THE DESIGN OF A TRANSONIC
GAS TURBINE STATOF

THESIS

AFIT/GAE/AA/78D-7   Robert N. Gamache
                        2Lt   USAF

DTIC
ELECT
MAR 13 1980

A

THE DESIGN OF A TRANSONIC
GAS TURBINE STATOR

Master's THESIS

Presented to the Faculty of the School of Engineering

of the Air Force Institute of Technology

Air Training Command

in Partial Fulfillment of the

Requirements for the Degree of

Master of Science

by

Robert N. Gamache, B.S.
2Lt   USAF

Graduate Aeronautical Engineering

December 78

Preface

In late 1977, the Turbine Technology Development Group of the Air Force Aero Propulsion Laboratory, identified the need to redesign the AFAPL Heat Transfer Facility's turbine stator blade profile. This report presents the results of my efforts to analytically design a turbine stator which yields optimum aerodynamic performance at transonic flow conditions.

I take this opportunity to thank Dr. Kervyn Mach, Air Force Aero Propulsion Laboratory, for his suggestions and advice during this study. I also wish to thank my thesis advisor, Dr. John R. Shea, for his assistance and direction. Acknowledgement is extended to Dr. James E. Hitchcock and Dr. Harold E. Wright for their counsel in the preparation of this document. I wish to specially thank my wife, Amy, for her encouragement, understanding, and patience during the course of this thesis project.

Finally, I would like to dedicate this report to the memory of my grandfather, Mr. Wilfrid A. Gendron.

Robert N. Gamache

i

Contents

List of Figures

List of Tables

List of Symbols

A	Normal flow area
C_p	Pressure coefficient = P_s/P_o
$\dot{m}$	Mass flow rate
M	Mach number
P	Pressure
PR	Cascade pressure ratio
ΔP	Change in pressure
R	Universal gas constant divided by molecular weight
S	Blade spacing cr pitch
t	Time
T	Temperature
u	Velocity in x direction
v	Velocity in y direction
V	Velocity
x	Axial coordinate direction
y	Blade-to-blade coordinate direction

Greek

α_1	Blade inlet angle
α_2	Blade exit angle
β_1	Gas inlet angle

β_2	Gas exit angle
γ	Specific heat ratio
δ	Gas exit deviation angle
θ	Trailing edge included angle
ρ	Density

Subscripts

a	Atmospheric conditions
b	Test facility conditions behind cascade test section
s	Local static value
z	Axial component
0	Total or stagnation value
1	Static value at cascade inlet plane
2	Static value at cascade exit plane

Abstract

A turbine stator profile that is analytically predicted
to exhibit good aerodynamic performance over a wide range of
transonic operating conditions has been designed for the Air
Force Aero Propulsion Laboratory's Heat Transfer Facility.
Analytical Turbine Design System computer programs developed
by General Electric Company were used to generate blade pro-
files/coordinates and perform 2-Dimensional cascade through-
flow calculations (streamline curvature technique). Two
aerodynamic performance standards were applied to pressure
distribution predictions of the blade contours produced from
a parametric variation study; 1) equal flow expansion over
both the suction and pressure surfaces, and 2) minimum suction
surface diffusion. The influence of the following geometric
parameters upon the design of a transonic turbine stator were
investigated; axial location of maximum section thickness,
stagger angle, leading edge bluntness factor, and trailing
edge taper factor. Results of this study show that a good
transonic turbine stator design must have a convergent-
divergent flow passage and a flat suction surface aft of the
throat location.

THE DESIGN OF A TRANSONIC
GAS TURBINE STATOR

I. Introduction

Background

Modern high pressure gas turbines operate in temperature environments in excess of $1055^\circ K$ ($1900^\circ R$). Due to the thermal limitations of existing materials, the requirement for blade cooling has become an essential feature of gas turbine design.

The mission objective of the Air Force Aero Propulsion Laboratory's Heat Transfer Facility (Figure 1) is to test and evaluate high temperature turbine blade cooling schemes for advanced turbopropulsion applications. The current test section, a rectilinear turbine stator cascade (Figure 2), was designed during the mid-1960's using a subsonic turbine blade design philosophy. Subsonic blade shapes are characterized by high aspect (span/chord) ratios, and relatively thick profile shapes.

Present day gas turbines are designed to function at pressure ratios which cause the working gas medium to approach sonic flow conditions. These designs are motivated by the high overall thermodynamic efficiency possible with a transonic pressure ratio. Small cross-sectional areas and

1
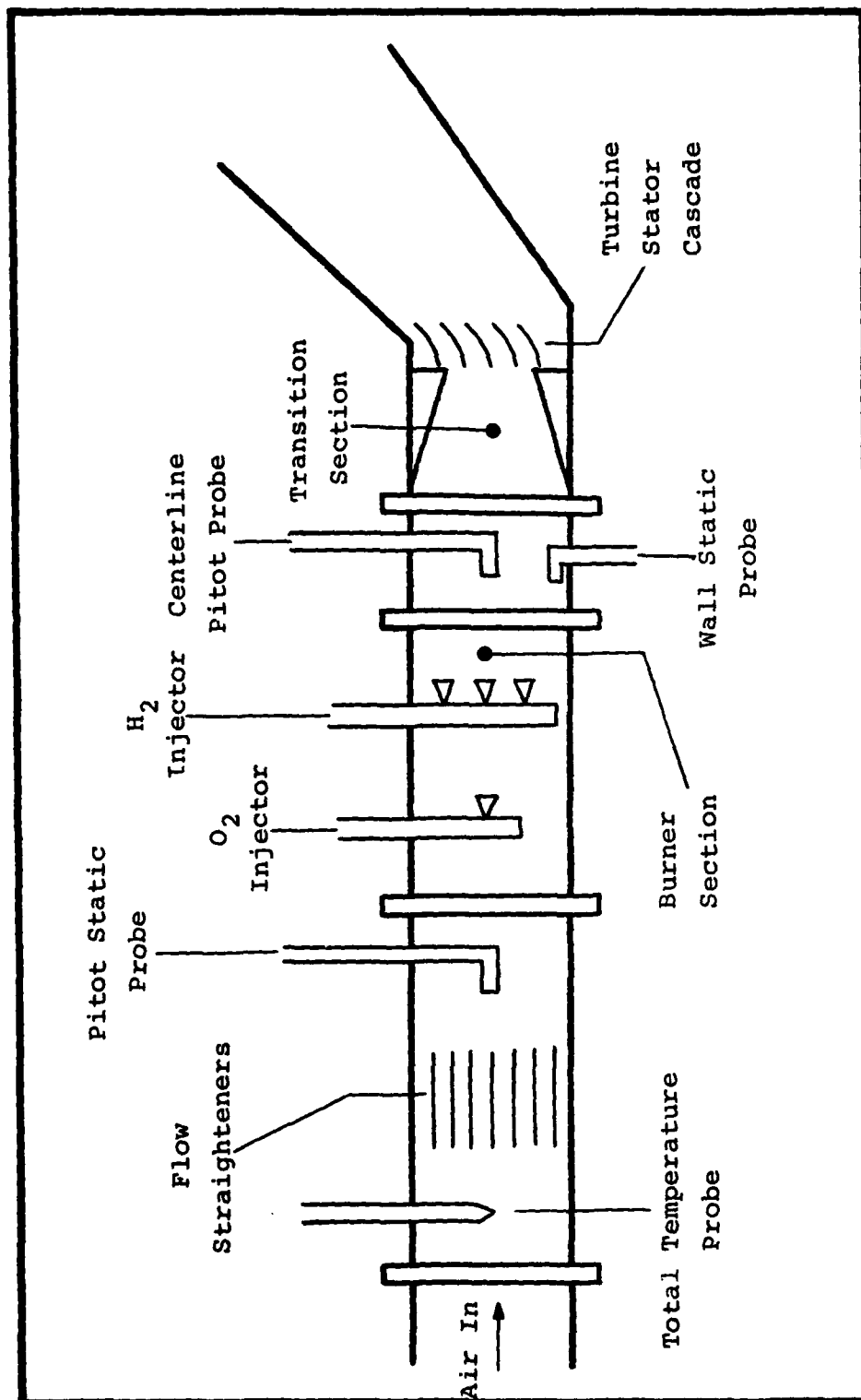
Figure 1 Heat Transfer Test Facility Schematic
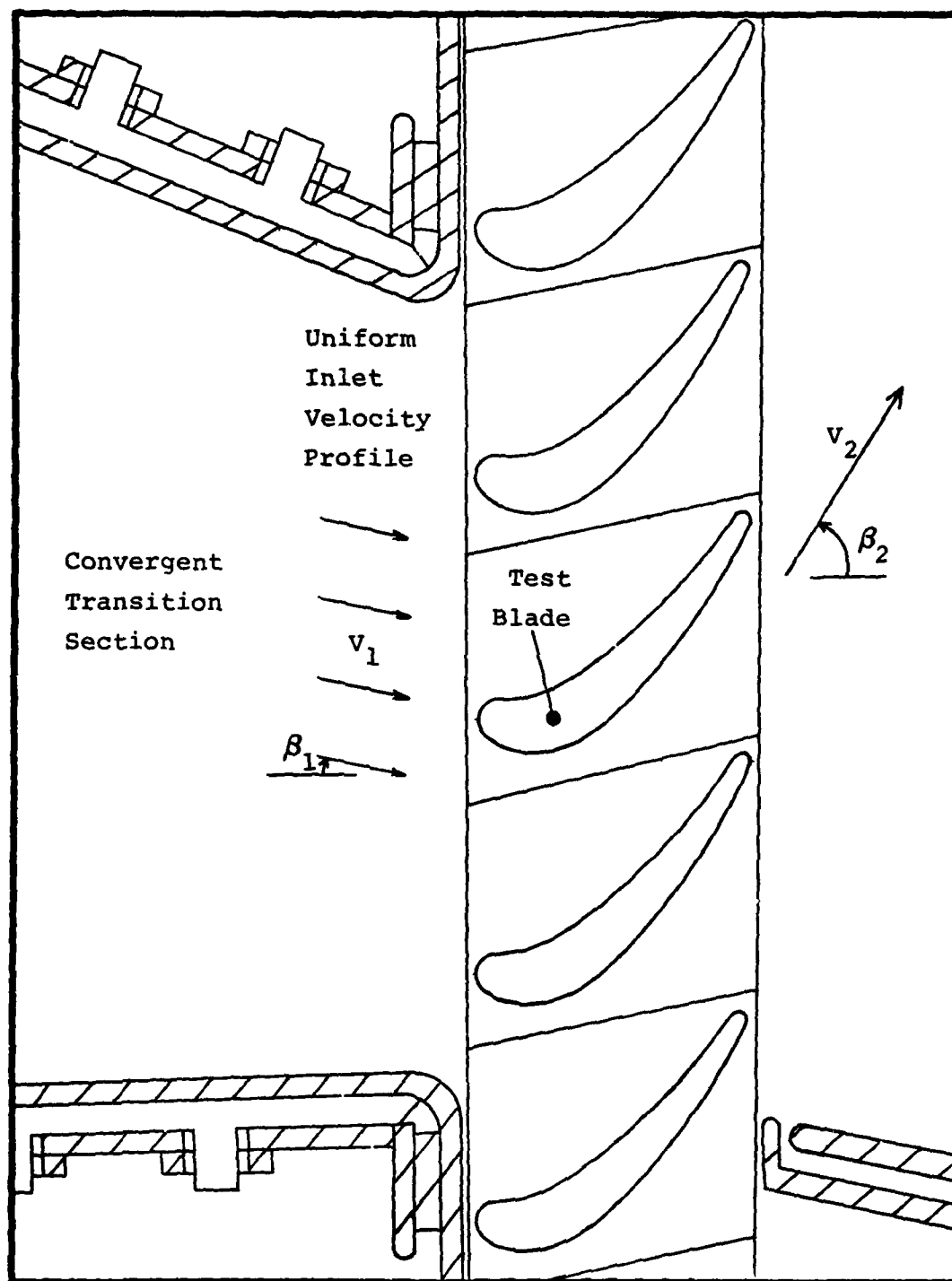
Figure 2 Schematic of Test Section Cascade

thin trailing edges are generally required to achieve acceptable aerodynamic performance in a transonic flowfield. These requirements must be balanced with the need to permit interior cooling systems while allowing the blade to retain mechanical strength at high temperatures.

Because the heat transfer loads and thermal stresses associated with a transonic profile are substantially more severe than those associated with a subsonic blade shape, relevant test conditions can no longer be established in the AFAPL Heat Transfer Facility. The facility's mission objective is seriously compromised until a new transonic turbine stator contour that simulates modern gas turbine environments is designed.

Problem

The basic intent of this study is to design a modern turbine blade shape that exhibits a high level of aerodynamic performance characteristics in a transonic flow regime. Flow through a transonic cascade passage is subsonic at the cascade inlet, choked at the flow passage throat (minimum area location), and slightly supersonic (M = 1.17) at the exit plane. Two tasks associated with the accomplishment of this design objective are: 1) the establishment of aerodynamic performance criteria based upon inviscid, shock-free flowfield calculations, and 2) the development of an analytical design optimization procedure.

4

The major analyatic design tool that will be used to generate and evaluate various balde contours is a set of computer programs entitled, "Turbine Design System" (TDS). Because the codes were recently developed and have not been sufficiently verified for accuracy and consistency, a secondary problem of verifying the TDS programs arises. The computer codes were generated by General Electric Company (Evendale, Ohio) under contract to AFAPL/TBC.

Scope

Experimental testing and evaluation of analytically derived blade geometries are an integral part of this AFAPL Heat Transfer Facility blade design upgrade program. However, it is beyond the scope of this thesis research effort to conduct the experimental portion of the transonic blade development program.

All flowfield calculations and estimates are valid for the mid-span 2-D streamsurface only. Aerodynamic performance and flowfield behavior are predicted for the design point, plus a number of off-design test conditions. The determination of heat transfer loads and mechanical stress analyses are also beyond the scope of this study.

The design point environment can be expressed in terms of the following gas property and velocity vector information: 29.0 N/cm^2 (42.0 psia) total pressure, 13.1 N/cm^2 (19.0 psia) back pressure, 1666.3°K (3000°R) total temperature, 1.26 specific heat ratio, 315.0 m^2/sec^2-$^\circ$K (1883.7 ft^2/sec^2-$^\circ$R)

5

gas constant, 8.0^O gas incidence angle, and 65.0^O gas exit angle.

Four geometric shape parameters are varied and optimized during the parametric design process: location of maximum section thickness, stagger angle, leading edge bluntness factor, and trailing edge taper factor. These parameters are defined in Chapter V. Performance sensitivity to off-design gas incidence angle, total temperature, and pressure ratio are also investigated.

Assumptions

A number of assumptions are inherent to the TDS flow-field calculation procedure. The most notable assumptions are: 1) the flow is steady, 2) the flow is inviscid, 3) the flow is isentropic (shock-free), 4) the fluid behaves as an ideal gas, and 5) mass, momentum and/or energy are not transported across a two-dimensional streamsurface.

The first assumption implies that the inlet velocity profile to the test blade is uniform. Because the transition section immediately upstream of the test section is a convergent duct (see Figures 1 and 2) with favorable decreasing pressure gradients, viscous boundary layer growth has negligible effect on the inlet velocity profile. The test section is assumed to be located far enough downstream that any residual freestream turbulance from the upstream combustion process is damped out. A condition of steady, irrotational flow is assumed to exist.

The next assumption is the shock-free flowfield. This assumption breaks down near the trailing edge wake region of the cascade. Viscous effects become significant in this region also. However, shock-free isentropic flow is a reasonable assumption for the rest of the cascade flowfield where velocities are subsonic or slightly sonic and pressure gradients are negative.

Finally, the fifth assumption is applied to a theoretical blade-to-blade streamsurface at the cascade mid-span location. This two dimensional flow assumption is justified on the basis of the rectilinear test section cascade geometry and the symmetrically convergent upstream transition duct.

The accuracy and validity of the experimental data contained in AFAPL-TR-67-147[1] is tacitly accepted. This assumption became a necessary premise during the TDS verification process.

General Approach

The basic approach toward solving the problem of designing a transonic turbine stator via analytical techniques is roughly a four phased process; 1) The flowfield calculation procedure is verified for correctness; 2) Blade design criteria are developed, and the existing blade profile deficiencies are identified; 3) Blade shape parameters are optimized along aerodynamic considerations to yield a final, transonic design; and 4) Off-design performance is investigated.

The first phase of this design project is concerned with establishing the validity of the preceding initial assumptions and the TDS calculation techniques. Verification of the analytical calculation techniques. Verification of the analytical calculation method as well as confirmation of the assumptions is achieved through correlation of subsonic test data[1] for the present airfoil cascade with TDS flowfield predictions. Further substantiation of the TDS program is obtained through comparison of TDS estimates for a transonic flow case with General Electric Company test data, and other analytical prediction programs.

Accomplishment of the phase two objective requires the development of suitable aerodynamic performance criteria. Next, these criteria are applied to TDS generated flowfield predictions for the current blade profile in a transonic flow regime (design point).

Finally, trends are established in phase three between the effect of varying various geometric blade shape parameters and their corresponding influence on aerodynamic performance. A final transonic design results from optimization of the blade shape trends. Off-design cases are also investigated.

Sequence of Presentation

The next chapter, entitled "Analytical Design Methods", contains a brief historical summary of the development of analytical calculation techniques for the turbomachinery

cascade throughflow problem. In addition, a description of the TDS computer design tool developed by General Electric Company under U.S. Air Force contract #F33615-75-C-2073 appears in Chapter II.

The phase one results from the TDS verification process, including correlation of theoretical predictions with experimental data for the current blade design, are presented in Chapter III.

Transonic design operating conditions and performance standards are defined in the first two sections of Chapter IV. These criteria are applied to an analytical prediction of the flowfield surrounding the present design in a transonic environment. The resulting deficiencies and shortcomings of the current blade are then identified and documented in the last section of Chapter IV.

The phase three parametric design study results are discussed in Chapter V. The final design coordinates appear in both tabular and graphical form. Estimates of aerodynamic performance sensitivity to various off-design conditions appear in Chapter VI. The influence of viscous effects on performance is also addressed.

Conclusions and recommendations for further study are offered in Chapter VII.

II. Analytical Design Method

The design of turbomachine cascade sections has tradi-
tionally been based upon empirical relations and/or one-
dimensional flow analyses. Thus, the standard practice for
the design of compressor and turbine cascades has primarily
consisted of a "build and try" approach. The advent of
advanced gas turbine engines for aircraft application, along
with their staggering development costs and stringent perfor-
mance requirements (high temperature operation, lightweight,
high thermodynamic efficiency), has necessitated a revolu-
tionary change in compressor and turbine design procedures.
Today, the performance of modern designs is analytically
predicted before a commitment is made to proceed with an
expensive fabrication and test program. Large, high speed,
digital computers have made this approach more attractive
from a cost effectiveness standpoint.

Pursuant to the goal of analytically predicting turbo-
machine cascade performance, a substantial number of
investigators from industry, government, and academia, have
developed cascade through-flow calculation techniques. There-
fore, one objective of this chapter is to present an overview
of the various methods currently used to compute turbomachine
cascade flowfields. However, the basic intent of this
section is to provide a detailed description about the nature
and operation of the major analytical design tool (i.e., the

10

TDS computer programs) that will be used to generate new transonic blade profiles and to determine the corresponding cascade flowfield characteristics.

Cascade Through-Flow Calculation Techniques

The cascade through-flow problem is three-dimensional, time-dependent and viscous in nature. Most modern analysis techniques dealing with three-dimensional cascade flowfields are based upon an approximate method set forth by Wu[2] in 1951. Wu's paper is primal to the field because he was one of the first investigators to make the necessary assumptions and simplifying approximations for transforming the overall three-dimensional problem into a series of two dimensional computations.

Wu's basic through-flow theory proposes that the three-dimensional flowfield should be modeled as a set of two-dimensional flows; one of these flows is located in blade-to-blade surfaces (the S1 stream surfaces), while the other flow lies on hub-to-shroud surfaces (the S2 stream surfaces). The relative orientation of the S1 and S2 stream surfaces is depicted in Figure 3.

Two classical solution approaches to the problem of calculating flows on either the S1 or S2 stream surfaces are reported in literature; the matrix method, and the streamline curvature method. Iterative numerical techniques are an inherent feature of both solution procedures. Iterative methods guess an initial stream function/velocity distribution from which the rest of the fluid properties in the flowfield are

11
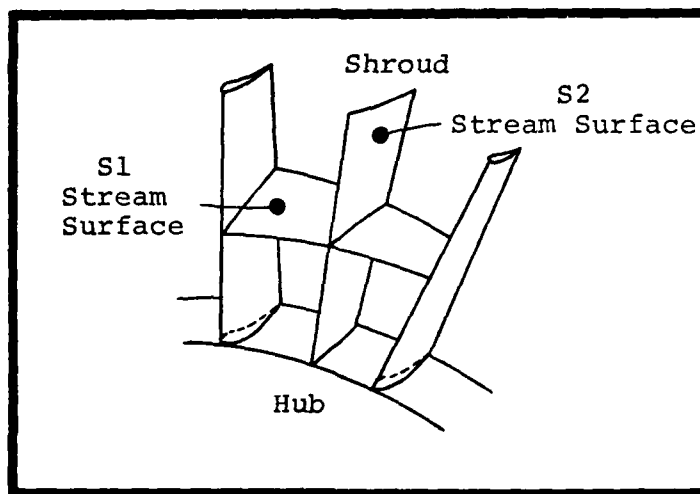
Figure 3   S1 and S2 Stream Surfaces

determined.   The equation of motion is solved by either the matrix or streamline curvature approach, and thus, a new velocity field is predicted.   This iterative process continues until a set of specified convergence criteria are satisfied.

Wu[2][3] suggested the use of matrix methods.   In this type of approach, sometimes referred to as a finite-element method, the iterations are performed on a fixed set of grid lines. The matrix method has recently been used to compute cascade flowfields by Bosman and El-Shaarawi[4], Bosman[5], Katsanis and McNally [6][7], and others[8][15].   Gopalakrishnan and Bozzola[16], and McDonald[17] pose the through-flow problem in time dependent form and use finite-element techniques to solve for transonic flows in turbomachinery cascades.   Ives and Liutermoza[18] use conformal mapping techniques in conjunction with a finite-difference grid to obtain transonic cascade solutions.

In the streamline curvature method, the grid is composed of the streamlines themselves and a set of semi-orthogonals.

12

During the iteration sequence, the grid lines and points are repositioned after each iteration to satisfy mass, momentum and energy balances. Novak and Hearsey[19], Smith[20], Frost[21], and Wilkinson[22] have reported the development of computer programs which employ streamline curvature techniques.

The concept of quasi-three-dimensional, numerical solutions of flow through cascades refers to the simultaneous solution of flow on the S1 and S2 streamsheets. A number of investigators[4,19] use coordinated computer programs in which the S1 stream surface shape is dependent on the S2 solutions while the S2 shape is dependent on the S1 solutions. These methods are indicative of the state-of-the-art and have established good convergence for steady, inviscid and subsonic flow conditions.

Turbine Design System (TDS)

The specific intent of this research is to establish an analytical procedure for designing transonic turbine blades. Fundamental geometric blade shape parameters were identified, and the influence of these parameters upon cascade performance for a given set of operating conditions was determined. The final design is simply the geometric parameter set which yields the highest amount of aerodynamic performance.

A parametric variation and evaluation study was conducted to realize the basic intent outlined above. The major analytical tool that was used to accomplish this study is the Turbine Design System (TDS) computer programs developed by
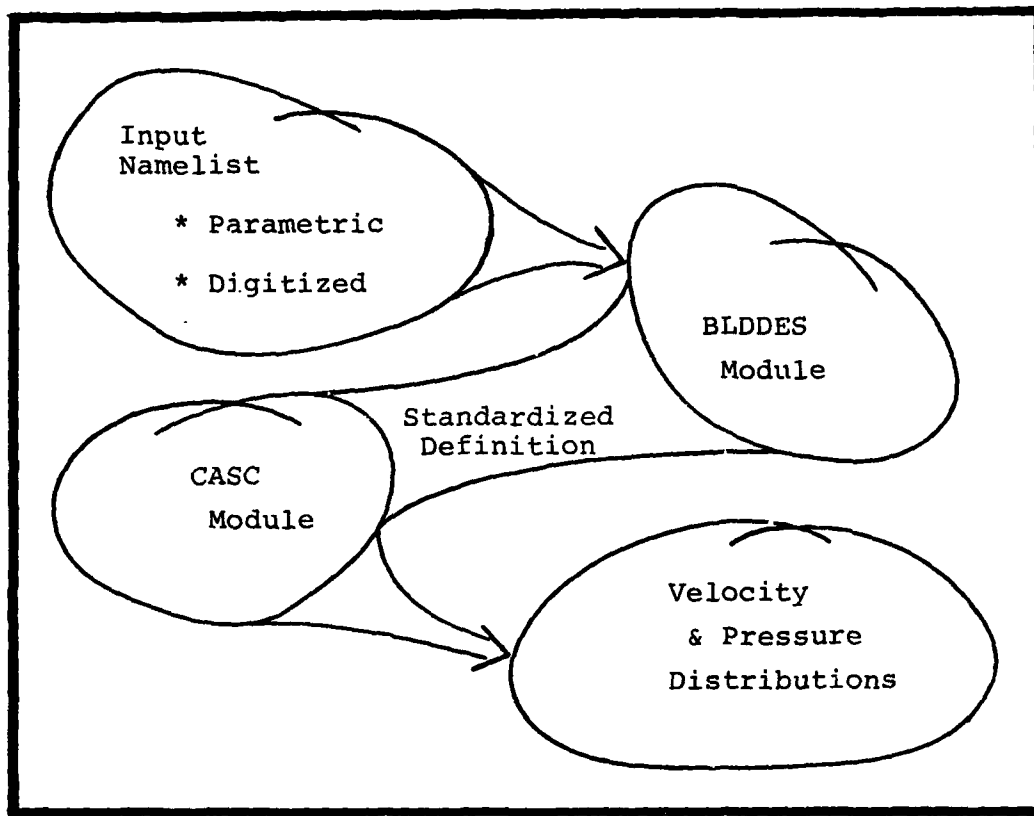
Figure 4   TDS Schematic Diagram

General Electric Company under contract to AFAPL/Turbine
Components Branch.   Two TDS subprograms were utilized:
the BLDDES and CASC modules.

Given a relatively simple blade shape definition, the
Blade Design (BLDDES) module generates an output file with
a standardized set of blade shape coordinates and surface
curvature information.   The Cascade Analysis by Streamline
Curvature (CASC) module returns the inviscid, shock-free
flowfield solution for a cascade of airfoils defined by the
BLDDES output file.   Figure 4 is a schematic diagram which
graphically displays the function and role of each module.

14

Further information about the operation of the TDS computer programs can be found in the TDS User's Manual[23] and AFAPL TR-78-92[24].

BLDDES MODULE. Two modes of data input to the BLDDES module are possible. Input may consist of a parametric blade definition or as an array of digitized blade coordinate data taken from a layout drawing or design report. The latter mode of data input was used to obtain a standardized definition of the current test blade profile. This information was required to perform the TDS verification process (Chapter III) and to arrive at an analytic evaluation of the current blade at transonic operating conditions (Chapter IV). The parametric definition input mode option was utilized to generate blade profiles for aerodynamic analysis during the parametric design study (Chapter V).

The standard definition returned by BLDDES is composed of blade surface coordinates that are tabulated with respect to the blade section stacking point. BLDDES output is consistent with the input requirements for the aerodynamic analysis module; CASC.

CASC Module. The CASC module yields steady-state, inviscid, shock-free flow solutions for a cascade of airfoils. CASC solutions for any particular blade section will lie on the blade-to-blade S1 streamsurface normal to the blade (see Figure 3).

The streamline curvature calculation technique employed by CASC requires the input of accurately determined boundary

surface coordinates from the standardized BLDDES output $BB

Namelist. The position and curvature of the streamlines are

found such that the continuity equation, the cross-stream

momentum equations, and the boundary surface curvature in-

formation are satisfied.

Although the inviscid assumption costs CASC a small

amount of inaccuracy, it reduces the complexity of the cal-

culations considerably. CASC's main asset is that it requires

substantially less central processor time and core space to

process a given airfoil contour as compared with other aero-

dynamic analysis programs reported in literature. Thus, the

"quick-look" capability offered by CASC makes the program

ideally suited towards performing a parametric design study

involving a number of cases to be analyzed.

III. TDS Verification Investigation

Purpose

Verification of the General Electric TDS computer programs was included as a major step in this research study for two reasons. First, the TDS codes had been recently procured by the U.S. Air Force in November 1977, and had not been sufficiently verified for accuracy and consistency. Second, it was necessary to determine whether or not the Heat Transfer Facility's rectalinear cascade geometry along with the simplifying inlet velocity profile assumptions could be analyzed by TDS to yield accurate results.

Pressure distributions for the existing turbine airfoil were experimentally determined by Quick, Henderson, and Tall during a 1967 cold-flow investigation study. The results are tabulated in AFAPL Technical Report 67-147[1].

Hence, the overall TDS verification objective was to obtain pressure distribution predictions for the present blade geometry that match available experimental data at two different sets of operating conditions. Comparison of analytical TDS pressure distribution predictions with actual Heat Transfer Facility experimental data was expected to substantiate the validity of the initial assumptions and the computer programs.

Procedure

The general approach used to verify the TDS programs consisted of three distinct phases. First, thermodynamic and geometric boundary conditions, as well as an inlet velocity profile, were specified for input into the TDS programs. These boundary conditions were chosen so that they were a direct reflection of the test conditions under which the experimental data were obtained.

Next, verification criteria were developed. In theory, the analytical codes should yield matching pressure distributions for the two known sets of test conditions that were considered. Additionally, the computer programs should yield predictable flowfield solutions for small variations of the inlet boundary conditions.

Finally, the results of the verification investigation were evaluated. The conclusions are presented in the last section of this chapter.

Boundary Conditions

Thermodynamic. During the 1967 experimental cold flow investigation of the present turbine airfoil[1], pressure distributions were obtained for various gas operating conditions. Two of these cases were selected for analytical correlation purposes. The thermodynamic properties for each of the two cases are tabluated in Tables I and II.

Geometric. Establishment of geometric boundary conditions for aerodynamic analysis by the CASC module consists

18

Table I

Case One Thermodynamic Boundary Conditions

| Thermodynamic Quantity | | Value | |
Description	Symbol	Metric	English
Mass Flow Rate	$\dot{m}$	2.23 kg_m/sec	4.92 lb_m/sec
Total Temperature	T_O	286.8 $^{\circ}K$	517.0 $^{\circ}R$
Total Pressure	P_O	14.543 N/cm^2	21.046 psia
Atmospheric Pressure	P_a	9.885 N/cm^2	14.3 psia
Specific Heat Ratio	γ	1.4	1.4
Gas Constant	R	287.1 $\dfrac{m^2}{sec^2-^{\circ}K}$	1717.0 $\dfrac{ft^2}{sec^2-^{\circ}R}$

Table II

Case Two Thermodynamic Boundary Conditions

Thermodynamic Quantity		Value	
Description	Symbol	Metric	English
Mass Flow Rate	$\dot{m}$	2.74 kg_m/sec	6.05 lb_m/sec
Total Temperature	T_O	286.8 $^\circ K$	517.0 $^\circ R$
Total Pressure	P_O	17.328 N/cm^2	25.074 psia
Atmospheric Pressure	P_a	9.885 N/cm^2	14.3 psia
Specific Heat Ratio	γ	1.4	1.4
Gas Constant	R	287.1 $\dfrac{m^2}{sec^2 - ^\circ K}$	1717.0 $\dfrac{ft^2}{sec^2 - ^\circ R}$

of defining the current blade profile, and then standardizing
the definition with respect to a stacking point origin via
the BLDDES module. The portion of the BLDDES input $BB
namelist (FORTRAN) that defines the present turbine airfoil
shape appears in Table III. Figure 5 is a scaled drawing
of the existing turbine airfoil section.

The philosophy used to define the current blade section
is the following; 1) represent the leading edge as an ellipse,
2) represent the trailing edge as a circle, and 3) input the
pressure and suction surfaces as digitized coordinate pairs.
This philosophy becomes obvious when the quantities contained
in Table III are clarified in the following paragraphs.

The pressure and suction surfaces are defined by the
(X,Y) pairs in the PRESS and SUCTN arrays. These coordinates
are taken from the original Allison Division blade design
report[25]. The coordinate system that was employed fixes the
X-axis parallel to the axial centerline, positions the leading
edge highlight point at (0,3), and the suction surface is the
upper surface.

ISTK is the stacking point indicator. A value equal
to unity locates the stacking point at the center of gravity
of the airfoil section. The choice of stacking point location
is academic; since choice of any stacking point location will
yield identical stacking results for a rectalinear two-
dimensional cascade.

A zero value for IVANE notifies the software logic that
the airfoil has a blade input orientation, i.e., the suction

21

Table III

Geometric Boundary Conditions

```
PRESS=
    0.0740   2.9205      0.1273   2.9126      0.1826   2.9033
    0.2337   2.8945      0.2851   2.8822      0.3342   2.8698
    0.3827   2.8558      0.4305   2.8404      0.4771   2.8234
    0.5232   2.8045      0.5912   2.7729      0.6574   2.7372
    0.7399   2.6859      0.8153   2.6334      0.8910   2.5756
    0.9654   2.5131      1.0348   2.4479      1.1023   2.3801
    1.1673   2.3093      1.2301   2.2357      1.2879   2.1593
    1.3429   2.0802      1.4015   1.9865      1.4317   1.9340
    1.4619   1.8815
SUCTN=
    0.0466   3.0730      0.1016   3.0984      0.1665   3.1205
    0.2294   3.1380      0.3027   3.1420      0.3728   3.1418
    0.4422   3.1343      0.5108   3.1210      0.5787   3.1006
    0.6442   3.0741      0.7366   3.0228      0.8203   2.9590
    0.9053   2.8744      0.9709   2.7994      1.0362   2.7195
    1.1006   2.6381      1.1611   2.5568      1.2194   2.4742
    1.2746   2.3894      1.3274   2.3034      1.3771   2.2167
    1.4253   2.1294      1.4781   2.0278      1.5054   1.9744
    1.5327   1.9209
ISTK=1
IVANE=0
LEDGE=1
ITMODE=1
TE=0.08335
E=1.45
EPSI=8.0
SCALIN=1.0
ZLE=0.0
ZTE=1.5327
RLE=23.87324
RREF=23.87324
RTE=23.87324
NBLDS=100
```

22

Suction
Surface

Pressure
Surface

center of gravity

Scale 3.75:1
  AXW 3.894 cm (1.533 in)
  Chord 4.834 cm (1.903 in)
  Stagger 34.65°
  Area 2.503 cm^2 (0.388 in^2)
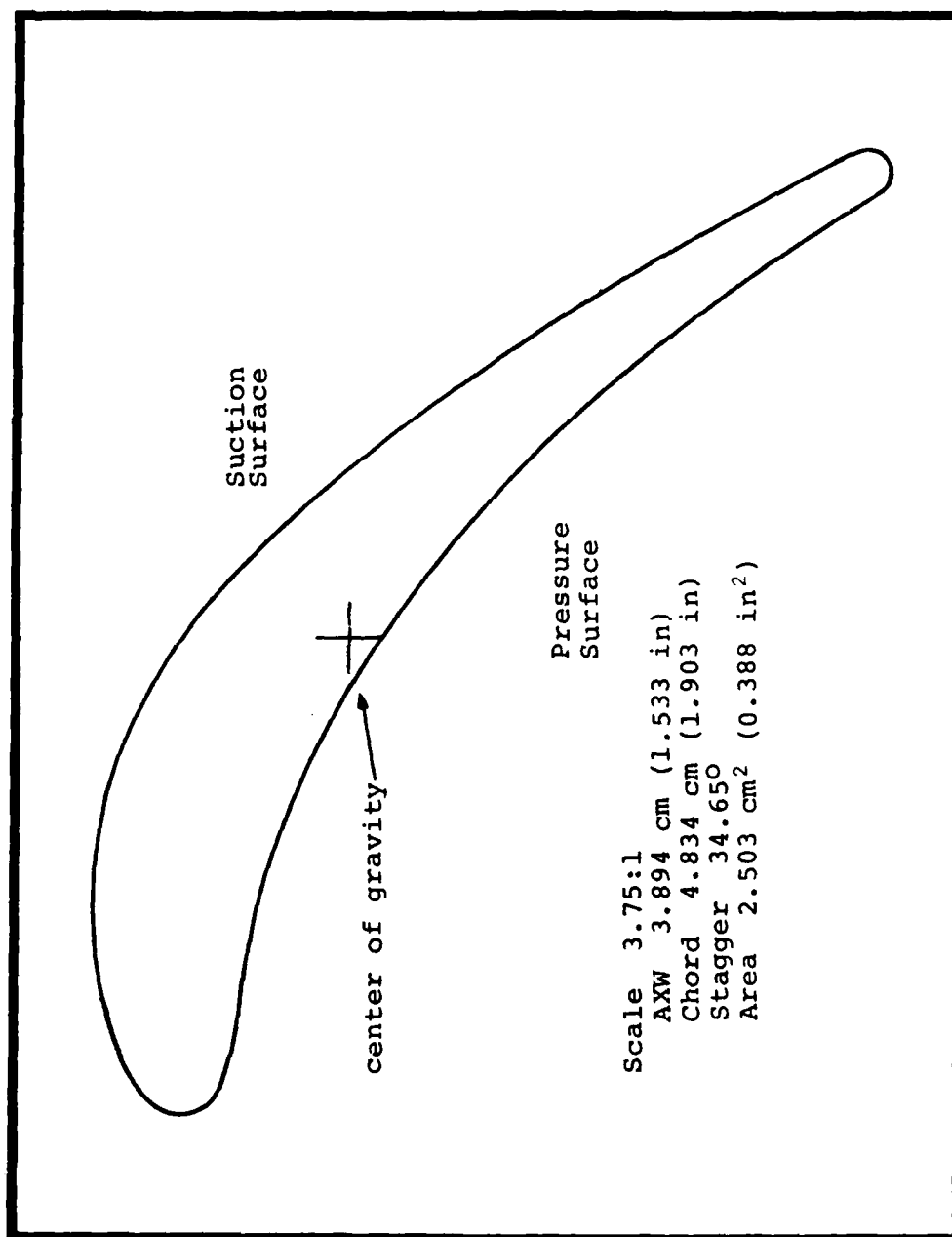
Figure 5 Existing Turbine Airfoil Section

side is uppermost. LEDGE equal to one means that the PRESS and SUCTN coordinate arrays do not include the leading and trailing edge. BLDDES will then generate an ellipse for the leading edge while either a square or circle will be fitted to the trailing edge.

ITMODE is the trailing edge shape indicator. A value of one causes the BLDDES programming to define the trailing edge as a circle with diameter equal to the trailing edge thickness (TE). From a plot of the original design coordinates, the trailing edge thickness, TE, was determined to be 0.2117 cm (0.08335 in).

The eccentricity parameter, E, is the ratio of leading edge ellipse semi-major to semi-minor axes. After a plot of the blade was made from coordinate data and several itertions were performed to obtain the best curve fit, a value for E of 1.45 was determined. EPSI is an estimate of the leading edge ellipse semi-major axis inclination angle.

SCALIN defines the scale size of the input data. Actual coordinates were used. ZLE and ZTE refer to the axial location of the leading and trailing edge highlight planes. RLE, RREF, and RTE are the radii which define the airfoil section radial location in a hypothetical curvalinear engine. Because the facility test section is rectalinear, a large radius value was chosen to simulate this condition. Thus, a radius value of 60.638 cm (23.87324 in) was chosen along with 100 blades (NBLDS) to yield a pitch value of 3.81 cm (1.5 in) which is the blade spacing in the two-dimensional cascade.

24

Inlet Velocity Profile. A condition of steady, turbulent, and fully-developed flow has been assumed to exist at the test section inlet. Because fully-developed, turbulent velocity profiles are characterized by fairly uniform core regions, the test blade inlet velocity profile is a set of constant, uniform velocity vectors. The direction of the velocity vectors is the gas incidence angle, β_1, and the magnitude is expressed in non-dimensional form as the inlet Mach number, M_1.

Due to the geometry of the upstream transition section, a slight gas incidence angle is known to exist. The gas incidence angle is estimated to be $8^{\circ} \pm 8^{\circ}$. As will be shown in the theoretical development of the third verification criterion, small gas incidence angles ($\pm 15^{\circ}$) have negligible effect on the pressure distribution of an airfoil in a turbine cascade. Therefore, the amount of error associated with $\pm 8^{\circ}$ is insignificant. Because gas incidence angle is primarily a function of hardware geometry and not gas operating conditions, it is assumed to remain constant for both experimental cases under consideration.

The inlet Mach number was approximated for each case through application of the following one-dimensional, isentropic equation;

$$\frac{\dot{m}}{A} \sqrt{\frac{T_0 R}{\gamma g_c^2}} \frac{1}{P_0} = M_1 \left(1 + \frac{\gamma-1}{2} M_1^2 \right)^{\frac{\gamma+1}{2(1-\gamma)}} \tag{1}$$

where ṁ is the mass flow rate, A is the cross-sectional area normal to the flow, T_O is the total temperature, R is the universal gas constant divided by the molecular weight of air, γ is the specific heat ratio, and P_O is the total pressure. When the appropriate Table I and II values are inserted into equation one, along with a cross-sectional area of 148.4 cm^2 (23 in^2), the inlet Mach number is estimated to be 0.29 and 0.30 for cases one and two respectively. Because of the significant amount of error associated with the figures for mass flow rate and the cross-sectional area normal to the flow, these approximations are only useful as a general estimate of the inlet Mach number level. Therefore, a number of cases with varying inlet mach numbers were analyzed before a precise analytical-experimental correlation was reached.

The case one and two BLDDES output files (CASC input files) which contain the standardized blade definition of the existing airfoil, plus the respective thermodynamic and inlet velocity profile boundary information, are listed in Appendix A. Further explanation of the Appendix A $BB namelist variables can be found in the TDS User's Manual[23].

Standards

Criterion One. For a given input combination of thermo-dynamic, geometric and inlet velocity profile information, the CASC module returns a value for the cascade exit static pressure, P_2, the gas exit angle, β_2, plus a listing of the

26

airfoil pressure distribution. For each of the two test cases, the first verification criterion requires that the analytical pressure distribution prediction matches the experimental data. Analytical-experimental correlation must occur for the boundary conditions stated in the previous section, plus a small change in the inlet Mach number value.

Since the exit static pressure, P_2, must equal the cascade back pressure, P_b, for a subsonic cascade operating condition, the exit static pressure is equal to the atmospheric pressure, plus exhaust duct line losses, ΔP;

$$P_2 = P_b = P_a + \Delta P \tag{2}$$

Because case one is at a lower mass flow rate operating condition than is case two, lower exhaust duct exit velocities will exist during case one. Thus, the line pressure losses are expected to be less for case one. In addition, the line pressure losses for either case should be greater than zero, but less than 20 percent of the atmospheric pressure level. Therefore, another requirement of the first verification criterion is that the following inequality must be staisfied;

$$0.0 < \Delta P_{\text{case one}} < \Delta P_{\text{case two}} < 0.20 \ P_a \tag{3}$$

Criterion Two. The gas exit angle, β_2, is primarily fixed by the cascade blade outlet angle, α_2. The blade outlet angle is defined in Figure 6 as the angle formed by

27
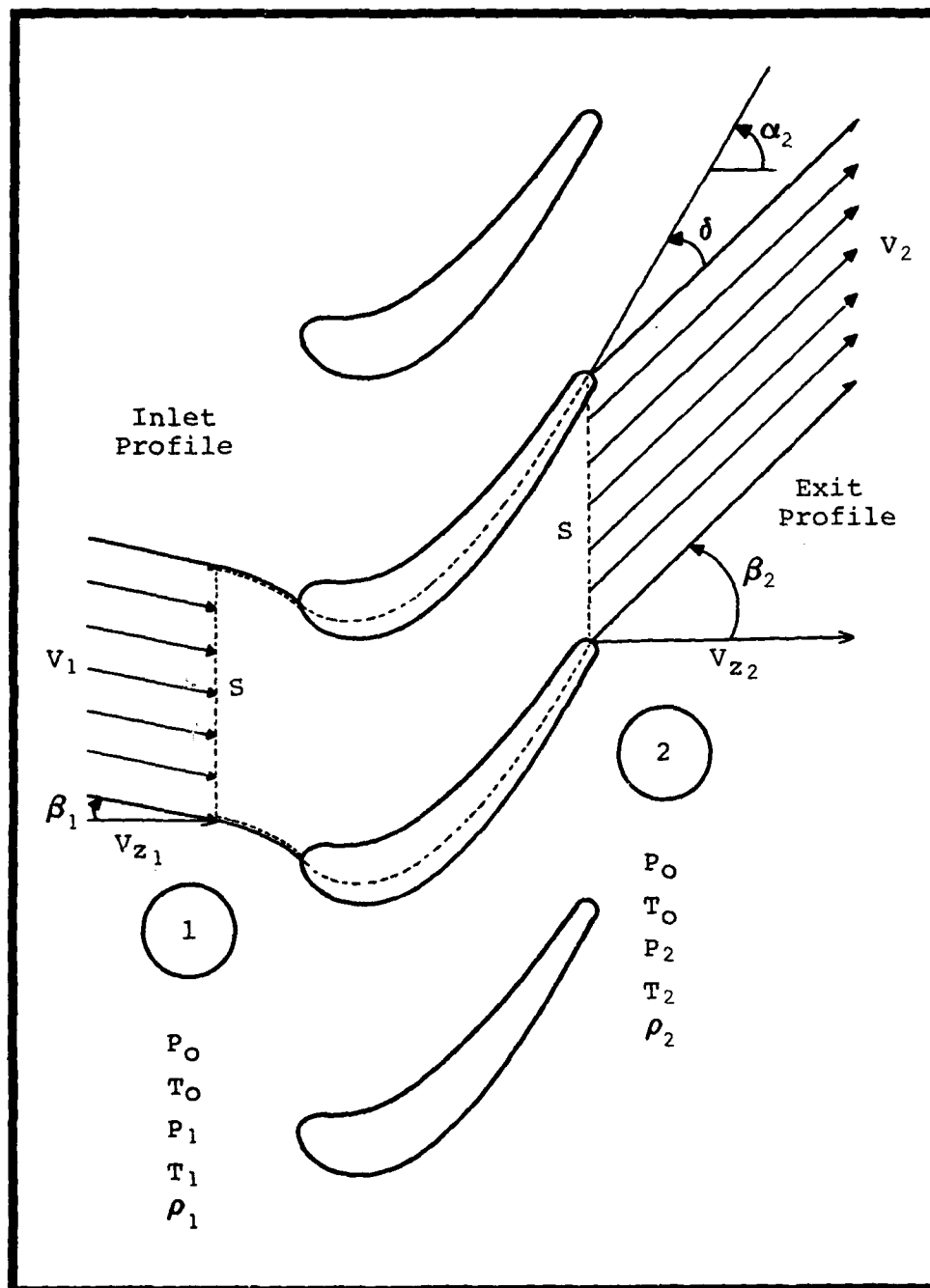
Figure 6   Turbine Cascade Control Volume

28

the tangent line to the trailing edge camberline and the axial chord line. The existing turbine cascade has an outlet blade angle of $61.2°$.

In most turbine and compressor cascades, a slight gas deviation angle, δ, will exist. Gas deviation angles for subsonic cascades are small and result from the pressure equilibrium process that occurs in the trailing edge wake region of the blades. Vincent[26] estimates that deviation angles are $\pm2°$ for most turbine cascades. Cox[27] reports deviation angles of the order of $5°$ from cascade test data.

Hence, the second verification criterion requires that the gas exit angle computed by CASC be equal to $61.2° \pm \delta$, where:

$$-5° < \delta < 5° \tag{4}$$

Criterion Three. The governing two-dimensional conservation of mass law is expressed in differential form by the following equation:

$$\frac{\partial \rho}{\partial t} + \frac{\partial \rho u}{\partial x} + \frac{\partial \rho v}{\partial y} = 0 \tag{5}$$

When the preceeding continuity equation is applied to the mid-span turbine cascade control volume depicted in Figure 6, the equation reduces to the following steady-state, one-dimensional expression:

$$\frac{\partial \rho u}{\partial x} = \dot{m}_1 - \dot{m}_2 = 0 \tag{6}$$

or

$$\dot{m}_1 = \dot{m}_2 \tag{7}$$

Equation 7 is a simple continuity balance which states that the mass flow through the inlet plane is equal to mass flow out the exit plane. Upon substitution of isentropic gas relationships and an algerbraic rearrangement of terms (see Appendix B), Equation 7 becomes;

$$(\cos \beta_1) \ M_1 \left(1 + \frac{\gamma-1}{2} M_1^2 \right)^{\frac{\gamma+1}{2(1-\gamma)}}$$

$$= (\cos \beta_2) \ M_2 \left(1 + \frac{\gamma-1}{2} M_2^2 \right)^{\frac{\gamma+1}{2(1-\gamma)}} \tag{8}$$

where

β_1 = gas incidence angle

M_1 = inlet Mach number

β_2 = gas exit angle

M_2 = exit Mach number

Equation 8 is non-dimensional and it relates the cascade inlet conditions to the exit conditions.

The pressure distribution around an airfoil of a typical turbine cascade has been observed to be a function of channel flow characteristics rather than parameters associated

with external airfoil theory. Moreover, for a given airfoil
in a cascade, the pressure coefficient distribution is a
function of one unique cascade pressure ratio (i.e., mass
flow rate):

$$C_p \text{ Distribution} = f(PR) \tag{9}$$

where

C_p = pressure coefficient

PR = cascade pressure ratio

The pressure coefficient, C_p, is defined as the local
static pressure divided by the total pressure. Cascade
pressure ratio, PR, is equal to the exit static pressure
divided by the total pressure. Exit Mach number, M_2, can be
defined in terms of the cascade pressure ratio, P_2/P_0, by
the following relationship:

$$\frac{P_2}{P_0} = \left(1 + \frac{\gamma-1}{2} M_2{}^2 \right)^{\frac{\gamma}{1-\gamma}} \tag{10}$$

or

$$M_2 = \sqrt{5 \left[\left(\frac{P_2}{P_0} \right)^{-0.2857} - 1 \right]} \tag{11}$$

where

$\gamma = 1.4$

31

Two points regarding Equation 8 require further clari-
fication. First, the right hand side of Equation 8 remains
constant for a given pressure distribution (matching or
otherwise) because the gas exit angle is relatively invari-
ant with varying inlet combinations and the exit Mach number
is also constant as defined by Equations 11 and 9. Second,
for small gas incidence angles, $\cos \beta_1$, is approximately
equal to unity. Thus, turbine cascades are insensitive to
small gas incidence angles and the inlet Mach number is
relatively fixed for a given pressure distribution.

Consequently, if a matching pressure distribution is
found such that the first two verification criteria are
satisfied, the gas exit angle, β_2, and the cascade pressure
ratio, P_2/P_O, returned by CASC are a pair of unique quantities.
Substitution of these gas exit conditions into Equations 11
and then 8 will yield a relationship which involves only
two variables; the inlet Mach number and the gas incidence
angle. Hence, the third verification criterion requires
that the TDS programs should yield matching pressure distri-
butions for the inlet velocity profile combinations defined
by Equation 8, where the right side of the equation is a
previously determined constant.

Results

For the specified boundary conditions which define either
verification case, analytical pressure distributions were
obtained that match the experimental data. At a gas incidence

32

angle of eight degrees, the inlet Mach number values which yield the matching data are 0.2842 and 0.2990 respectively. Note that the difference between these inlet Mach number values and the Equation 1 approximations are negligible.

The CASC output files for both cases are presented in Appendix C. Figures 7 and 8 are pressure coefficient distribution plots which graphically demonstrate the correlation between the experimental and analytical results.

Comparison of the Figure 7 and 8 curves indicates that a small (1-5 percent) discrepancy exists between predicted and and actual data. The analytic pressure coefficients are slightly higher than the corresponding experimental results. This situation occurs primarily because CASC is an inviscid analysis tool. Due to the fact that CASC neglects the presence of boundary layers, it does not consider displacement thickness effects. Thus, lower velocities (higher pressures) are predicted due to larger effective flow areas.

The six to eight percent error associated with the prediction of the minimum throat location is a function of three probable causes. First, boundary layer induced displacement thickness can cause the minimum throat location to shift forward. Second, local blade surface curvature effects from manufacture of the test specimen could also have advanced the minimum area location. Finally, small inaccuracies inherent in the experimental procedure could have accounted for misrepresentation of the minimum throat location.
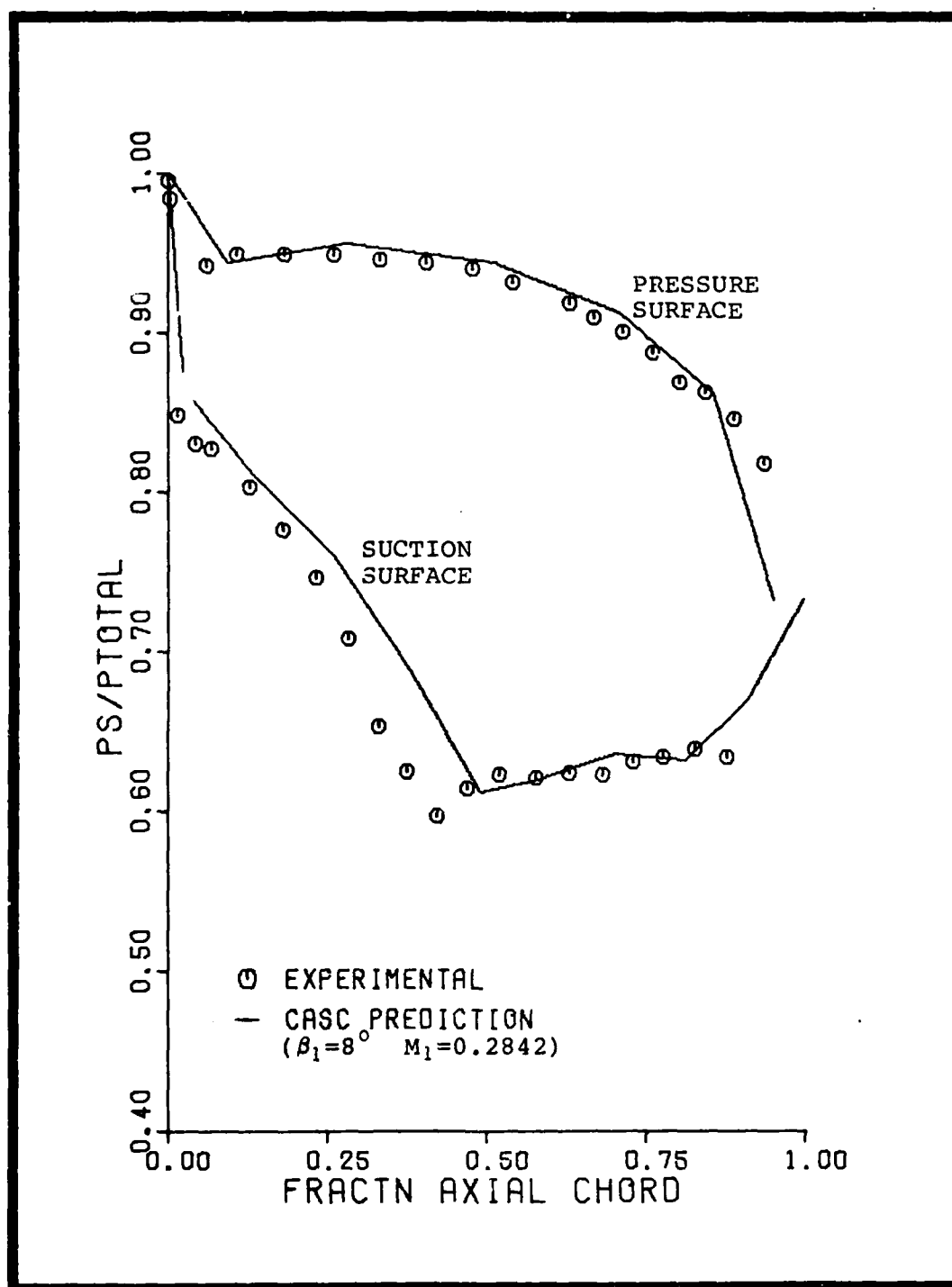
Figure 7   Case One Pressure Coefficient Distribution
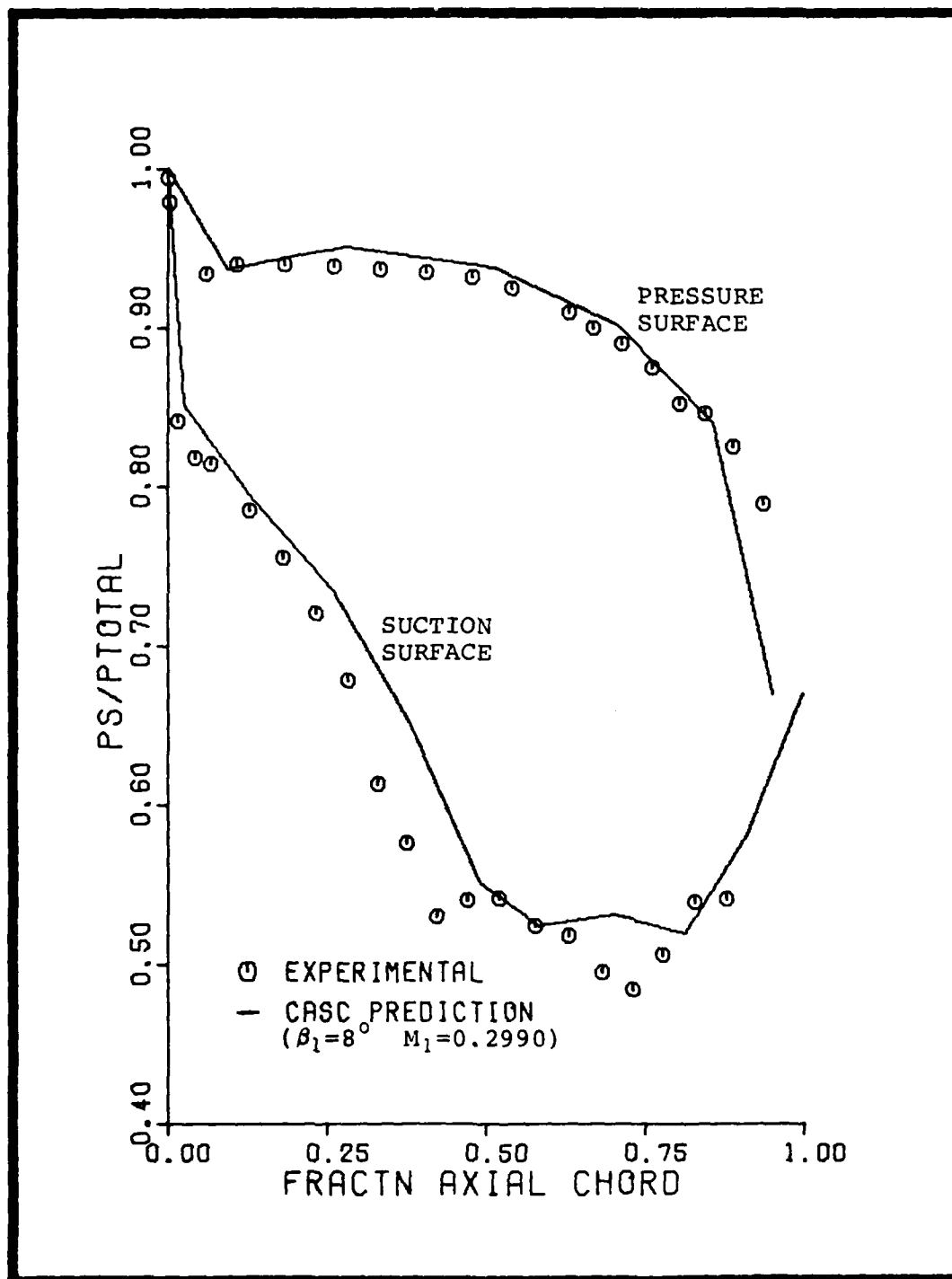
Figure 8   Case Two Pressure Coefficient Distribution

Table IV

Trailing Edge Gas Properties

Test Case	P_2 (N/cm^2)	(psia)	M_2	β_2 (deg)
1	10.434	15.1	0.7053	59.64
2	11.052	16.0	0.8275	60.08

Table IV contains the trailing edge conditions returned by CASC for the matching pressure coefficient distributions plotted in Figures 7 and 8. Line pressure losses, ΔP, are calculated by inserting the Table IV exit static pressures into Equation 2. For an atmospheric pressure of 9.885 N/cm^2 (14.3 psia), the line losses are 0.549 N/cm^2 (0.8 psi) and 1.167 N/cm^2 (1.7 psi). These ΔP values satisfy the relationship expressed by Equation 3.

The gas deviation angle, δ, is the difference between the blade outlet angle and the gas exit angle. The computed deviation angles of 1.56° and 1.12° for the two test cases are within the Equation 4 requirements.

In order to satisfy the third verification criterion, the effect of varying the inlet Mach number and gas incidence angle was investigated. A combined total of ninety-one different inlet combinations were analyzed for both cases. Appendicies D and E contain the pressure coefficient distri-
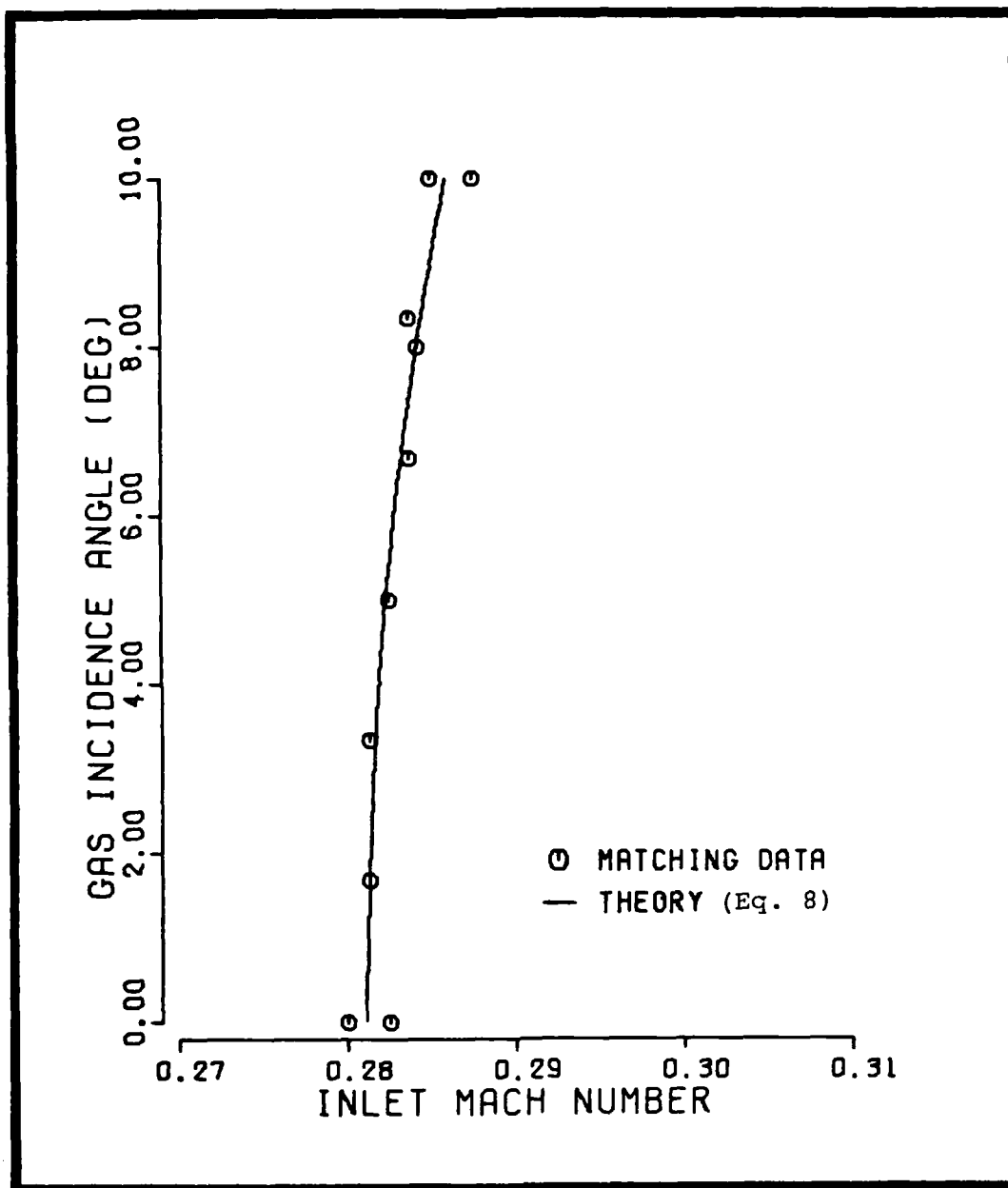
Figure 9   Case One Inlet Velocity Profiles
Yielding Matching C_p Distributions
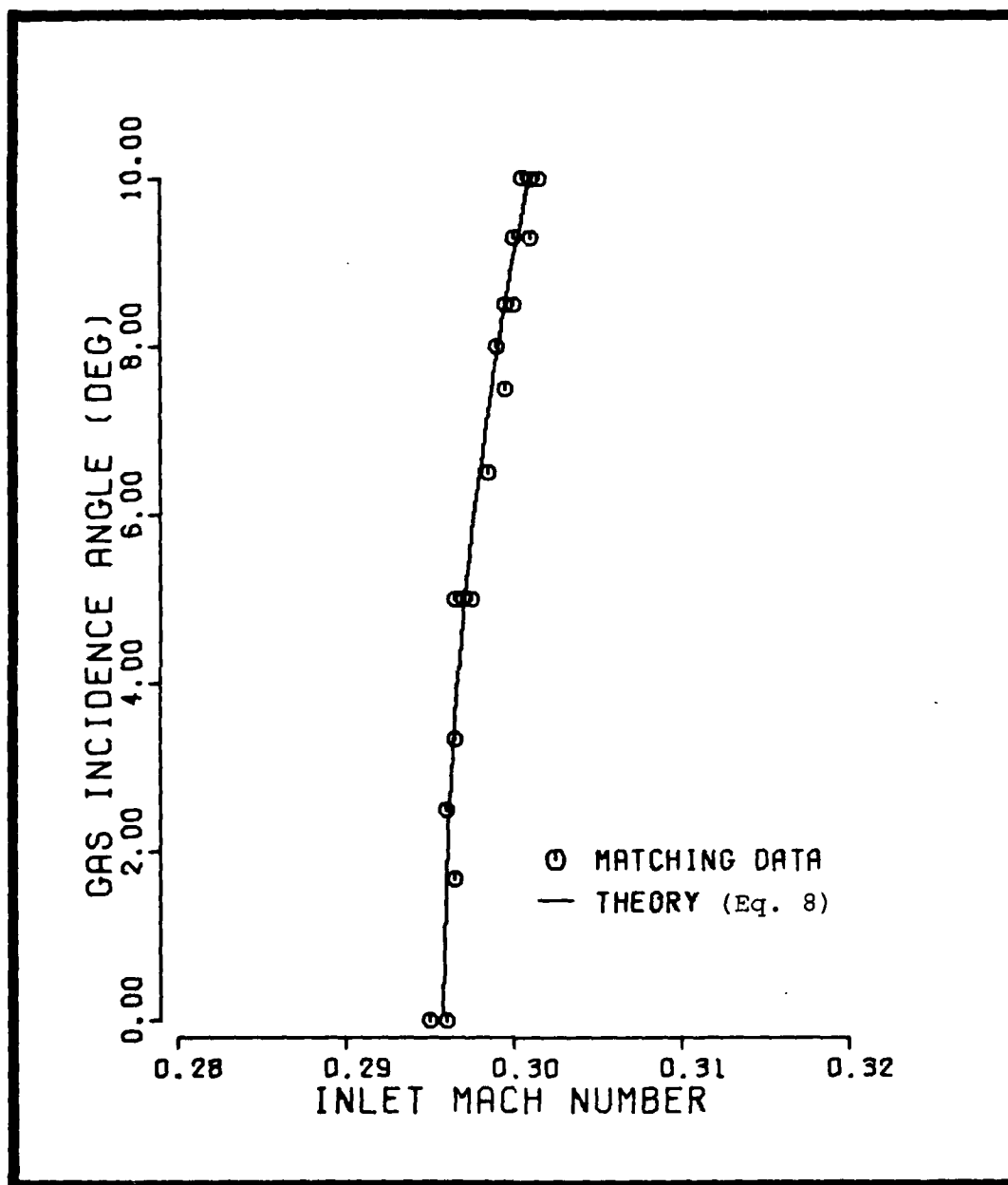
Figure 10   Case Two Inlet Velocity Profiles
Yielding Matching C_p Distributions

bution plots for a representative sampling of the ninety-one point data field.

Figures 9 and 10 were generated from a visual inspection of the entire set of pressure coefficient distributions. Distributions which match the appropriate set of experimental data are plotted as points on a β_1 versus M_1 coordinate system. The matching data collapse along an exit static pressure (P_2) curve whose value is listed in Table IV. This result is predicted by the Equation 9 functional relationship.

A line defined by Equation 8, where the right side of the equation has been evaluated by the Table IV β_2 and M_2 constraints, is superimposed upon the matching data points. The agreement between the locus of expected and calculated matching pressure distributions is excellent. Note that the influence of small gas incidence angles upon the pressure distribution is negligible, while slight Mach number changes will define totally different pressure distribution curves.

Conclusions

The results presented in the previous section satisfy all three verification criteria for the two test cases considered. In addition, the simplifying inlet velocity profile assumptions in the test facility have been substantiated. Thus, the ability of the TDS computer programs to calculate two-dimensional cascade flowfields accurately in the Heat Transfer Facility test environment has been established.

IV. Blade Design Criteria

The objective of this blade design study is to provide
the Air Force Aero Propulsion Laboratory with a updated blade
profile to be used in an "in-house" turbine cooling test
program. The final blade design must be compatible with the
static test facility in which the blades are to be tested.
The airfoil shape must also exhibit maximum aerodynamic per-
formance in the transonic flow regime specified by AFAPL/TBC.

In order to accomplish the objectives stated above,
certain criteria must be established and incorporated into
the design process. The threefold intent of this chapter is
to define the specified transonic design point, to present
the aerodynamic performance standards used for selecting
superior designs, and to document a transonic evaluation of
the existing design using the previously identified perfor-
mance standards.

Design Point Operating Conditions

The primary conditions which governed the design of the
turbine airfoil were based on the anticipated operating con-
ditions of the test facility in which the blades are to be
tested. A compilation of the design point gas properties
specified by AFAPL/TBC appears in Table V.

The total pressure and back pressure values listed in
Table V are within the operating limits of the test facility

40

Table V

Design Point Thermodynamic Boundary Conditions

Thermodynamic Quantity		Value	
Description	Symbol	Metric	English
Max Mass Flow Rate	$\dot{m}$	2.27 kgm/sec	5.00 lbm/sec
Total Temperature	T_O	1666.3 °K	3000.0 °R
Total Pressure	P_O	29.0 N/cm²	42.0 psia
Back Pressure	P_b	13.1 N/cm²	19.0 psia
Specific Heat Ratio	γ	1.26	1.26
Gas Constant	R	315.0 $\frac{m^2}{sec^2 - °K}$	1883.7 $\frac{ft^2}{sec^2 - °R}$

for a mass flow rate less than 2.27 kg_m/sec (5 lb_m/sec).
Together, the two quantities define a transonic environment
with an exit Mach number equal to 1.169.

The design point total gas temperature of 1666.3°K
(3000°R) is substantially greater than most modern turbine
inlet temperatures. However, advanced gas turbines are ex-
pected to encounter this type of temperature environment.
The AFAPL Heat Transfer Facility has a hot gas temperature
generation capability of 2500°K (4500°R) for stoichometric
hydrogen-oxidant ratios.

The mass flow rate limitation of 2.27 kg_m/sec (5 lb_m/sec)
is imposed as a constraint because this is the maximum mass
flow rate that the facility's compressors can sustain while
maintaining a total pressure level greater than 29.0 N/
cm^2 (42.0 psia). The gas constant and specific heat ratio
are derived from the hydrogen combustion reaction which pro-
duces a cascade total inlet temperature of 1666.3°K (3000°R).

Although small gas incidence angles have negligible ef-
fect on turbine cascade performance (determined in Chapter
III), a design point gas incidence angle of eight degrees was
chosen as a best estimate in lieu of firm evidence to the
contrary. When the maximum mass flow rate, along with the
other Table V thermodynamic quantities, are substituted into
Equation 1, the maximum allowable design point inlet Mach
number is found to be 0.46.

Aerodynamic Performance Standards

Transonic blade performance is usually measured experimentally because of the inability of present day analytical procedures to successfully model complicated blade trailing edge flowfields where most pressure losses occur. Streamline curvature flow calculation programs, including CASC, require simplifying shock-free and inviscid assumptions which make it impossible to compute an estimate of total pressure losses. Thus, the establishment of aerodynamic performance standards based on minimum pressure loss gives rise to a fundamental question; can the standards be applied to isentropic loss-free CASC predictions? The purpose of this section is to answer the question by presenting a generalized discussion of the theory behind the evaluation of transonic criteria that will be applied to select superior designs.

Trailing Edge Pressure Gradient. The primary function of turbine stator blade rows is to accelerate the working gas medium across a static pressure drop. For a turbine cascade where the flow is subsonic (low pressure ratios), the fluid is accelerated through a convergent flow passage as shown in Figures 2 and 6. The total pressure loss in a subsonic turbine stator row is very small. Viscous losses are of the order of five percent. There are no shock-related losses because the flow is everywhere subsonic. Finally, losses due to separation usually do not occur because the pressure gradients in an accelerating flowfield are favorable.

If the pressure ratio across a blade row is large enough to choke the flow, a sonic line will appear at the flow passage throat location. In a typical convergent turbine cascade, the throat (sonic line) is formed at the trailing edge of a blade's pressure surface and extends to the suction surface of the adjacent blade. The transonic flowfield surrounding the trailing edge of a blade in a convergent turbine stator row is depicted in Figure 11.

At the trailing edge of the Figure 11 blades, the flow over the suction surface is supersonic ($M > 1$). The flow over the pressure surface is subsonic ($M < 1$) until a sonic condition is realized at the trailing edge. Thus, a region of relatively high pressure exists on the lower surface, while a region of low pressure is present on the upper surface. Hence, the existence of an extremely large pressure gradient at the trailing edge of the blades would seem to be indicated.

According to Amana, Demuren and Louis[28], this condition is reconciled by an expansion of the flow around the pressure surface trailing edge and then a subsequent compression as the flow turns into the downstream wake (see Figure 11). This phenomena occurs in order to satisfy the Kutta condition of zero pressure gradient at the trailing edge. The compression shock wave formed during this process originates from the trailing edge wake region and then impinges on the suction surface of the adjacent blade. The boundary layer-shock interation on the suction surface of the blade usually
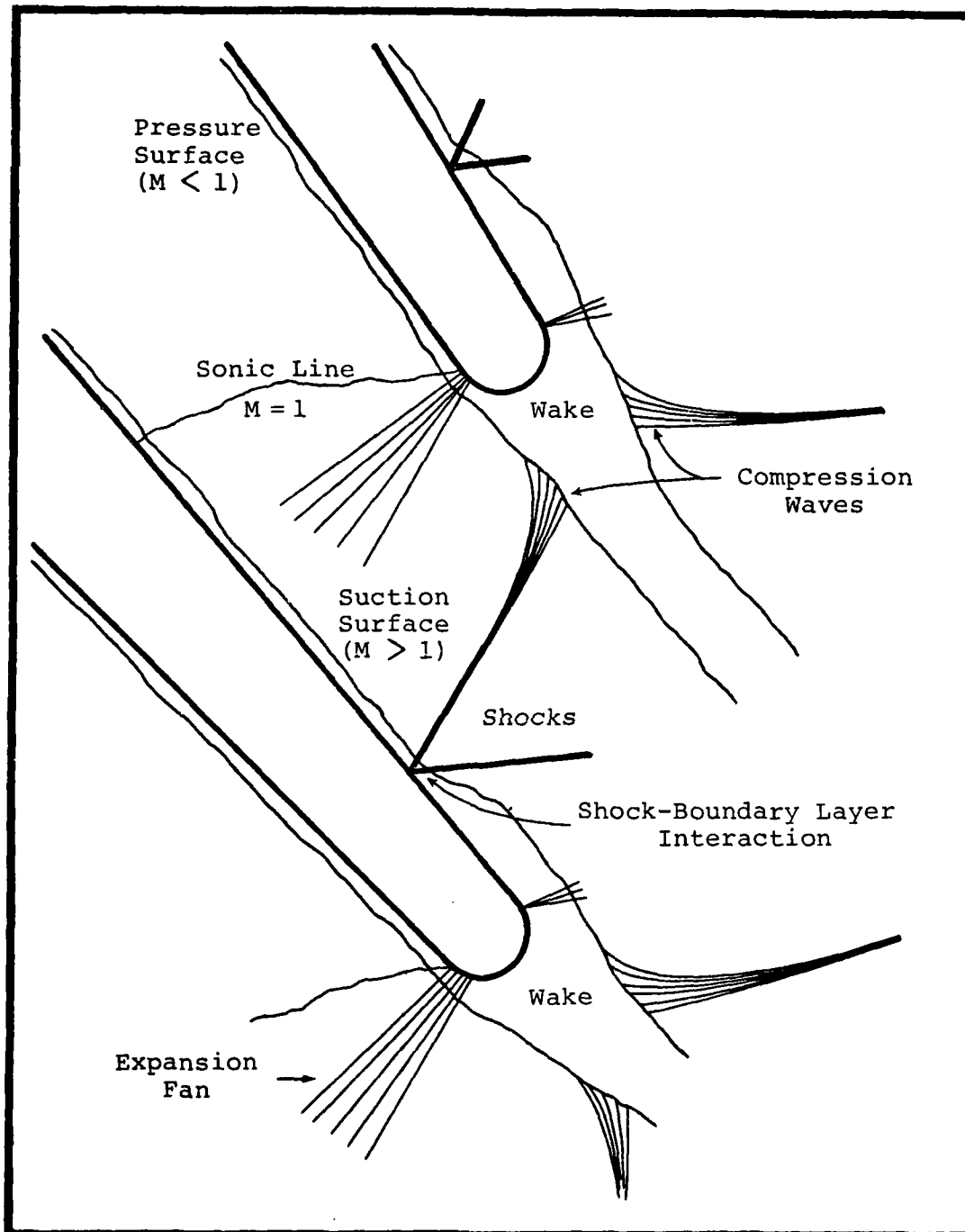
Figure 11   Trailing Edge Transonic Flowfield

45

results in flow separation or a change in the boundary layer
thickness. This, in turn, changes the suction surface trail-
ing edge boundary conditions and thus, fluctuating (time-
dependent) trailing edge pressure gradients are set up. This
is the loss mechanism which substantially reduces the perfor-
mance of convergent cascades under transonic pressure ratios.
Amana et al[28] and Heinemann[29] have reported this phenomenon
in literature and they also present corroborating photographic
evidence.

Although the CASC program is unable to predict the total
pressure losses which accompany these complicated transonic
flow patterns, inviscid, shock-free theory can yield a rough
estimate of the pressure gradient that must be reconciled
at the blade trailing edge due to poor design. Because the
pressure gradient is primarily caused by isentropic flow over-
expansion on the suction surface and underexpansion on the
pressure surface, the CASC estimate of pressure gradient mag-
nitude is an indication of the magnitude of the resultant
flow turning, shock strength, and total pressure losses that
must occur to satisfy the Kutta condition. Therefore, the
first aerodynamic performance criterion requires that the
predicted trailing edge pressure gradient is zero.

$$\left. \frac{dP}{dY} \right)_{T.E.} = 0 \qquad (12)$$

In order to satisfy the criterion represented by equa-
tion 12, the flow on either surface must be expanded to a

46

single static pressure, i.e., the blade row back pressure. Thus, the flow passage through the stator row will necessarily be convergent-divergent in nature for transonic pressure ratios.

Suction Surface Diffusion. Any number of blade contours can be designed to satisfy the first performance criterion at the design point described in the first section of this report. Thus, a second performance criterion that can be applied to quantitatively distinguish between isentropic CASC results is required.

In the absence of experimental data, it is common analytical design practice to predict aerodynamic performance by estimating the amount of diffusion which occurs on the surface of a given airfoil design. Prince[15], McDonald[17], Szanca and Schum[30] address the topic of turbine airfoil diffusion and concur that diffusion control is a significant transonic blade design performance criterion.

Diffusion or flow deceleration causes the formation of adverse pressure gradients which thickens the boundary layer on the surface of the blade. Under rapid or long term decelerations, the flow separates completely. The possibility of a shock wave interaction with the boundary layer of a diffusing flow will almost certainly cause a flow separation. Thus, an inviscid prediction of the amount of diffusion which occurs on the blade suction surface is an indication of the

tendency for the flow to separate and thereby significantly increase pressure losses.

The second performance criterion that will be applied to the various blade designs is summarized in the following statement: the airfoil shape yielding the least amount of flow overexpansion and subsequent diffusion is the better design. This flow overexpansion standard is applied to proposed designs through use of the following equation;

$$\Delta P_{overexpansion} = P_{s_{exit}} - P_{s_{minimum}} \tag{13}$$

Evaluation of Existing Design

The present design was evaluated in terms of the aerodynamic performance criteria developed in the previous section for the transonic design point. Highlighting the deficiencies of the existing airfoil in this manner demonstrates the need for design of a transonically well-behaved blade shape.

Since there is no transonic experimental data for the existing turbine airfoil, the CASC flow analysis was used to obtain predictions of the flowfield surrounding the existing airfoil at the transonic design point. In this case, the CASC input $BB namelist is exactly the same as those depicted in Appendix A, except that the Table V thermodynamic data are substituted in lieu of the verification operating conditions. For choked, transonic flow cases, CASC iterates

48

upon the upstream inlet Mach number (mass flow rate), while holding the back pressure constant. CASC also returns exit static pressure for either blade surface that satisfy the isentropic equations and boundary conditions. These calculated exit pressures may or may not equal each other, or the back pressure depending on the design.

Figure 12 is a plot of the pressure distribution resulting from the evaluation investigation. Regions of rapid acceleration can be observed to occur on both the pressure and suction surfaces. Note that the flow over the suction surface overexpands to a very high Mach number (low pressure) immediately behind the sonic throat at 51 percent of axial chord. After this initial overexpansion, the velocity (pressures) on the suction remain relatively constant. Because the flow on the pressure surface does not exceed a Mach number greater than one, a large pressure gradient at the trailing edge is 6.649 N/cm^2 (9.63 psi). The amount of overexpansion which occurs on the upper surface is determined to be 4.197 N/cm^2 (6.08 psi).

The current blade behaves poorly because too much turning occurs on the suction surface after the throat location. After sonic conditions are reached, convex surface curvature causes the remaining suction surface to act as a supersonic diverging nozzle. By the time the turning becomes small, a high velocity has been attained and must be diffused, separated or shocked-down to satisfy the exit conditions and
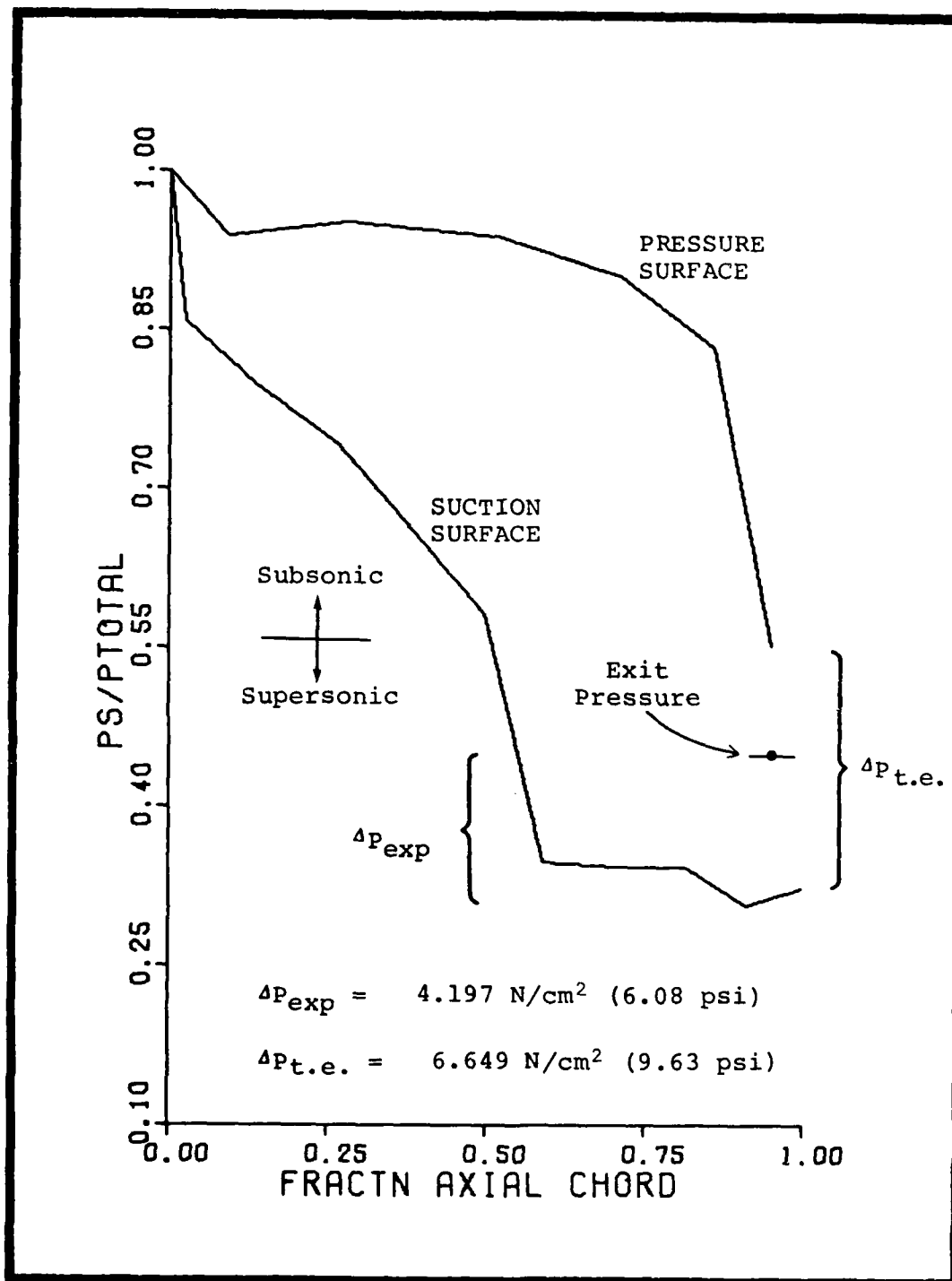
Figure 12 CASC Prediction of the Transonic Design Point C_p Distribution for the Existing Blade

trailing edge Kutta boundary requirements. Finally, lack of
a convergent-divergent flow passage prevents the flow on the
pressure surface from undergoing supersonic expansion to reach
the exit static pressure level.

V. Parametric Design Study

The geometry of the existing airfoil typifies most sub-
sonic turbine cascades. A turbine airfoil that is designed
to operate at subsonic pressure ratios is easily identified
by the following geometric characteristics; a convergent flow
passage, significant suction surface curvature after the throat
location, a maximum blade thickness position at 30-50 percent
of axial chord, and a moderate stagger angle. The net effect
of these blade shape trends is a turbine cascade that is to-
tally unsuited for transonic flow environments.

During the course of this design study, the observation
was made that a well designed transonic cascade exhibits two
distinguishing geometric features. First, in order to expand
the flow on the pressure surface to the proper exit pressure
level, a convergent-divergent flow passage is a necessary hall-
mark of any transonic turbine cascade. Second, practically
all of the suction surface flow turning must occur ahead of
the throat location to prevent supersonic overexpansion and
subsequent diffusion on that surface.

Consequently, the twofold objective of this parametric
design study is to identify the geometric parameters that
have a major influence on the two features discussed in the
previous paragraph, and then, to determine the parameter
combination which yields the maximum amount of aerodynamic
performance at the design point operating conditions.

Parametric Design Approach

Two modes of data input to the BLDDES module were discussed in Chapter II. The parametric option requires utilization of a BLDDES subroutine called BSGEN, which analytically generates blade surface coordinate arrays using parametric input in lieu of digitized data. The blade section generation (BSGEN) calculation procedure involves the computation of a section meanline derived from a fourth-order polynomial and a thickness distribution derived from the conformal transformation of a fifth-order polynomial. The coefficients of these polynomials are governed by the blade shape input parameters.

When the resulting standardized airfoil definitions are evaluated by the aerodynamic analysis module, CASC, a pressure distribution prediction for the original set of blade shape input parameters is obtained. Four input parameters were found to have a substantial effect upon the airfoil pressure distribution predictions. Thus, the design study was limited to variations of these four input parameters. The influence of each input parameter upon overall aerodynamic performance was determined by generating a total of 72 different blade profiles, and then, evaluating the associated pressure distribution predictions.

The remaining required BLDDES input parameters were held constant throughout the parametric variation study. These fixed parameters generally tended to relate to the physical dimensions of a given airfoil configuration rather than the blade profile itself. The assigned values chosen for the

fixed parameters are physically compatible with the static
test facility.

Definition of Blade Shape Parameters

The primary intent of this section is to identify and
adequately describe both the fixed and varied blade shape
input parameters. A complete description of the parametric
input variables and the BSGEN calculation procedure appears
in AFAPL-TR-78-92[24].

Fixed Parameters. Table VI contains a listing of the
parameters that were assigned fixed values during the para-
metric variation study. A schematic of the BSGEN coordinate
system in which these parameters are employed is presented
in Figure 13. The following paragraphs provide a brief
description of the parameters tabulated in Table VI.

The velocity vector diagram information that is consis-
tent with the test facility geometry, is represented by the
first two Table VI entries. BETA1 and BETA2 are the specified
gas inlet and gas exit angles respectively. Together, the
two quantities fix the amount of flow turning to be accom-
plished in the cascade passage.

Throat size parameter, CF, influences the size of the
flow passage geometric throat or the minimum clearance be-
tween blades. The throat is calculated in the following
manner;

$$\text{THROAT} = \text{CF} * \text{S} * \cos(\text{BETA2}) \tag{14}$$

Table VI

Fixed Blade Shape Parameters

Parameter	Description	Fixed Value
BETA1	gas inlet angle	8.0°
BETA2	gas exit angle	62.0°
CF	throat size parameter	0.9
C3	meanline curvature control factor	0.1
DELTA1	angle of attack	0.0°
ISTK	stacking point indicator	1
ITMODE	trailing edge shape indicator	1
IVANE	blade-vane indicator	0
NBLDS	number of blades	100
RLE	leading edge section radius	60.6 cm (23.9 in)
RREF	reference radius	60.6 cm (23.9 in)
RTE	trailing edge section radius	60.6 cm (23.9 in)
TE	trailing edge thickness	0.127 cm (0.050 in)
TMAXX	maximum section thickness	0.7798 cm (0.307 in)
ZLE	leading edge axial position	0.0 cm (0.0 in)
ZTE	trailing edge axial position	3.893 cm (1.5327 in)

55

Table VII

Varied Blade Shape Parameters

Parameter	Description
SF	stagger factor
C1	maximum section thickness location (fraction of axial chord)
C2	trailing edge taper factor
TI	leading edge bluntness factor
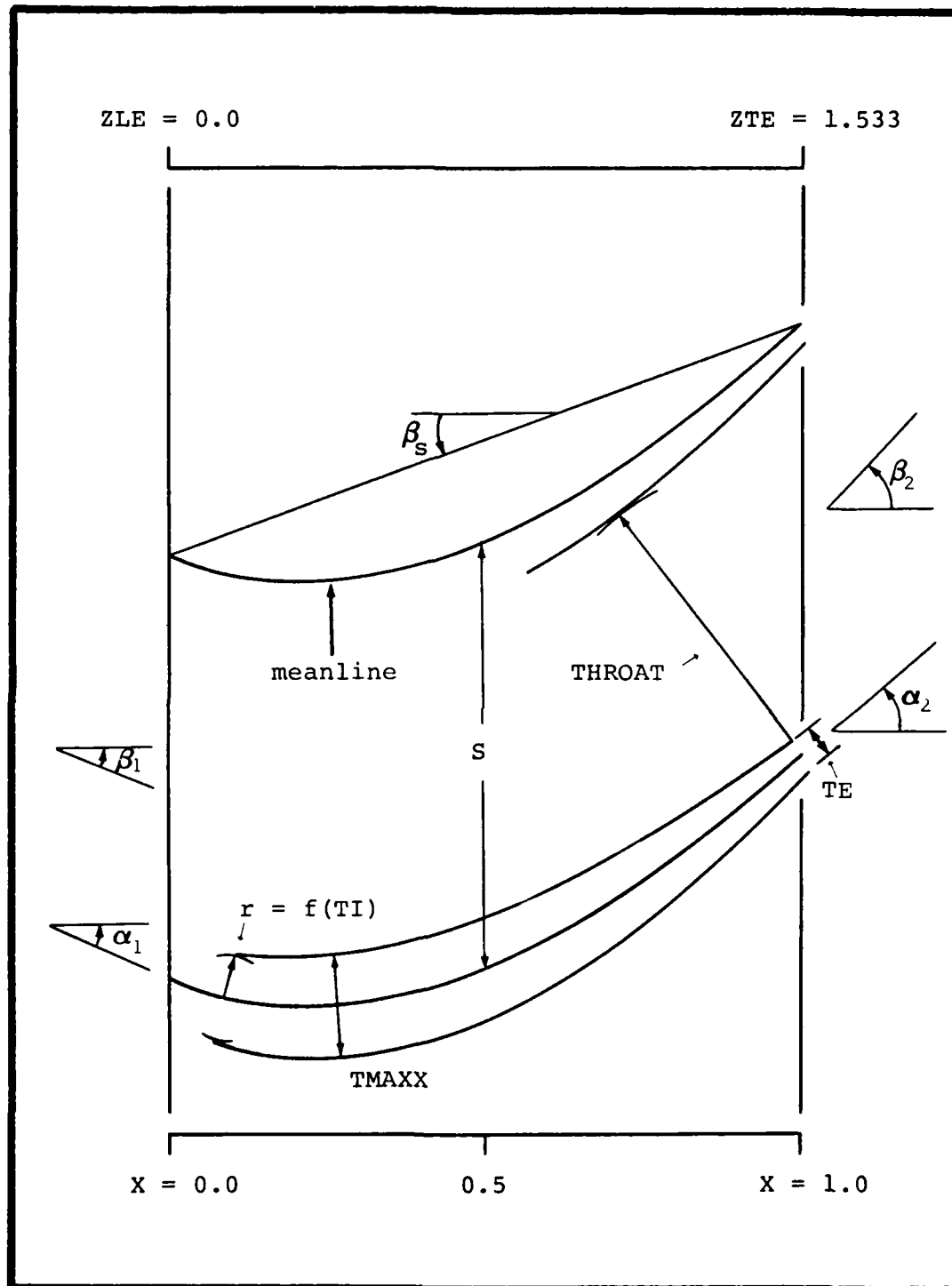
Figure 13   Blade Generator Coordinate System

57

where S is the blade spacing (see Figure 13). Initially, the blade exit angle, α_2, is set equal to the gas exit angle, β_2. If the throat (minimum blade clearance) calculated by BSGEN is not equal to the desired throat represented by equation 14, a new blade exit angle is computed. The value chosen for CF insures that the mass flow rate through the test facility will not exceed 2.27 kg_m/sec (5 lb_m/sec).

Although the parameter C3 controls the intermediate curvature of the section meanline, this factor has a minor effect on the overall blade shape when compared to the effects of the varied parameters. The Table VI value for C3 is favorably consistent with decreasing the suction surface unguided turning.

The angle of attack to the blades in the cascade is specified by DELTA1. Since an angle of attack was not desired, DELTA1 was set equal to zero. Because DELTA1 is the angular difference between the tangent line to the section meanline at the leading edge and the inlet velocity vector, the following relationship exists when DELAT1 is zero;

$$\alpha_1 = \beta_1 \tag{15}$$

where α_1 and β_1 are the blade inlet and gas inlet angles respectively.

ISTK, ITMODE, and IVANE are minor blade shape indicators. These quantities were defined in Chapter III and the fixed values listed in Table VI are consistent with the previous

discussion. NBLDS, RLE, RREF, and RTE have been previously
defined in Chapter III. The number of blades and the radii
lengths that were assigned, define a cylindrical blade section
with a cascade blade spacing, S, of 3.894 cm (1.533 in). The
cylindrical section is almost rectalinear because of the large
radial values chosen. ZLE and ZTE define the axial width of
the blades. Note that the blade spacing and axial width for
the proposed transonic designs is the same as that for the
existing cascade.

Fifty mils is the minimum tolerable trailing edge thick-
ness required for advanced turbine blading with trailing edge
coolant holes. The maximum section thickness for typical
transonic turbine stators is usually 20 percent of the axial
chord length. This general rule-of-thumb was applied to fix
TMAXX.

Varied Parameters. The four blade shape input parameters
that were varied are listed in Table VII. The input parameter
SF, stagger factor, indirectly controls the stagger angle, β_s,
in the following way;

$$SF = \frac{\tan \beta_2 - \tan \beta_s}{\tan \beta_s - \tan \beta_1} \tag{16}$$

Hence, the relationship between stagger factor and stagger
angle is an inverse function, i.e., increasing SF decreases
β_s. The stagger angle of a turbine cascade is an important
transonic design parameter. For a given amount of flow

turning (velocity vector diagram), large stagger angles tend to reduce surface curvature in the aft portion of the blades. Blades with high stagger angles are characterized by long, straight tails with relatively no suction surface curvature after the throat location. The primary consequence of increasing stagger angle is to shift most of the flow turning to the foreward portion of the blades, thereby, enhancing transonic performance. Therefore, the stagger factor was treated as a variable design parameter.

The input parameter C1, the non-dimensional axial location of maximum section thickness, was also treated as a design parameter. In order to promote higher stagger angles and substantial flow turning ahead of the throat location, most of the blade mass (i.e., maximum section thickness), must be concentrated towards the leading edge of the blade. The maximum section thickness location along with stagger angle primarily determines whether or not the flow passage will have a convergent-divergent nature.

Trailing edge taper factor, C2, controls the trailing edge included angle, θ, as defined by the following equation;

$$\theta = 2\tan^{-1}\left[\sqrt{C2}\left(\frac{TMAXX-TE}{ZTE - ZLE}\right)\cos\beta_2\right] \qquad (17)$$

The trailing edge taper factor was considered to be a significant design parameter because trailing edge taper heavily influences the throat location and the ratio of throat to exit area.

Finally, the leading edge bluntness factor, TI, is related to the leading edge radius of curvature as shown in Figure 13. Bluntness increases with increasing TI values. The flowfield behavior over the midchord portion of the blades is a strong function of the leading edge bluntness. Although the parameter TI is somewhat dependent on the maximum section thickness magnitude and location, it has been included as an independent design parameter.

Transonic Performance Maximization

Procedure. The four blade shape input parameters (Cl, C2, SF, TI) were systematically varied to generate seventy-two different blade design versions for analysis by the CASC module. Then, the resultant pressure distributions were evaluated in terms of the two aerodynamic performance standards that were developed in Chapter IV.

The specific approach that was used to maximize the relationships between the input parameters and the aerodynamic performance standards was a two phased procedure. Under phase one, the input parameter combinations which yielded designs with trailing edge pressure gradients, off design exit static pressures, etc., were identified and eliminated from consideration. This objective was achieved for four separate values of maximum section thickness location (Cl), by varying the other three input parameters until a unique design was found that satisfied the first performance criterion at the design point exit pressure. The second phase

61

of the performance maximization process was concerned with
selecting one of the four design versions from phase one.
In phase two, determination of the superior design was based
upon the pressure distribution prediction which exhibited the
least amount of suction surface diffusion.

The final design selection is presented in the last sec-
tion of this chapter. Description of the input parameter/
aerodynamic performance relationships that were discovered
during the parametric variation study is the subject of the
next two subsections.

Elimination of Trailing Edge Pressure Gradients. For a
given value of maximum section thickness location (C1), the
other three variable blade shape input parameters (SF, C2, TI)
were individually varied to determine whether or not any
characteristic effect upon pressure distribution shape could
be attributed to a specific input parameter. Although each
of the three input parameters did not exhibit completely
uncoupled influences upon the predicted pressure distributions,
well defined aerodynamic trends were related to each input
parameter.

The stagger factor, SF, primarily determines the mag-
nitude of the pressure gradient across the blade's trailing
edge. If the stagger factor is too large (i.e., the stagger
angle is too small) for a given set of operating conditions,
the predicted pressure distribution from the resulting blade
profile will feature a pressure surface that is underexpanded
and a suction surface that is overexpanded. Thus, an increase

62

in the stagger factor tends to decrease the convergent-divergent nature of the flow passage. A limiting case is encountered when the stagger factor becomes great enough to cause the flow passage to become entirely convergent. The opposite extreme condition is a stagger factor that is too small, which yields a design that has an overexpanded pressure surface and an underexpanded suction surface. Appendix F contains various selected design versions that illustrate proper and improper combinations of these input blade shape parameters. Design version two is an example of a blade contour with not enough stagger angle, while design version eighteen typifies the case with too much stagger angle.

Once the appropriate stagger factor is found such that the trailing edge pressure gradient is eliminated, the input parameter C2 is varied to adjust the trailing edge taper ratio. Although, the trailing edge pressure gradient may be zero, the cascade exit static pressure to which both surfaces are expanded may not necessarily equal the design back pressure. Design version twelve (Appendix F) is an example of a design case where the trailing edge pressure gradient is zero but the exit static pressure is considerably lower than the design back pressure. Decreasing the value of the taper factor has the effect of decreasing the trailing edge included angle (see Equation 17). The ratio of the flow passage throat to exit area is thereby decreased and the exit static pressure of an overexpanded flow is raised. Hence, for a given maximum thickness location and stagger factor, proper positioning

of the throat location with reference to the flow passage exit plane is accomplished by varying the taper factor, C2.

The last variable input parameter that was incorporated into the design parameter investigation, is the leading edge bluntness factor, TI. The combination of stagger factor and taper factor that yields a design with zero trailing edge pressure gradient for a particular exit static pressure is still not a unique combination until the parameter, TI is introduced. The characteristic effect on predicted pressure distribution shape that is associated with leading edge bluntness is midchord overexpansion and recompression phenomena. The predicted pressure distribution for design version fourteen (Appendix F) shows jagged peaks and troughs that are commensurate with unstable flow accelerations and decelerations on the suction surface. A larger amount of leading edge bluntness alleviates this problem.

Versions fifty-two, fifty-nine, sixty-five, and seventy-two are the design versions that exhibited zero trailing edge pressure gradient at the design exit static pressure with no significant midchord overexpansions and recompressions. These four versions respectively correspond to decreasing values of maximum section thickness location.

Table VIII contains a complete listing of the variable input parameter combinations used to generate these design versions. Figures 14, 15 and 16 are plots of SF, C2 and TI versus the maximum section thickness location, C1, for the

64

Table VIII

Varied Input Parameter Combinations

Yielding Maximum Aerodynamic Performance Designs

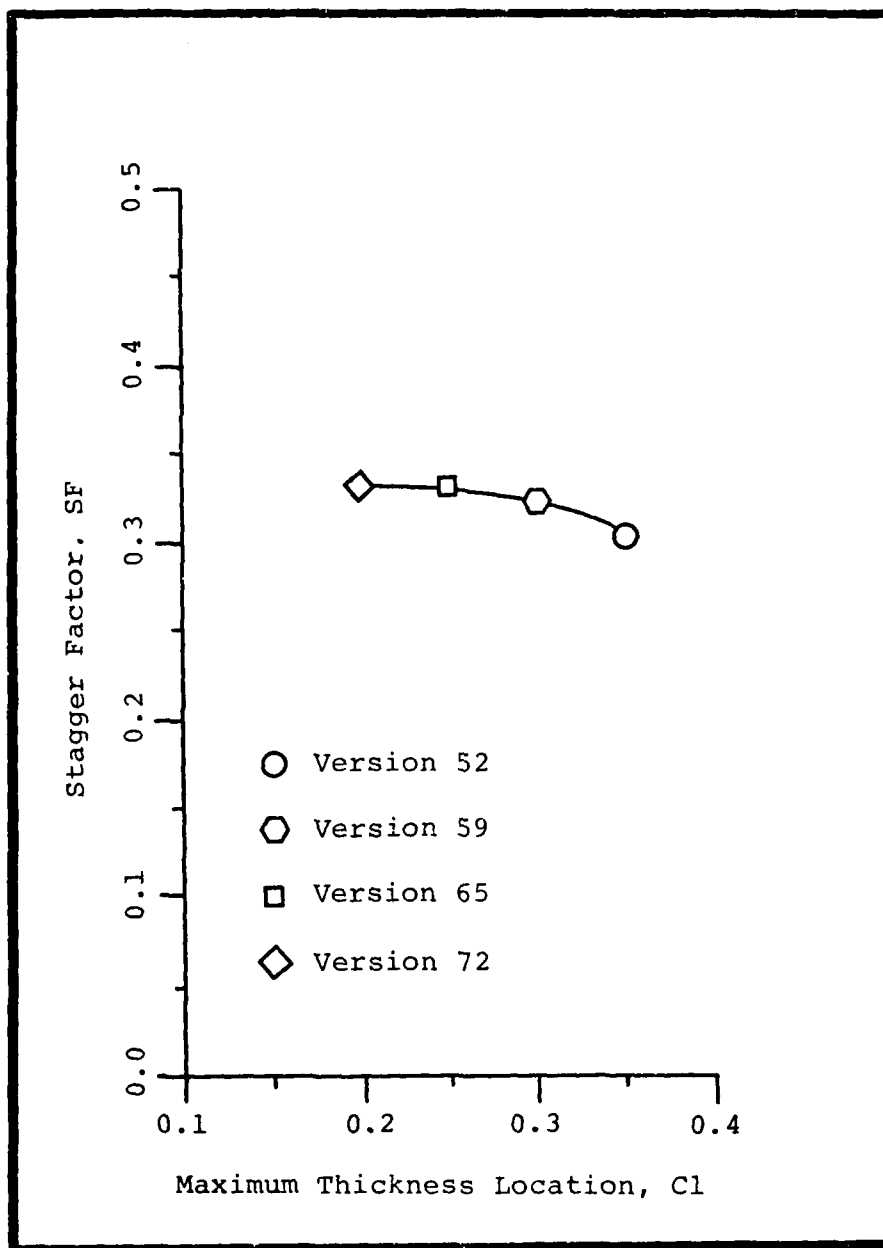| Design Version	C1	SF	C2	TI
52	0.35	0.309	0.950	0.6
59	0.30	0.3234	0.870	0.9
65	0.25	0.335	0.757	1.2
72	0.20	0.3368	0.600	1.65

Figure 14   Stagger Factor versus Location
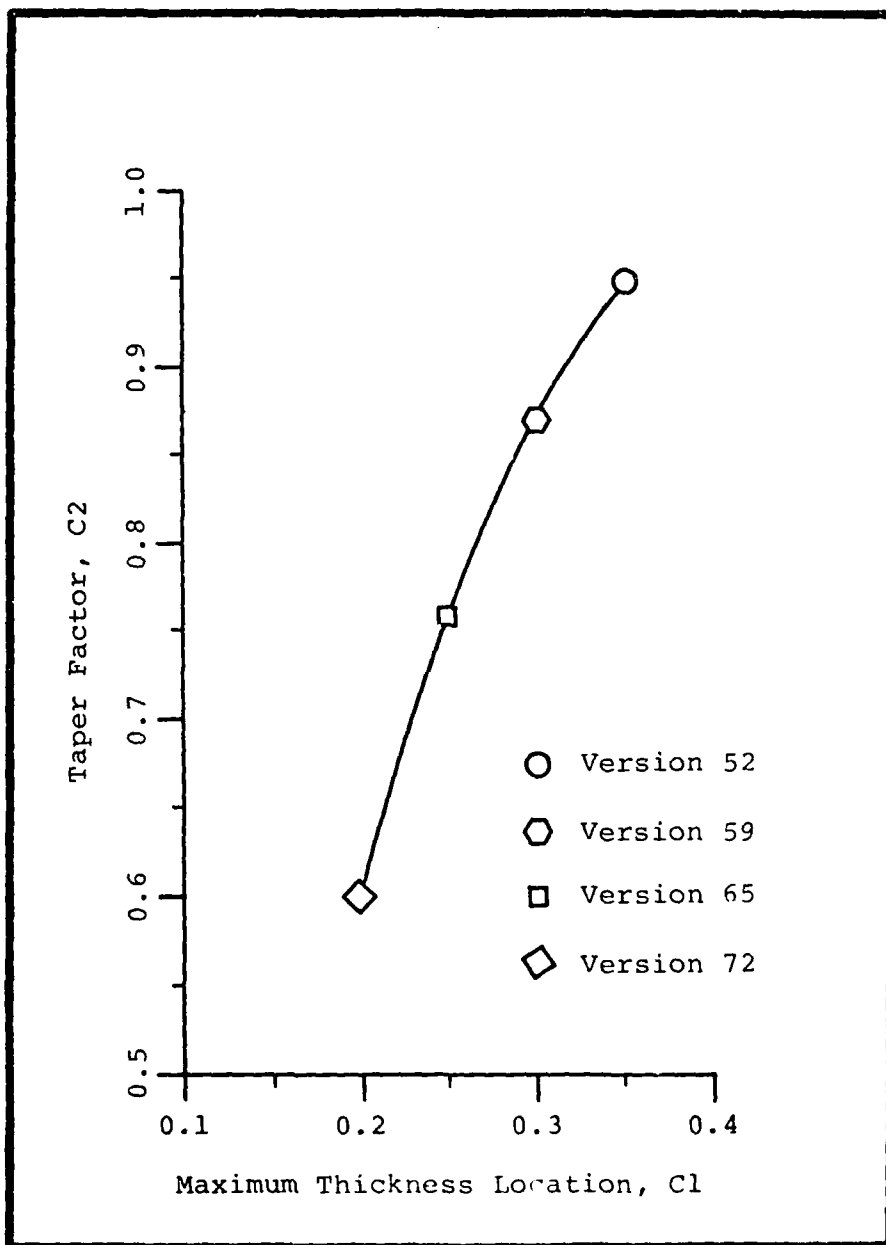of Maximum Section Thickness

Figure 15   Taper Factor versus Location
of Maximum Section Thickness

67
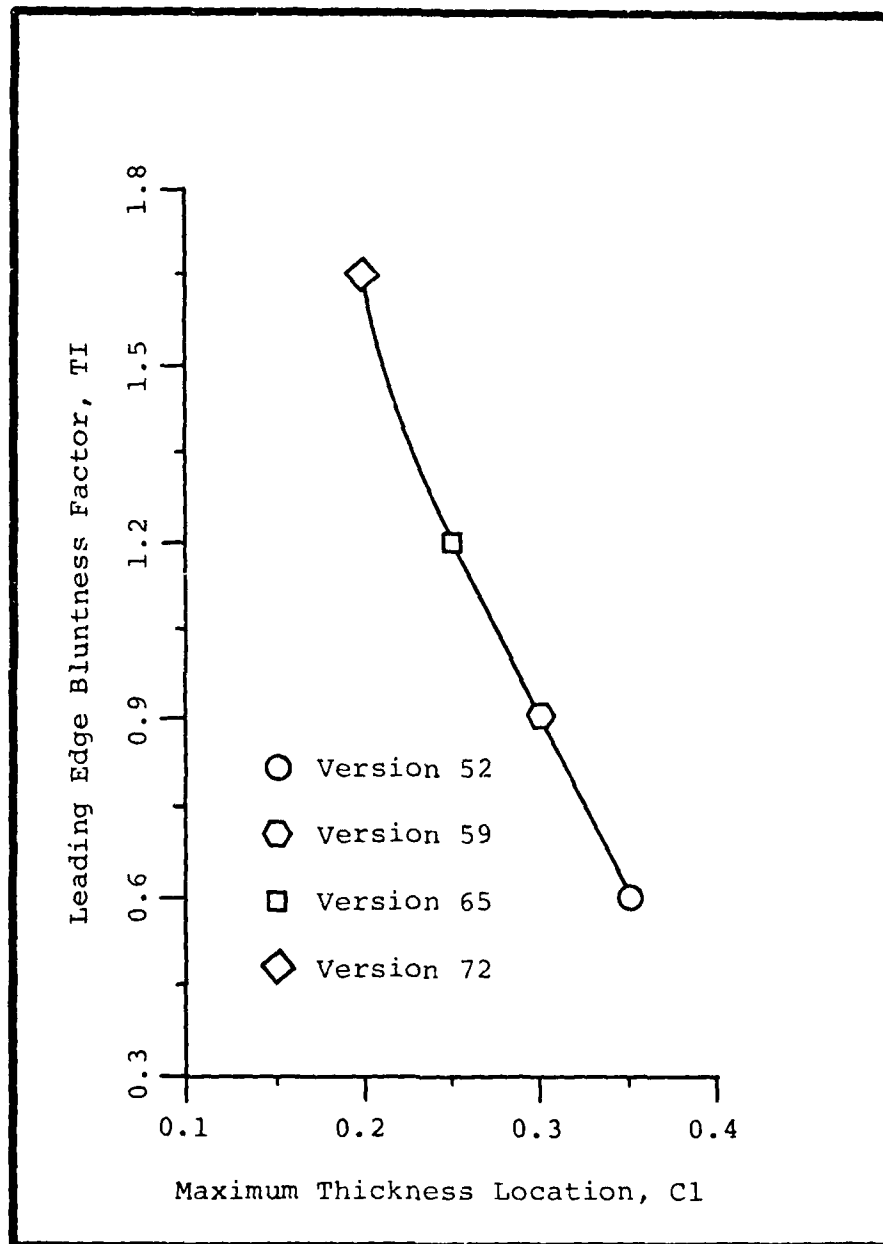
Figure 16   L.E. Bluntness Factor versus Location
of Maximum Section Thickness

four unique design versions which satisfied the first aero-
dynamic performance standard. The parametric relationships
expressed in these figures define the locus of designs which
yield maximum aerodynamic performance as a function of max-
imum section thickness location. Version seventy-two was
selected as the best design and therefore, its blade contour,
coordinates and predicted pressure distribution appear in
the last section of this chapter. The remaining versions
are presented in Appendix F.

Minimizing Suction Surface Diffusion. The design ver-
sions listed in Table VIII are the superior aerodynamic blade
contours for each respective maximum section thickness lo-
cation. Selection of the best aerodynamic profile is deter-
mined from suction surface diffusion considerations. Dif-
fusion data for each of the designs is tabulated in Table
IX and plotted in Figure 17.

Application of the second performance criterion to the
diffusion data yields version seventy-two as the best overall
aerodynamic blade design. Although the Figure 17 diffusion
trend indicates that better aerodynamic designs may exist
at lower maximum section thickness locations, design versions
with maximum section thickness location ahead of the 20 per-
cent axial chord position were not considered due to practical
mechanical and thermal limits.

Shifting the maximum section thickness location foreward
while maintaining a maximum aerodynamic performance profile
tends to increase mechanical and thermal stresses. The

69

Table IX

Diffusion Data

for Maximum Aerodynamic Performance Designs

Design Version	P_{smin}		Axial Location (percent)	ΔP_{diff}	
	N/cm^2	psia		N/cm^2	psi
52	7.375	13.574	71.6	3.765	5.426
59	9.659	13.985	71.3	3.472	5.015
65	10.022	14.499	71.1	3.109	4.501
72	10.395	15.041	70.8	2.736	3.959
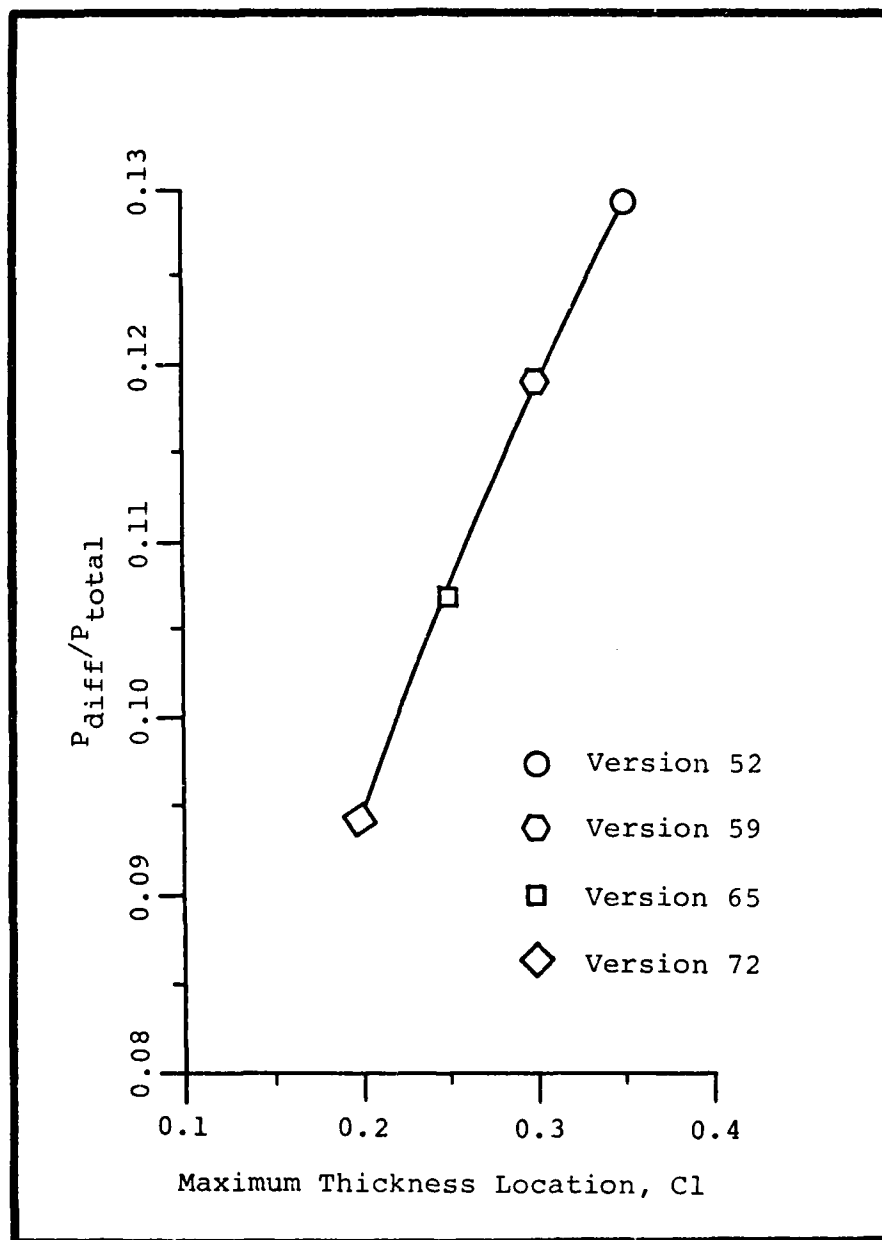
Figure 17   Normalized Diffusion versus Location
of Maximum Section Thickness

71

effective *crossectional* area for interior cooling systems and structural integrity continuously reduces with decreasing Cl values. Not only does the overall crossectional area become smaller, but the area distribution within the profile changes unfavorably, i.e., the area in the front portion of the blade increases while the area in the already thin aft portion decreases even further.

Because thermal and mechanical analyses were not included within the scope of this study, an arbritrary thermal-mechanical limit was imposed upon the foreward movement of the maximum section thickness position. The Figure 14, 15, and 16 relationships can be used to generate new designs should a thermal-mechanical analysis establish that this arbitrary limit is not sufficiently restrictive.

Final Design

On the basis of the preceeding analysis, the blade contour which yielded the maximum amount of aerodynamic performance is design version seventy-two. A scaled drawing of the blade coordinates, a schematic of the cascade formed by the final blade profile, and the predicted pressure distribution of the new transonic design appears in Figures 18, 19, and 20. The blade section profile coordinates are given in Table X. These coordinates are tabulated with respect to an origin located at the leading edge highlight point, and are normalized as a fraction of the axial width, 3.894 cm (1.533 in).

Suction
Surface

+

center of gravity

Pressure
Surface

Scale 2.35:1
AXW 3.894 cm (1.533 in)
Chord 6.134 cm (2.415 in)
Stagger 48.77°
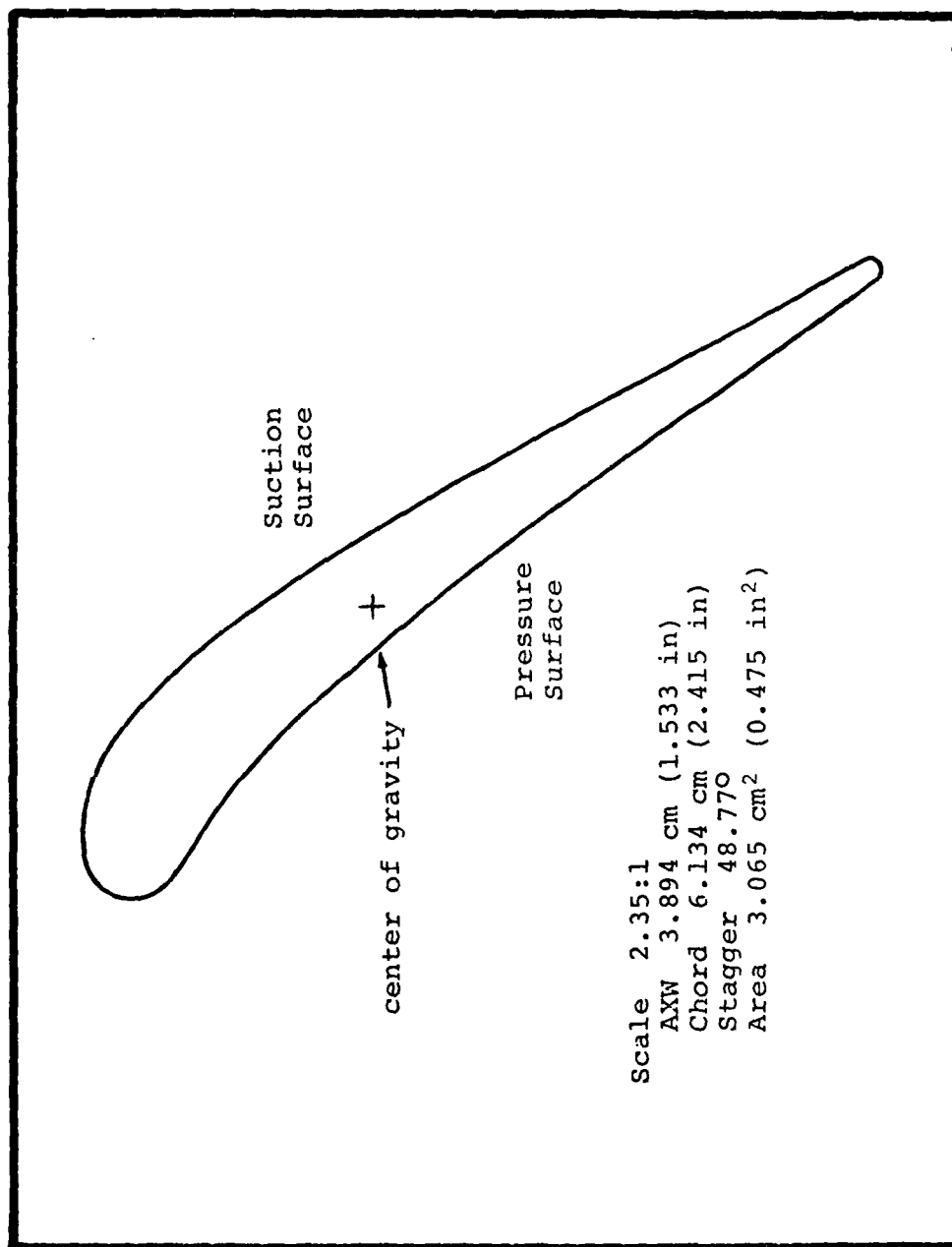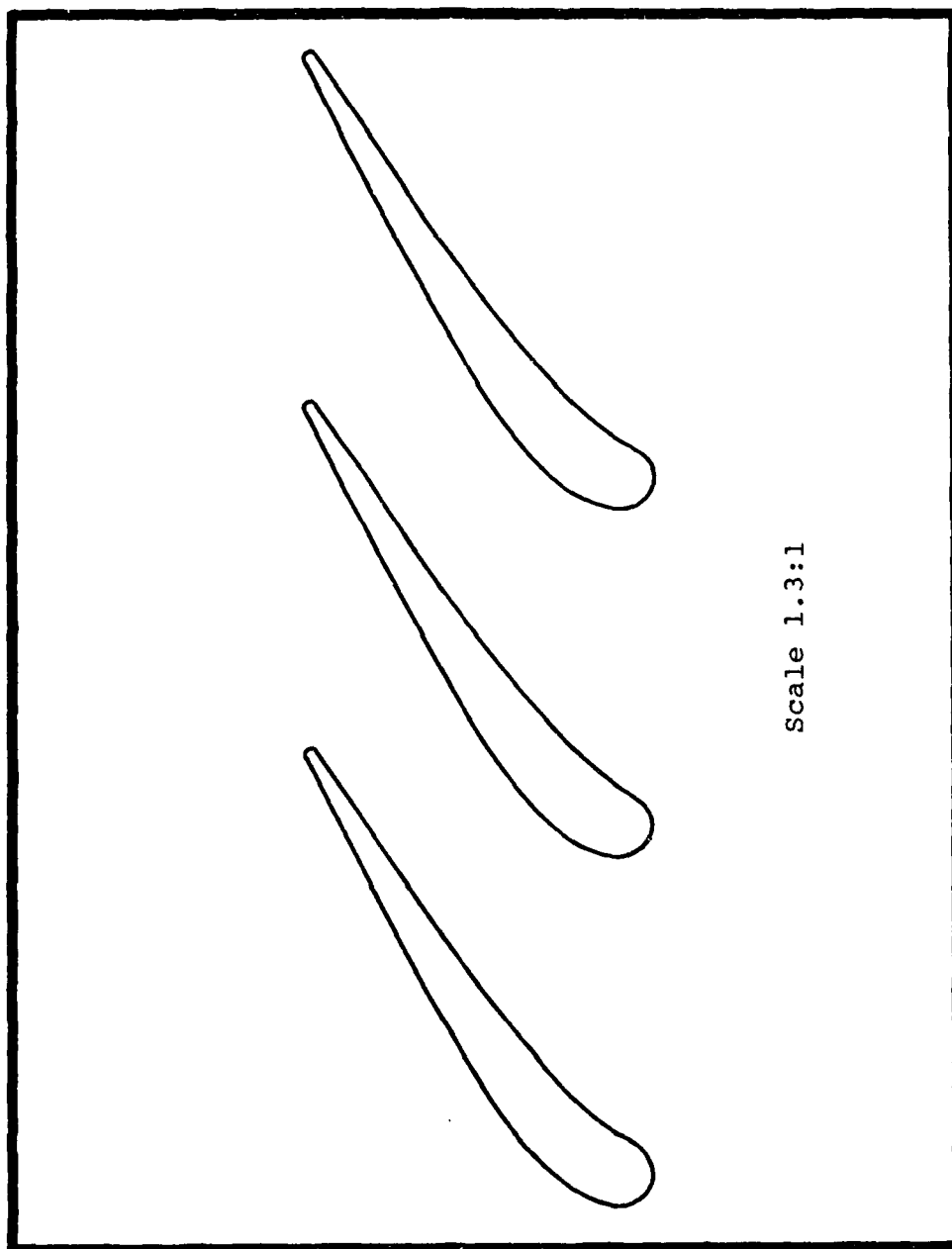Area 3.065 cm² (0.475 in²)

Figure 18 Final Transonic Turbine Stator Design

73

Scale 1.3:1

Figure 19 Final Transonic Turbine Cascade
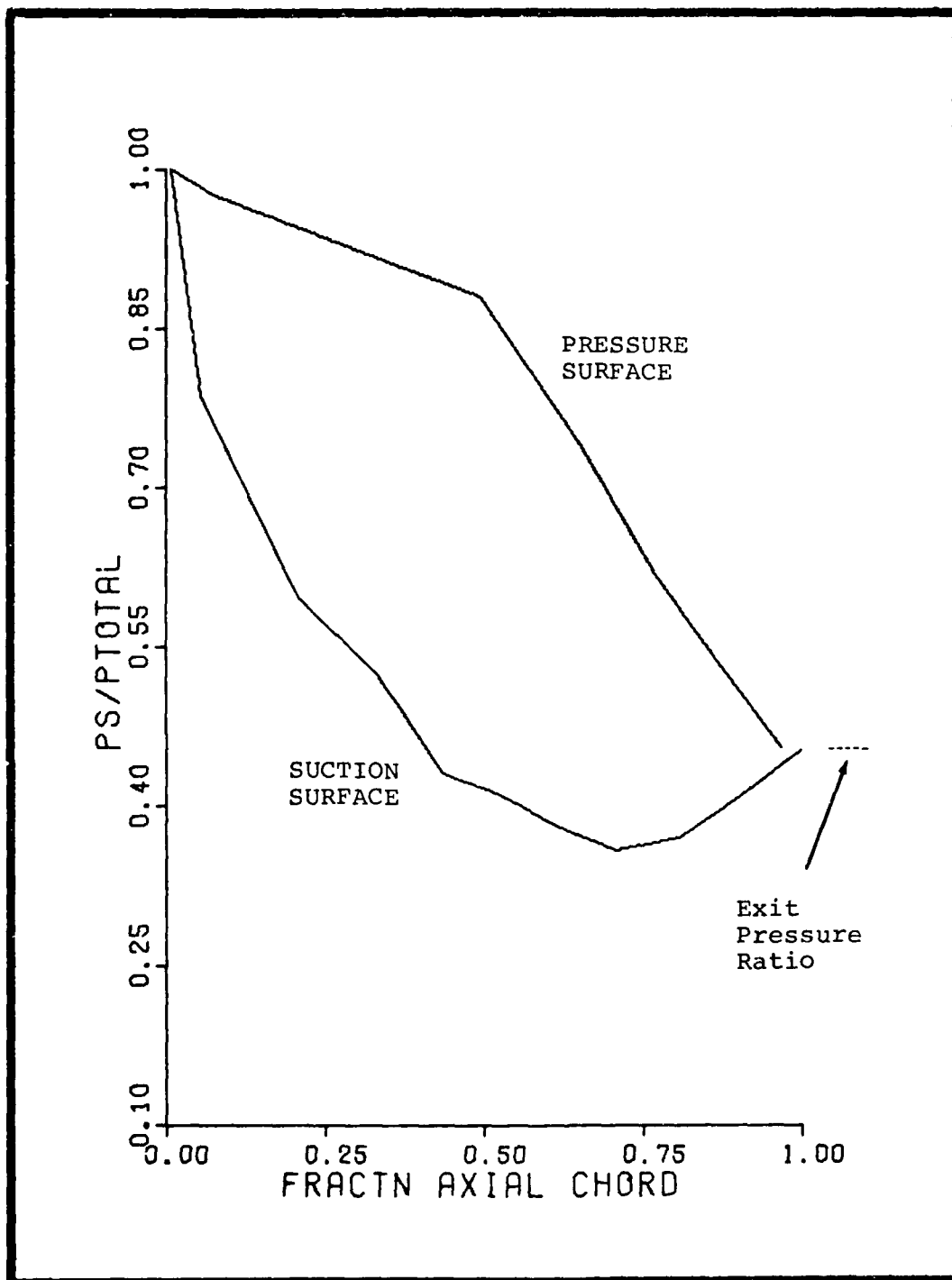
Figure 20   Predicted C_p Distribution of the Final
Transonic Turbine Stator Design

Table X

Final Transonic Turbine Airfoil Coordinates

	Suction Surface		Pressure Surface
XU	YU	XL	YL
.00254794	.0126342	.00254794	.0126342
.00449475	.0185607	.00114627	.00655564
.00699983	.0243537	.00029135	.00030234
.0100907	.0300264	.00000000	-.00615117
.0246569	.0475173	.00341009	-.0286552
.0482701	.0630423	.0155778	-.0541594
.0697609	.0776025	.0548640	-.0856713
.124253	.0780460	.0777952	-.102742
.177667	.0605864	.101686	-.116643
.210417	.0468422	.109689	-.123935
.258595	.0161234	.139988	-.145285
.303582	-.0209306	.173479	-.171138
.346041	-.0630353	.209497	-.201732
.386578	-.109334	.247436	-.236931
.425683	-.159205	.286809	-.276414
.463730	-.212160	.327239	-.319783
.501004	-.267788	.368443	-.366616
.537714	-.325729	.410210	-.416491
.574016	-.385660	.452385	-.469004
.610022	-.447287	.494856	-.523774
.645814	-.510342	.537541	-.580448
.681448	-.574583	.580384	-.638700
.716962	-.639791	.623347	-.698233
.752380	-.705773	.666407	-.758780
.787715	-.772357	.709549	-.820104
.822974	-.839396	.752767	-.881995
.858156	-.906769	.796062	-.944275
.893260	-.974375	.839435	-1.00679
.928280	-1.04214	.882892	-1.06943
.963211	-1.11000	.926438	-1.13210
.998188	-1.17786	.970286	-1.19462

Although the scaling in the two figures is different comparison of the Figure 18 transonic design with the existing subsonic profile depicted in Figure 5 graphically demonstrates the dissimilarities between the two blade contours. The slightly convergent-divergent flow passage geometry of the new transonic turbine cascade is evident in Figure 19. Finally, the inviscid pressure coefficient distribution prediction of the new blade profile (Figure 20), is a significant improvement over the current design (Figure 12), in terms of the Chapter IV performance standards.

VI. Off-Design Performance

An important aspect of turbine blade design is the pre-
diction of cascade performance at off-design operating
conditions. Usually, the environment under which the turbine
airfoil actually operates is significantly different from the
originally intended design operating conditions. Therefore,
the new transonic turbine stator design must not only exhibit
maximum aerodynamic performance at the transonic design point
specified in Chapter IV, but it should exhibit reasonable
performance over a wide range of possible test environments.

The four most probable off-design scenarios that the
new design is anticipated to encounter are as follows:
1) an angle of attack other than zero, 2) a different gas
total temperature, 3) cold flow tests, and 4) an alternate
pressure ratio. Hence, the predicted performance of the
proposed airfoil design in these off-design test environments
is reported in the following sections of this chapter. In
addition, the last section is addressed to the topic of
viscous boundary layer influence upon aerodynamic performance.

Angle of Attack Sensitivity

The final turbine stator profile presented in Chapter V
was designed for an angle of attack equal to zero. However,
there is a good possibility that the new design may experience
a slight angle of attack if the gas inlet angle in the test

facility is not eight degrees. Although the Equation 8 continuity relationship indicates that turbine cascades are insensitive to small angles of attack, the effect upon performance of both positive and negative angles of attack was analytically investigated.

Pressure distribution predictions for the new airfoil were obtained at off-design gas inlet angles, β_1, ranging from zero to sixteen degrees. In every case, the results were identical to the pressure coefficient distribution plotted in Figure 20. Thus, the recently designed transonic turbine cascade, sketched in Figure 19, is relatively insensitive to small angles of attack.

Effect of Total Temperature Variations

In accordance with the requirement for a design that is based on an extremely high gas temperature, a design point gas total temperature of 3000^OR was selected. At the present time, most cooled or uncooled turbine stators can not withstand these temperatures at transonic blade loadings. Therefore, most cascade tests in the immediate future will probably occur at lower gas total temperatures until superior materials and/or cooling systems are developed.

Thus, the effect of lowering the operating gas total temperature to values of 2000^OR and 2500^OR was investigated. Since the governing continuity and momentum equations do not have explicit temperature terms, the effect of total temperature variation was expected to be negligible. This outcome

was realized by the resulting lower temperature pressure distributions which were identical to the Figure 20 pressure profile.

Cold Flow Test Conditions

Cold flow tests are conducted in the static test facility on certain occasions. When the nature of the experimental program requires use of low temperature instrumentation, cold flow testing becomes essential. Therefore, the performance of the new design was estimated for operation in this type of test environment.

Although the effect of total temperature variation upon cascade performance was reported to be negligible in the previous section, cold flow test conditions marginally effect aerodynamic performance. The reason for this apparent discrepancy is due to the fact that the major difference between the design point operating condition and cold flow testing is the change in the working gas medium, not the total temperature difference.

During the design point operating condition, the high gas temperatures are generated by an upstream chemical combustion reaction between hydrogen and compressed air. When this combustion reaction does not occur (cold flow), the nature of the working gas medium considerably changes. Thus, it is the specific heat ratio and molecular weight of compressed air at low temperatures which causes the observable difference in aerodynamic performance.

Figure 21 is a plot of the pressure distribution prediction for a cold flow test condition defined by the following thermodynamic quantities;

$$T_o = 300^\circ K \ (540^\circ R)$$
$$\gamma = 1.4$$
$$R = 286.9 \ \frac{m^2}{sec^2 - ^\circ K} \ \left(1716.2 \ \frac{ft^2}{sec^2 - ^\circ R}\right)$$

The isentropic pressure distribution prediction returned by CASC indicates that the flow on the suction surface will tend to undergo an increased amount of diffusion until an under-expanded exit pressure of 13.563 N/cm^2 (19.63 psia) is reached. Meanwhile, the flow over the pressure surface is estimated to overexpand to an exit static static pressure of 12.405 N/cm^2 (17.96 psia). This situation does not occur in an actual test environment because loss mechanisms, including flow separation and shock wave phenomenon, equalize the trailing edge pressure gradient. Hence, overall aero-cynamic performance degrades during cold flow operation. On the basis of the design parameter relationships discussed in Chapter V, this performance problem can be partially alleviated by slightly decreasing the cascade stagger angle, i.e., increase the stagger factor, SF.

Alternate Pressure Ratio

According to the qualitative functional relationship expressed by Equation 9, the pressure coefficient distribution is heavily dependent upon the cascade pressure ratio.
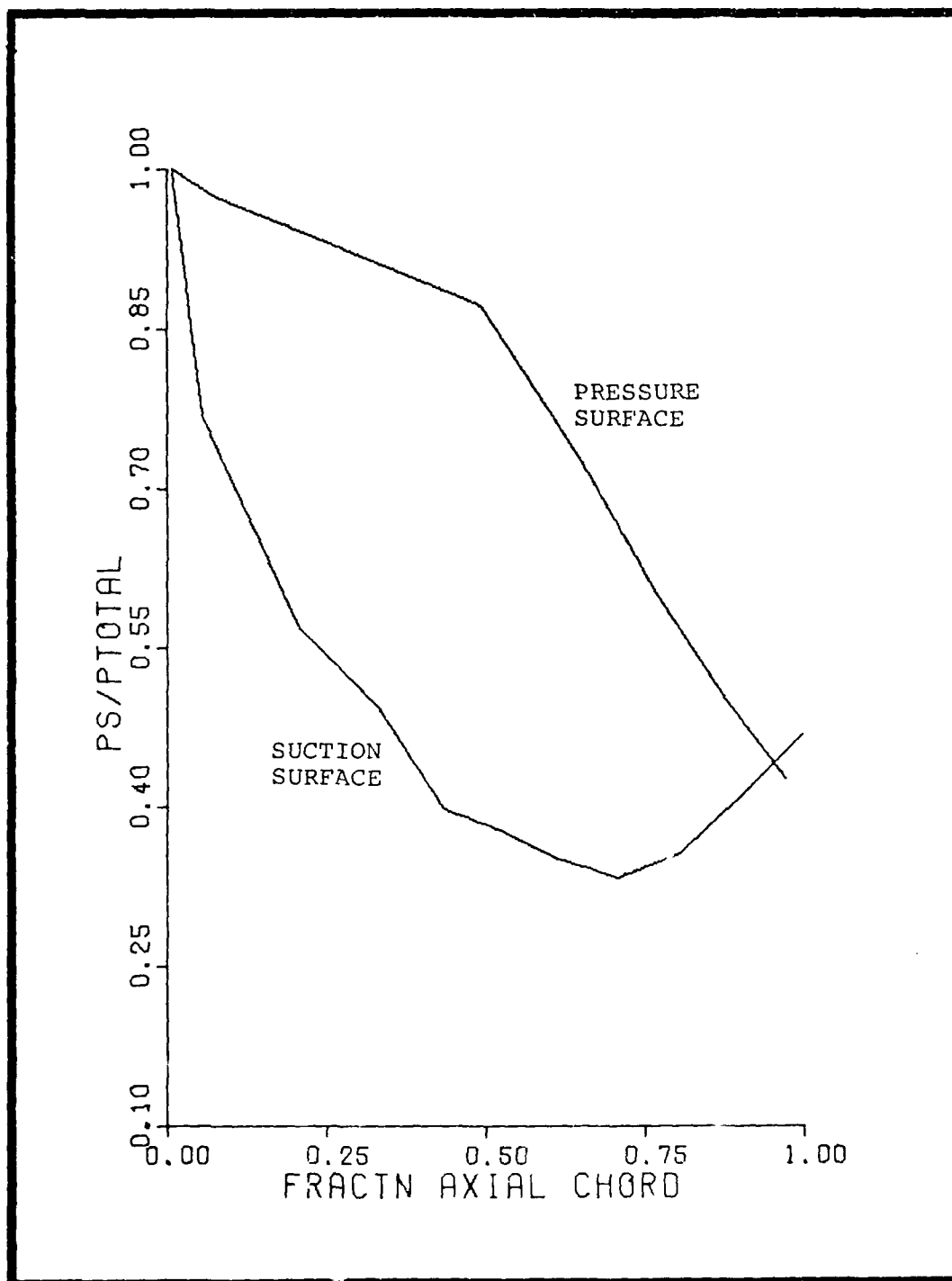
81

Figure 21   Off-Design C_p Distribution Prediction
(Cold Flow Test Condition)

Therefore, both subsonic and transonic off-design pressure ratios were analytically applied to the new design. In terms of significant loss in cascade performance, the results of this off-design pressure ratio investigation are the most dramatic.

Subsonic. An evaluation of the existing design determined that subsonic blade geometries exhibit poor aerodynamic performance at transonic flow conditions. In Chapter V, the geometric qualities which distinguish a subsonic turbine shape from a transonic contour were discussed. This section is concerned with presenting the performance characteristics of the new transonic design with respect to a subsonic pressure ratio.

When the recently developed transonic design is analytically subjected to a subsonic pressure ratio, the isentropic pressure coefficient distribution displayed in Figure 22 is generated. Large amounts of flow overexpansion are predicted on both the pressure and suction surfaces. In fact, the existence of a supersonic bubble on the suction surface is estimated to occur at 30-50 percent of axial chord. Along the divergent portion of the flow passage, flow on both surfaces diffuses drastically. Again, the situation depicted in Figure 22 is not realistic at the trailing edge because flow separation and other loss mechanisms will cause the flows over the aft portion of both surfaces to separate, rather than isentropically diffuse to meet exit static pressure boundary conditions.
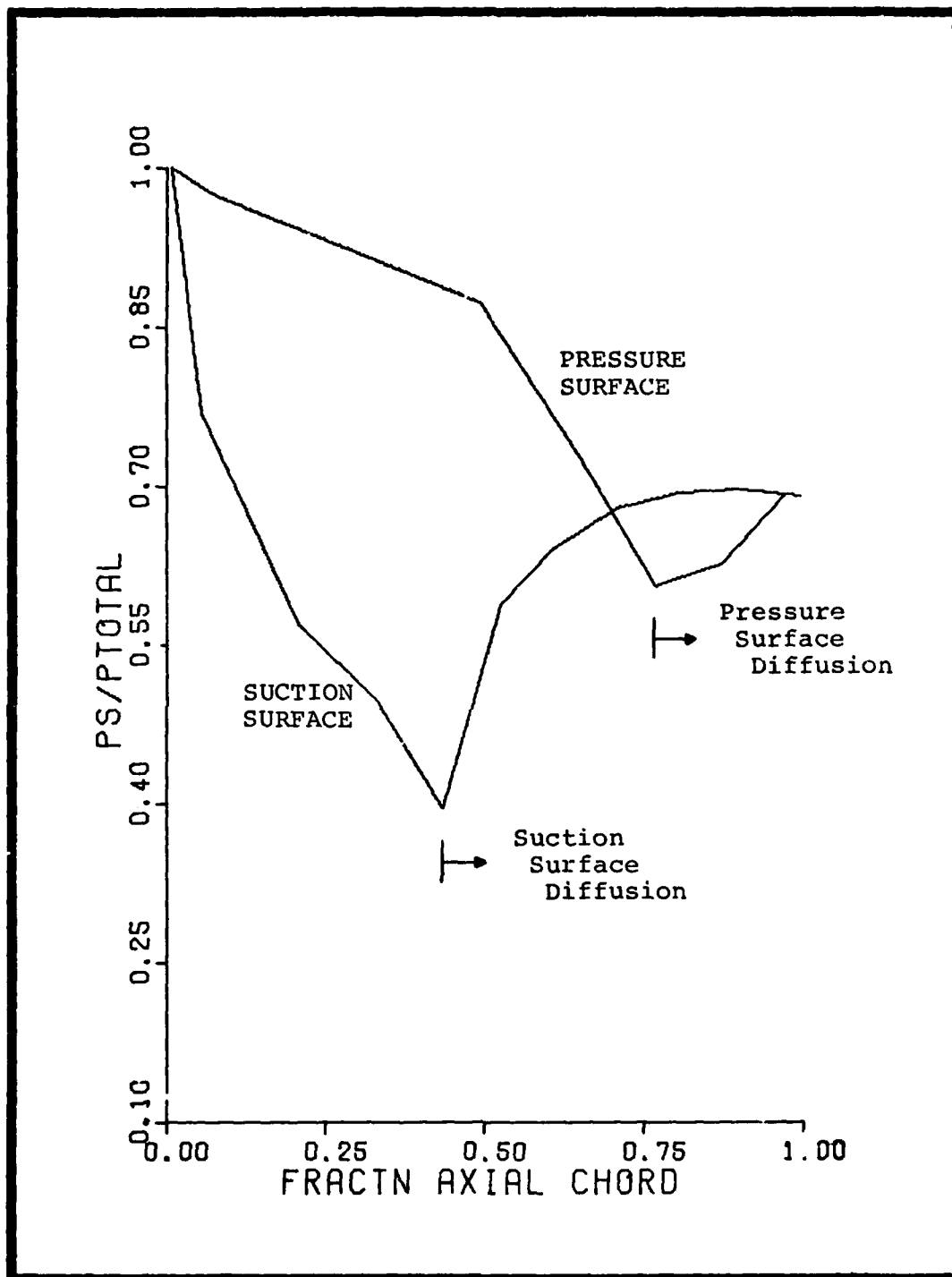
Figure 22   Off-Design C_p Distribution Prediction
(Subsonic Pressure Ratio)

84

Transonic. Figures 23 and 24 show the effect of respectively increasing and decreasing the pressure ratio while maintaining a transonic operating condition. The cascade pressure ratio can be increased by either increasing the total pressure, P_O, or decreasing the back pressure, P_b. The opposite relationships apply for decreasing the pressure ratio.

Increasing the cascade pressure ratio above the design point enhances the tendency of a negative trailing edge pressure gradient to be predicted, i.e., the suction surface overexpanded and the pressure surface underexpanded. A decrease in the cascade pressure ratio below the design point has the opposite effect; positive trailing edge pressure gradients are predicted. These tendencies are demonstrated in Figures 23 and 24 respectively. Stagger angle can be adjusted to correct these adverse aerodynamic effects in the following manner; reduce stagger angle to compensate for negative pressure gradients, increase stagger angle to compensate for positive pressure gradients.

Effect of Viscous Boundary Layer

The final transonic design is based upon maximization of aerodynamic performance. However, the flowfield calculation procedure and thermodynamic standards utilized to achieve this result are predicted upon isentropic, inviscid theory. In an actual flow situation, viscous boundary layers are present. The overall effect of boundary layer development
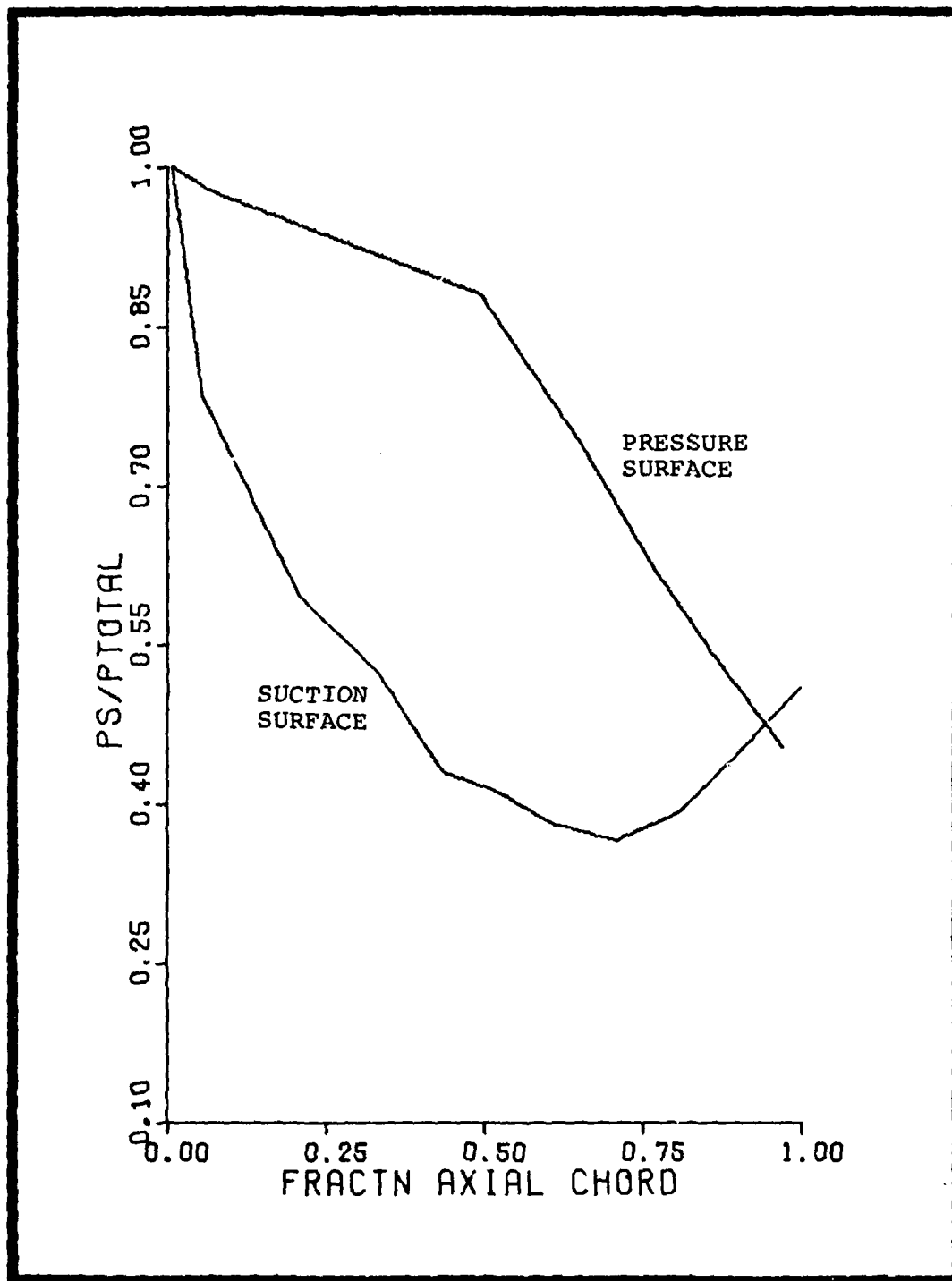
Figure 23   Off-Design C_p Distribution Prediction
(Transonic Pressure Ratio above Design Point)

86
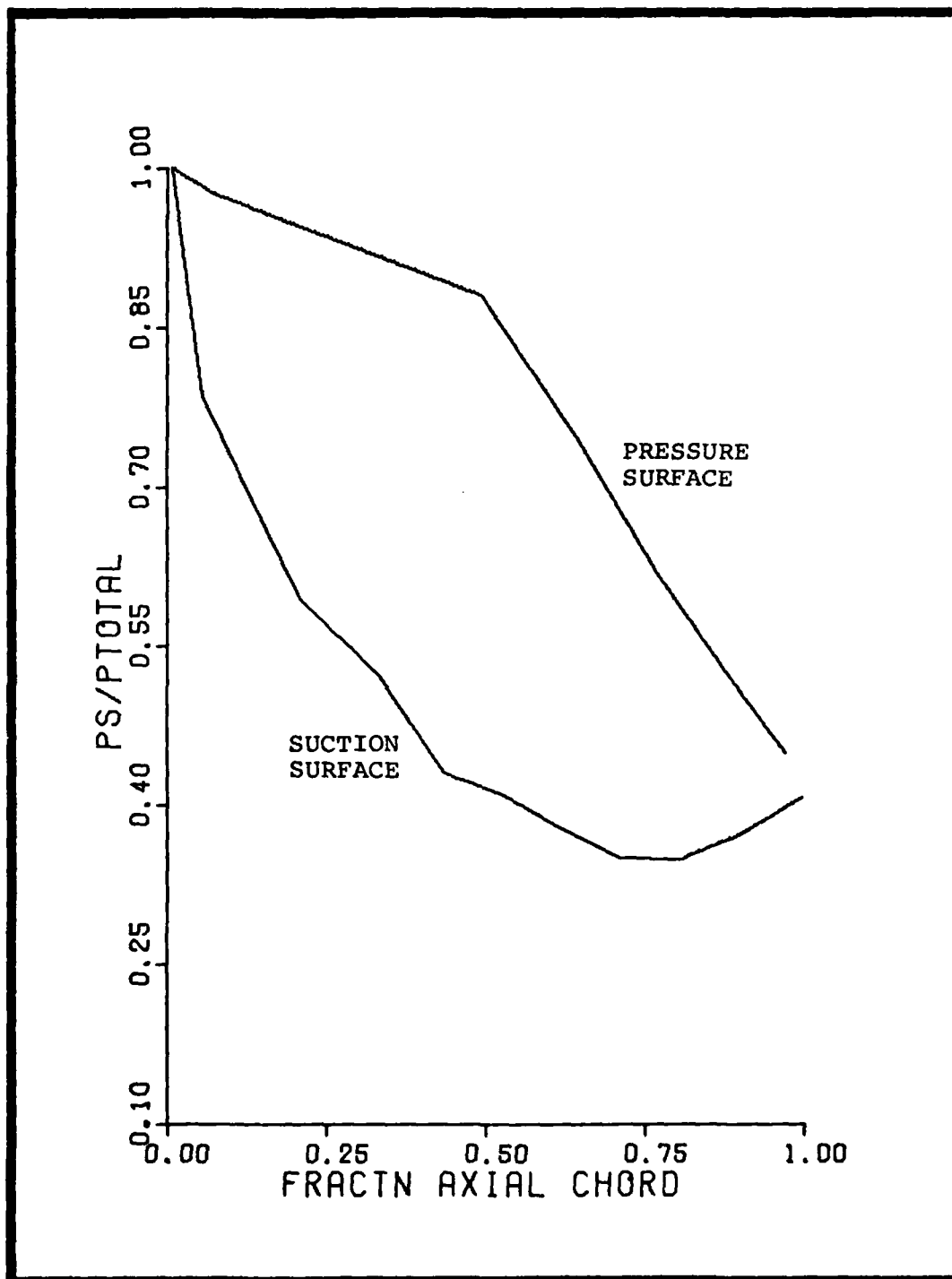
Figure 24   Off-Design C_p Distribution Prediction
(Transonic Pressure Ratio below Design Point)

is the existence of an additional displacement thickness.
Since the flow area is reduced, higher velocities result for
a given mass flow rate.

This situation was simulated by considering a design
version with a slightly larger thickness distribution along
the latter portion of the blade. Although the exit static
pressures at the trailing edge remain equal, the overall exit
static pressure decreases below the design back pressure by
2 percent. Thus, boundary layer induced effects upon perfor-
mance are relatively insignificant.

VII. Conclusions and Recommendations

A turbine stator profile that is analytically predicted
to exhibit good aerodynamic performance over a wide range
of transonic operating conditions has been designed for the
AFAPL Heat Transfer Test Facility. The design of the new
turbine airfoil section was based entirely upon analytical
methods. THis is a revolutionary approach to the turbine
blade design problem. During the course of this design
study, a number of significant conclusions were formulated.

First, the analytical TDS computer codes that were used
to generate blade profiles and perform cascade flow calcu-
lations were verified for accuracy and consistency. Analytical-
experimental correlation of TDS pressure distribution predic-
tions with existing test facility cascade data demonstrated
the ability of the computer programs to compute heat transfer
facility cascade flowfields successfully.

A set of aerodynamic performance standards to be applied
to isentropic cascade flowfield solutions has been developed.
Although experimental performance data is conclusive, appli-
cation of isentropic standards to state-of-the-art analytical
pressure distribution predictions is less time consuming,
more cost-effective, and reasonably valid.

A well designed transonic turbine stator must have a
convergent-divergent flow passage with most of the flow

turning occuring ahead of the throat location. Important geometric parameters for the design of transonic turbine airfoils have been identified. Transonic turbine stators require large stagger angles compared with typical subsonic designs. The stagger angle is the critical geometric parameter that determines whether or not the flow is equally expanded on both the pressure and suction surfaces. In addition, the location of maximum section thickness should be positioned ahead of the 25 percent axial chord location in order to minimize diffusion tendencies.

The results of the off-design investigation indicate that the performance of the final transonic design is not seriously compromised at ultimate angles of attack, and total temperature values. However, small changes in the operating pressure ratio will significantly change the pressure distribution of the new design. From an aerodynamic performance or diffusion control viewpoint, operation of the final transonic design at subsonic pressure ratios would be intolerable.

The scope of this transonic turbine stator design study was limited to maximization of aerodynamic performance. Further study is needed to develop a thermal and mechanical analysis suitable for incorporation into the performance maximization process.

A second area requiring further study is development of an improved aerodynamic analysis which incorporates non-

isentropic flow phenomena. For instance, formulation of viscous trailing edge wake model might significantly improve the predicted flowfield calculations.

The final recommendation is that the turbine stator design presented in this report be built and tested in the Air Force Aero Propulsion Laboratory Heat Transfer Test Facility. The results of these experimental tests could provide valuable data regarding the analytical concepts used to generate this design.

Bibliography

[1]Quick, D.H., Henderson, R.E., and Tall, W. "Experimental Cold-Flow Investigation of Chordwise Static Pressure Distribution Around a Turbine Airfoil," AFAPL-TR-67-147, March, 1968.

[2]Wu, C., "A General Through-Flow Theory of Fluid Flow With Subsonic or Supersonic Velocity in Turbomachines of Arbitrary Hub and Casing Shapes," NACA TN-2302, 1951.

[3]Wu, C., "A General Theory of Three-Dimensional Flow in Subsonic and Supersonic Turbomachines of Axial-, Radial-, and Mixed Flow Types," NACA TN-2604, 1952.

[4]Bosman, C., and El-Shaarawi, M.A.I., "Quasi-Three-Dimensional Numerical Solution of Flow in Turbomachines," Journal of FLuids Engineering, Transactions of the ASME, Vol. 99, Mar. 1977, pp. 132-140.

[5]Bosman, C., "The Occurrence and Removal of Indeterminacy from Flow Calculations in Turbomachines," Aeronautical Research Council Reports and Memoranda, R. & M. No. 3746, 1974.

[6]Katsanis, T., and McNally, W.D., "Fortran Programming for Calculating Velocities and Streamlines on the Hub-Shroud Mid-Channel Flow Surface of an Axial or Mixed Flow Turbomachine," Part I-Users Manual, NASA TN D-7343, 1973.

[7]Katsanis, T., and McNally, W.D., "Fortran Programming for Calculating Velocities and Streamlines on the Hub-Shroud Mid-Channel Flow Surface of an Axial or Mixed Flow Turbomachine," Part II-Programmers Manual NASA TN D-7344, 1974.

[8]Katsanis, T., "Fortran Program for Calculating Transonic Velocities on a Blade-to-Blade Streamsurface of a Turbomachine," NASA TN D-5427, 1969.

[9]Marsh, H., "A Digital Computer Program for the Through-Flow Fluid Mechanics in an Arbitrary Turbomachine Using a Matrix Method," Aeronautical Research Council Reports and Memoranda, R. & M. No. 3509, 1968.

[10]Marsh, H., "Through-Flow Calculations in Axial Turbomachinery: A Technical Point of View," AGARD Conference Proceedings No. 195 on Through-Flow Calculations in Axial Turbomachinery, 1976.

[11]Hill, M.J., "Numerical Solutions for Mixed Flow Turbomachines." PhD thesis, Department of Mechanical Engineering, The University of Manchester Institute of Science and Technology, Manchester, England, 1974.

[12]Hirsch, CH., and Warzee, G., "A Finite-Element Method for Through-Flow Calculations in Turbomachines," Journal of Fluids Engineering, Transactions of the ASME, Vol. 98, Sept. 1976, pp. 403-421.

[13]Smith, D.J.L., "Computer Solutions of Wu's Equations for the Compressible Flow Through Turbomachines," Symposium on the Fluid Mechanics & Design of Turbomachinery, Pennsylvania State University, 1970.

[14]Davis, W.R., "Through-Flow Calculations Based on Matrix Inversion: Loss Prediction," AGARD Conference Proceedings No. 195 on Through-Flow Calculations in Axial Turbomachinery, 1976.

[15]Prince, T., "Prediction of Transonic Inviscid Steady Flow in Cascades by Finite Element Methods," PhD Dissertation, Department of Mechanical Engineering, University of Cincinnati, 1976.

[16]Gopalakrishnan, S., and Bozzola, R., "A Numerical Technique for the Calculation of Transonic Flows in Turbomachinery Cascades," ASME Paper No. 71-GT-42, ASME Gas Turbine Conference, April 1971.

[17]McDonald, P.W., "The Computation of Transonic Flow Through Two-Dimensional Gas Turbine Cascades," ASME Paper No. 71-GT-89, ASME Gas Turbine Conference, April 1971.

[18]Ives, D.C., and Liutermoza, J.F., "Analysis of Transonic Cascade Flow Using Conformal Mapping and Relaxation Techniques," AIAA Journal, Vol, 15, May 1977, pp. 647-652.

[19]Novak, R.A., and Hearsey, R.M., "A Nearly Three-Dimensional Intrablade Computing System for Turbomachinery," Journal of Fluids Engineering, Transactions of the ASME, Vol, 99, Mar. 1977, pp. 154-166.

[20]Smith, L.H., "The Radial Equilibrium of Turbomachinery," Journal of Engineering for Power, Transactions of the ASME, Vol. 88, 1966, pp. 1-12.

[21]Frost, D.H., "A Streamline Curvature Through-Flow Computer Program for Analyzing the Flow Through Axial Flow Turbomachines," Aeronautical Research Council Reports and Memoranda, R. & M. No. 3687, 1970.

[22]Wilkinson, D.H., "Calculations of Blade-to-Blade Flow in a Turbomachine by Streamline Curvature," Aeronautical Research Council Reports and Memoranda, R. & M. No. 3704, 1972.

[23]Wysong, R.R., "Turbine Design System User's Manual," Contract F33615-75-C-2073, November 1977.

[24]Wysong, R.R., "Turbine Design System," AFAPL-TR-78-92, October 1978.

[25]Anderson, R.D., Davis, W.C., McLoed, R.N., and Nealy, D.A., "High Temperature Cooled Turbine Blades," AFAPL-TR-69-41, May 1969.

[26]Vincent, E.T., "The Theory and Design of Gas Turbines and Jet Engines," New York: McGraw-Hill, 1950.

[27]Cox, H., "Through-Flow Calculation Procedures for Application to High Speed Large Turbines," AGARD Conference Proceedings No. 195 on Through-Flow Calculations in Axial Turbomachinery, 1976.

[28]Amana, O.M., Demuren, H.O., and Louis, J.F., "Studies on Transonic Turbines with Film Cooled Blades: A Second Annual Report," Office of Naval Research TR-75-1, AD-A015-321, June 1975.

[29]Heinemann, H.J., "Influence of Secondary Flow Effects on Blade Surface Pressure Measurements in 2-D Transonic Turbine Cascades," AGARD Conference Proceedings No. 214 on Secondary Flows in Turbomachines, 1977.

[30]Szanca, E.M., and Schum, H.J., "Turbine Design and Application: Experimental Determination of Aerodynamic Performance," NASA SP-290, 1975.

APPENDIX A

CASC Input Files for
Test Cases One and Two

```
KEYS="HPTURB" "BLAD01" "DSEC02" "VERS01" 2*" "
$BB
QIDENT=
"TEST CASE ONE
ALPHAM=8. AREA= .387977 AXU=1.5327 BETA1=8. BET1UD=8.
BETAM1=8. BETA2=-61.2 BET2UD=-61.2 BETAM2=-61.2 CHORD=1.90338
CONE=0. C1=0. C2=0. C3=0. DELTA1=0. E=1.45 EPSI=8.36
EPSIM=8.36 FAX=0. FTAN=0. ICHOKE=1 ICOB=1 IOGU=0 IPLOT=2 ISKP=0
ISTK=1 ITMODE=1 ITURB=1 IVANE=0 JBLCKD=3 JBLCKU=3 LEDGE=1
MACH1= .2842 HMTE=1. NBLDS=100 NODENS=1 NPSI=4 NPTS=100
NRMLZD=0 NSLICE=0 PSIRAT=2. NSLPCT=10 PICH=1.5 PSPACE= .978665
PS2=15.1 PTO=21.046 RLE=23.8732 ROTATE=0. RPM=0. RSTKPT=23.8732
RTE=23.8732 SCALE=1. SCALIN=1. SF=0. STAGGR=34.6504 TE= .08335
TI=0. TMAX= .334468 TMAXX=0. TMXX= .722278 TTO=517.
WIDTH=1.5327 ZDOWN=4.5981 ZLE=0. ZTE=1.5327 ZREF=0. ZUP=-3.0654
Z1=0. Z2=1.5327 RREF=23.8732 0. STKPT= 2*0. TOLER= .001 5.E-7
.005 .01
SLICE=
 10.0000  20.0000   30.0000   40.0000   45.0000   50.0000
 55.0000  60.0000   70.0000   80.0000
HM= 13* 1.00000
RM= 13* 23.8732
ZM=
 -3.06540 -1.14953 -.766350 -.383175   2*       0.      .766350
 2* 1.53270 1.91588 2.29905 2.68223 4.59810
XU=
 3.4931E-4       0.     .00168803  .00590654  .0135776  .0260229
 .0427794  .0789374  .121598   .146603   .194427  .240163
 .285443   .330200   .374501   .417236   .477522  .532132
 .587589   .630390   .672994   .715011   .754484  .792522
 .828537   .862986   .895412   .926860   .961309  .979121
 .996932
```

96

YU=

1.95013	1.95913	1.96865	1.97893	1.99006	2.00175
2.01259	2.02752	2.04002	2.04737	2.04998	2.04985
2.04495	2.03628	2.02297	2.00568	1.97221	1.93058
1.87538	1.82645	1.77432	1.72121	1.66817	1.61428
1.55895	1.50284	1.44627	1.38931	1.32302	1.28818
1.25328					

AU=

98.3600	86.1607	73.9494	61.7870	45.4200	37.9022
28.0547	17.8086	17.4942	11.9048	-.0973627	-2.52968
-8.79797	-13.6974	-19.4487	-24.7651	-33.2527	-41.3069
-47.5167	-49.9909	-51.1833	-52.4521	-54.0216	-55.8528
-57.7360	-59.3750	-60.6617	-61.7974	-62.9126	-62.9399
-62.5914					

XL=

3.4931E-4	.00260447	.00696082	.0139572	.0245060	.6397873
.0623298	.0971623	.133302	.149408	.182944	.214979
.246622	.277809	.308213	.338291	.382657	.425849
.479675	.528869	.578259	.626801	.672081	.716121
.758529	.799503	.837214	.873099	.911332	.931036
.949143					

YL=

1.95013	1.94141	1.93277	1.92415	1.91569	1.90808
1.90301	1.89751	1.89108	1.88850	1.88047	1.87238
1.86325	1.85320	1.84211	1.82978	1.80916	1.78587
1.75240	1.71814	1.68043	1.63966	1.59712	1.55288
1.50669	1.45867	1.40882	1.35721	1.29608	1.26183
1.22736					

AL=

-81.6400	-69.4364	-57.2480	-44.9932	-33.0066	-19.8906
-7.25897	-10.2316	-8.94445	-10.4266	-14.3924	-14.8491
-17.0406	-18.8689	-21.1988	-23.3356	-26.6093	-30.0059
-33.5301	-36.1214	-38.5760	-41.7365	-44.2514	-46.2746
-48.3618	-51.1922	-54.1448	-56.4616	-59.2870	-61.0950
-63.4683					

PRESS=

.0740000	2.92050	.127300	2.91260	.182600	2.90330
.233700	2.89450	.285100	2.88220	.334200	2.86980
.382700	2.85580	.430500	2.84040	.477100	2.82340
.523200	2.80450	.591200	2.77690	.657400	2.73720
.739900	2.68590	.815300	2.63340	.891000	2.57560
.965400	2.51310	1.03489	2.44790	1.10230	2.38010
1.16730	2.30930	1.23010	2.23570	1.28790	2.15930
1.34290	2.08020	1.40150	1.98650	1.43170	1.93400
1.46190	1.88150				

SUCTN=

.0466000	3.07300	.101600	3.09840	.166500	3.12050
.229400	3.13800	.302700	3.14200	.372800	3.14180
.442200	3.13430	.510800	3.12100	.578700	3.10060
.644200	3.07410	.736600	3.62280	.820300	2.95900
.905300	2.87440	.970900	2.79940	1.03620	2.71950
1.10060	2.63810	1.16110	2.55680	1.21940	2.47420
1.27460	2.38940	1.32740	2.30340	1.37710	2.21670
1.42530	2.12940	1.47810	2.02780	1.50540	1.97440
1.53270	1.92090				

RF= 65% 23.8732

TF=

1.56007	1.55949	1.55898	1.55822	1.55751	1.55676
1.55606	1.55552	1.55506	1.55469	1.55433	1.55361
1.55366	1.55409	1.55497	1.55637	1.55840	1.56120
1.56492	1.56928	1.57398	1.57902	1.58458	1.59079
1.59762	1.60001	1.60241	1.60481	1.60532	1.60586
1.60637	1.60681	1.60714	1.60732	1.60734	1.60719
1.60689	1.60647	1.60607	1.60568	1.60529	1.59892
1.59354	1.58894	1.58487	1.58118	1.57791	1.57501
1.57241	1.57014	1.56825	1.56670	1.56546	1.56446
1.56372	1.56355	1.56339	1.56324	1.56310	1.56293
1.56265	1.56224	1.56171	1.56102	1.56007	

ZF=

-.748401	-.748936	-.746349	-.739883	-.728126	-.709051
-.683368	-.653797	-.624226	-.594655	-.565083	-.475346
-.385608	-.295871	-.206133	-.116395	-.0266577	.0630799
.152817	.242555	.332293	.422030	.511768	.601506
.691243	.720516	.749789	.779062	.783065	.783170
.779365	.772012	.761808	.749721	.736895	.724549
.713851	.705816	.700958	.696101	.691243	.601506
.511768	.422030	.332293	.242555	.152817	.0630799
-.0266577	-.116395	-.206133	-.295871	-.385608	-.475346
-.565083	-.587163	-.609243	-.631323	-.653403	-.675423
-.695237	-.712861	-.728217	-.740703	-.748401	

$

KEYS='HPTURB' 'BLAD01' 'DSEC02' 'VERS01' 2*' '
$BB
QIDENT='
'TEST CASE TWO
ALPHAM=8. AREA=.387977 AXU=1.5327 BETA1=8. BET1UD=8.
BETAM1=8. BETA2=-61.2 BET2UD=-61.2 BETAM2=-61.2 CHORD=1.90338
CONE=0. C1=0. C2=0. C3=0. DELTA1=0. E=1.45 EPSI=8.36
EPSIM=8.36 FAX=0. FTAN=0. ICHOKE=1 ICOB=1 IOGU=0 IPLOT=2 ISKP=0
ISTK=1 ITMODE=1 ITURB=1 IUANE=0 JBLCKD=3 JBLCKU=3 LEDGE=1
MACH1=.2990 HMTE=1. NBLDS=100 NODENS=1 NPSI=4 NPTS=100
NRMLZD=0 NSLICE=0 PSIRAT=2. NSLPCT=10 PICH=1.5 PSPACE=.978665
PS2=16.0 PT0=25.074 RLE=23.8732 ROTATE=0. RPM=0. RSTKPT=23.8732
RTE=23.8732 SCALE=1. SCALIN=1. SF=0. STAGGR=34.6504 TE=.08335
TI=0. TMAX=.334468 TMAXX=0. TMXX=.722278 TT0=517.
WIDTH=1.5327 ZDOWN=-4.5981 ZLE=0. ZTE=0. ZREF=0. ZUP=-3.0654
Z1=0. Z2=1.5327 RREF=23.8732 0. STKPT= 2*0. TOLER= .001 5.E-7
.005 .01
SLICE=
10.0000 20.0000 30.0000 40.0000 45.0000 50.0000
55.0000 60.0000 70.0000 80.0000
HM= 13* 1.00000
RM= 13* 23.8732
ZM=
-3.06540 -1.14953 -.766350 -.383175 2* 0. .766350
2* 1.53270 1.91588 2.29905 2.68223 4.59810
XU=
3.4931E-4 0. .00168803 .00590654 .0135776 .0260229
.0427794 .0789374 .121598 .146603 .194427 .240163
.285443 .330200 .374501 .417236 .477522 .532132
.587589 .630390 .672994 .715011 .754484 .792522
.828537 .862986 .895412 .926869 .961309 .979121
.996932

YU=

1.95013	1.95913	1.96865	1.97893	1.99006	2.00175
2.01259	2.02752	2.04002	2.04737	2.04998	2.04985
2.04495	2.03628	2.02297	2.00568	1.97221	1.93058
1.87538	1.82645	1.77432	1.72121	1.66817	1.61428
1.55895	1.50284	1.44627	1.38931	1.32302	1.28818
1.25328					

AU=

98.3600	86.1607	73.9494	61.7870	49.4200	37.9022
28.0547	17.8036	17.4942	11.9048	-.0973627	-2.52968
-8.79797	-13.6974	-19.4487	-24.7651	-33.2527	-41.3069
-47.5167	-49.9909	-51.1833	-52.4521	-54.0216	-55.8528
-57.7360	-59.3750	-60.6617	-61.7974	-62.9126	-62.9399
-62.9914					

XL=

3.4931E-4	.00260447	.00596082	.0139572	.0245060	.0397873
.0623298	.0971623	.133302	.149408	.182344	.214979
.246622	.277809	.308213	.338291	.382657	.425849
.479675	.528869	.578259	.626801	.672081	.716121
.758529	.799503	.837214	.873099	.911332	.931036
.949143					

YL=

1.95013	1.94141	1.93277	1.92415	1.91569	1.90808
1.90301	1.89751	1.89108	1.88850	1.88047	1.87238
1.86325	1.85320	1.84211	1.82978	1.80916	1.78587
1.75240	1.71814	1.68043	1.63966	1.59712	1.55288
1.50669	1.45867	1.40882	1.35721	1.29608	1.26183
1.22736					

AL=

-81.6400	-69.4364	-57.2480	-44.9932	-33.0066	-19.8906
-7.25897	-10.2316	-8.94445	-10.4266	-14.3924	-14.8491
-17.0406	-18.8689	-21.1988	-23.3356	-26.6093	-30.0059
-33.5301	-36.1214	-38.5760	-41.7365	-44.2514	-46.2746
-48.3618	-51.1922	-54.1448	-56.4616	-59.2870	-61.0950
-63.4683					

PRESS-

.0740000	2.92050	.127300	2.91260	.182600	2.90330
.233700	2.89450	.285100	2.88220	.334200	2.86980
.382700	2.85580	.430500	2.84040	.477100	2.82340
.523200	2.80450	.591200	2.77290	.657400	2.73720
.739900	2.68590	.815300	2.63340	.891000	2.57560
.965400	2.51310	1.03480	2.44790	1.10230	2.38010
1.16730	2.30930	1.23010	2.23570	1.28790	2.15930
1.34290	2.08020	1.40150	1.98650	1.43170	1.93400
1.46190	1.88150				

SUCTN-

.0466000	3.07300	.101600	3.09840	.166500	3.12050
.229400	3.13800	.302700	3.14200	.372800	3.14180
.442200	3.13430	.510800	3.12100	.578700	3.10060
.644200	3.07410	.736600	3.02280	.820300	2.95900
.905300	2.87440	.970900	2.79940	1.03620	2.71950
1.10060	2.63810	1.16110	2.56680	1.21940	2.47420
1.27460	2.38940	1.32740	2.30340	1.37710	2.21670
1.42530	2.12940	1.47810	2.02780	1.50540	1.97440
1.53270	1.92090				

RF= 65* 23.8732

TF=

1.56007	1.55949	1.55888	1.55822	1.55751	1.55676
1.55606	1.55552	1.55506	1.55469	1.55433	1.55361
1.55366	1.55409	1.55497	1.55637	1.55840	1.56120
1.56492	1.56928	1.57398	1.57902	1.58458	1.59079
1.59762	1.60001	1.60241	1.60481	1.60532	1.60586
1.60637	1.60681	1.60714	1.60732	1.60734	1.60719
1.60689	1.60647	1.60607	1.60568	1.60529	1.59892
1.59354	1.58894	1.58487	1.58118	1.57791	1.57501
1.57241	1.57014	1.56825	1.56670	1.56546	1.56446
1.56372	1.56355	1.56339	1.56324	1.56310	1.56293
1.56265	1.56224	1.56171	1.56102	1.56007	

ZF=

-.748401	-.748936	-.746349	-.739883	-.728126	-.709051
-.683368	-.653797	-.624226	-.594655	-.565083	-.475346
-.385608	-.295871	-.206133	-.116395	-.0266577	.0630799
-.152817	.242555	.332293	.422030	.511768	.601506
.691243	.720516	.749789	.779062	.783065	.783170
.779365	.772012	.761808	.749721	.736895	.724549
.713851	.705816	.700958	.696101	.691243	.601506
.511768	.422030	.332293	.242555	.152817	.0630799
-.0266577	-.116395	-.206133	-.295871	-.385608	-.475346
-.565083	-.587163	-.609243	-.631323	-.653403	-.675423
-.695237	-.712861	-.728217	-.740703	-.748401	

$

APPENDIX B

Derivation of the Non-Dimensional
Turbine Cascade Continuity Equation (Eq. 8)

Equation B-1 is the simple continuity balance which states that the mass flow through the inlet plane is equal to the mass flow out the exit plane. This is equation seven in the text (Chapter III).

$$\dot{m}_1 = \dot{m}_2 \qquad (B-1)$$

The subscripts 1 and 2 refer to the turbine cascade inlet and exit stations respectively (see Figure 6). Equation B-1 can be expressed in the Figure 6 terminology;

$$\rho_1 A_1 V_{z_1} = \rho_2 A_2 V_{z_2} \qquad (B-2)$$

where

ρ = local density

A = flow area

V_z = axial velocity

It should be readily apparent that the following definitions are valid for a turbine cascade geometry (see Figure 6 control volume):

$$A_1 = A_2 = S*L \qquad (B-3)$$

$$V_{z_1} = (\cos \beta_1) V_1 \qquad (B-4)$$

$$V_{z_2} = (\cos \beta_2) V_2 \qquad (B-5)$$

where

S = cascade pitch (blade spacing)

L = characteristic unit length

β_1 = gas incidence angle

β_2 = gas exit angle

V_1 = inlet velocity

V_2 exit velocity

Substituting Equations B-3. B-4, and B-5 into Equation B-2 and dividing through by the equal area term yields the following mass flux expression;

$$\rho_1 (\cos \beta_1) V_1 = \rho_2 (\cos \beta_2) V_2 \qquad (B-6)$$

From gas dynamic theory, velocity, density and temperature can be represented in the following manner:

$$V = M \sqrt{\gamma RT} \qquad (B-7)$$

$$\rho = \frac{P_O}{RT_O} (1 + \frac{\gamma - 1}{2} M^2)^{\frac{1}{1-\gamma}} \qquad (B-8)$$

$$T = T_O / (1 + \frac{\gamma - 1}{2} M^2) \qquad (B-9)$$

Substitution of Equation B-9 into B-7 yields:

$$V = \frac{M \sqrt{\gamma RT_O}}{\sqrt{1 + \frac{\gamma - 1}{2} M^2}} \qquad (B-10)$$

After the appropriate subscripts are introduced, Equations B-10 and B-8 can be inserted into Equation B-6 to produce the following:

$$\left(P_O \sqrt{\frac{\gamma}{RT_O}}\right)_1 (\cos \beta_1) M_1 \left(1 + \frac{\gamma-1}{2} M_1^2\right)^{\frac{\gamma+1}{2(1-\gamma)}}$$

$$= \left(P_O \sqrt{\frac{\gamma}{RT_O}}\right)_2 (\cos \beta_2) M_2 \left(1 + \frac{\gamma-1}{2} M_2^2\right)^{\frac{\gamma+1}{2(1-\gamma)}} \qquad (B-11)$$

Since no heat transfer and negligible viscous pressure loss is assumed to occur the Figure 6 control volume, the total property terms cancel. Thus, Equation B-11 becomes:

$$(\cos \beta_1) M_1 \left(1 + \frac{\gamma-1}{2} M_1^2\right)^{\frac{\gamma+1}{2(1-\gamma)}}$$

$$= (\cos \beta_2) M_2 \left(1 + \frac{\gamma-1}{2} M_2^2\right)^{\frac{\gamma+1}{2(1-\gamma)}} \qquad (B-12)$$

APPENDIX C

CASC Output Files for
Test Cases One and Two

```
$BBUPR
NI=11 UPPER=F QIDENT.
"TEST CASE ONE
PT= 11X
 21.0460
TT= 11X
 517.000
XII=
 15.5000    16.0000    17.0000    18.0000    19.0000    20.0000
 21.0000    22.0000    23.0000    24.0000    25.0000
SU=
 0.         .0873126   .276857    .466401    .655945    .845489
 1.03503    1.32490    1.61477    1.90464    2.19450
X=
 5.35524E-4 .0239491   .136139    .259548    .379786    .489239
 .581385    .702661    .812890    .909545    .996932
Y=
 1.94898    2.30009    2.04465    2.04838    2.02107    1.96428
 1.88210    1.73710    1.58347    1.42099    1.25328
ZAX=
 8.20796E-4 .0367067   .208660    .397809    .582097    .749855
 .891088    1.07697    1.24591    1.39406    1.52800
RAD= 11X
 23.8732
ANGU=
 ,  50.9556 11.7157    -5.57524   -20.1494   -34.6076   -45.0307
 -52.2170   -56.7931   -60.8654   -60.7490
CURUU=
 23.7544    6.31432    2.72494    2.00659    2.02143    1.97653
 .926145    .391419    .452151    .297413    -.318569
XLAMDA= 11X
 1.00000
PS=
 21.0460    18.1931    17.0574    15.9861    14.4764    12.8741
 13.0535    13.3713    13.3081    14.1020    15.4371
```

UE=
```
        0.      503.179     601.587     685.058     793.569     902.061
  890.127     868.882     873.121     819.381     725.499
```
XMACH=
```
        0.      .460963     .556214     .639286     .751115     .868233
  .855053     .831782     .836407     .778455     .680413
```
$
$BBLUR
NI=7 UPPER=T QIDENT=
*TEST CASE ONE
PT= 7*
```
   21.0460
```
TT= 7*
```
  517.000
```
XII=
```
  15.5000     16.0000     17.0000     18.0000     19.0000     20.0000
  21.0000
```
SU=
```
        0.      .159815     .457312     .861155     1.25497     1.61236
  1.89253
```
X=
```
5.35524E-4    .0913615    .279753     .511672     .706255     .854888
  .949143
```
Y=
```
  .970312     1.89854     1.85253     1.73049     1.56309     1.38396
  1.22736
```
ZAX=
```
8.20796E-4    .140030     .428776     .784238     1.08248     1.31028
  1.45475
```
RAD= 7*
```
   23.8732
```
ANGU=
```
  -23.7064    -19.6995    -34.3267    -45.7604    -55.1698    -56.3588
```

110

```
CURUU=
  23.7544  -1.73456   1.04852    .855157    .678118    .719452
  -.493824
XLAMDA=  7*
  1.00000
PS=
  21.0460   19.8567   20.1125   19.8757   19.2197   18.1348
  15.4374
UE=
   0.       319.950   282.827   317.334   398.770   508.577
  725.479
XMACH=
   0.        .289466   .255412   .287061   .362461   .466123
  .680393
$
```

```
$BBUPR
NI=11 UPPER=F QIDENT=
*TEST CASE TWO
PT= 11*
 25.0740
TT= 11*
 517.000
XI1=
 15.5000  16.0000  17.0000  18.0000  19.0000  20.0000
 21.0000  22.0000  23.0000  24.0000  25.0000
SW=
 0.        .0870026  .276494   .465986   .655478   .844970
 1.03446   1.32439   1.61432   1.90425   2.19418
X=
 4.95933E-4 .0239491  .136115   .259489   .379698   .489134
 .581275   .702586   .812846   .909526   .996932
Y=
 1.94921   2.00009   2.04464   2.04839   2.02110   1.96435
 1.88222   1.73722   1.58354   1.42103   1.25328
ZAX=
 7.60115E-4 .0367067  .208623   .397718   .581963   .749695
 .890919   1.07685   1.24585   1.39403   1.52800
RAD= 11*
 23.8732
ANGW=
 ,        56.8994   11.7192   -5.56765  -20.1386  -34.5942  -45.0200
 -52.2138  -56.7962  -60.8646  -60.7118
CURVW=
 23.7449   6.31028   2.72490   2.00686   2.02138   1.98314
 1.53704   .648168   .411850   .297436   -.325262
XLAMDA= 11*
 1.00000
PS=
 25.0740   21.3434   19.8403   18.4055   16.3322   13.8193
 13.1236   13.2830   12.9959   14.5786   16.8006
```

```
UE=
        0.      528.569   633.924   724.657   846.166   985.970
      1024.15   1015.40   1031.16   944.170   819.405
XMACH=
        0.      .485292   .588124   .679550   .807160   .963237
      1.00795   .997617   1.01626   .915380   .778481
$
$BBLWR
NI=7 UPPER=T QIDENT=
*TEST CASE TWO
PT= 7*
     25.0740
TT= 7*
     517.000
XI1=
     15.5000   16.0000   17.0000   18.0000   19.0000   20.0000
     21.0000
SW=
        0.      .160055   .454241   .857377   1.25112   1.61068
     1.89278
X=
  4.95933E-4   .0913615  .277700   .509525   .704383   .854167
      .949143
Y=
      .970541   1.89854   1.85324   1.73201   1.56500   1.38499
     1.22736
ZAX=
  7.60115E-4   .140030   .425631   .780948   1.07961   1.30918
     1.45475
RAD= 7*
     23.8732
ANGU=
    -23.7061  -19.5701  -34.1947  -45.6527  -55.1186  -56.2996
```

113

CURVU=
```
 23.7449   -1.76368    1.04815    .858522    .678202    .719137
-.496590
```
XLAMDA= 7*
```
 1.00000
```
PS=
```
 25.0740   23.4933    23.8345    23.5160    22.6132    21.0579
 16.8014
```
UE=
```
 0.        338.357    298.853    335.856    425.000    549.688
 819.355
```
XMACH=
```
 0.         .306423    .270090    .304116    .386994    .505653
 .778428
```
$

APPENDIX D

Pressure Coefficient Distributions
for Various Combinations of β_1 and M_1
(First Test Case)
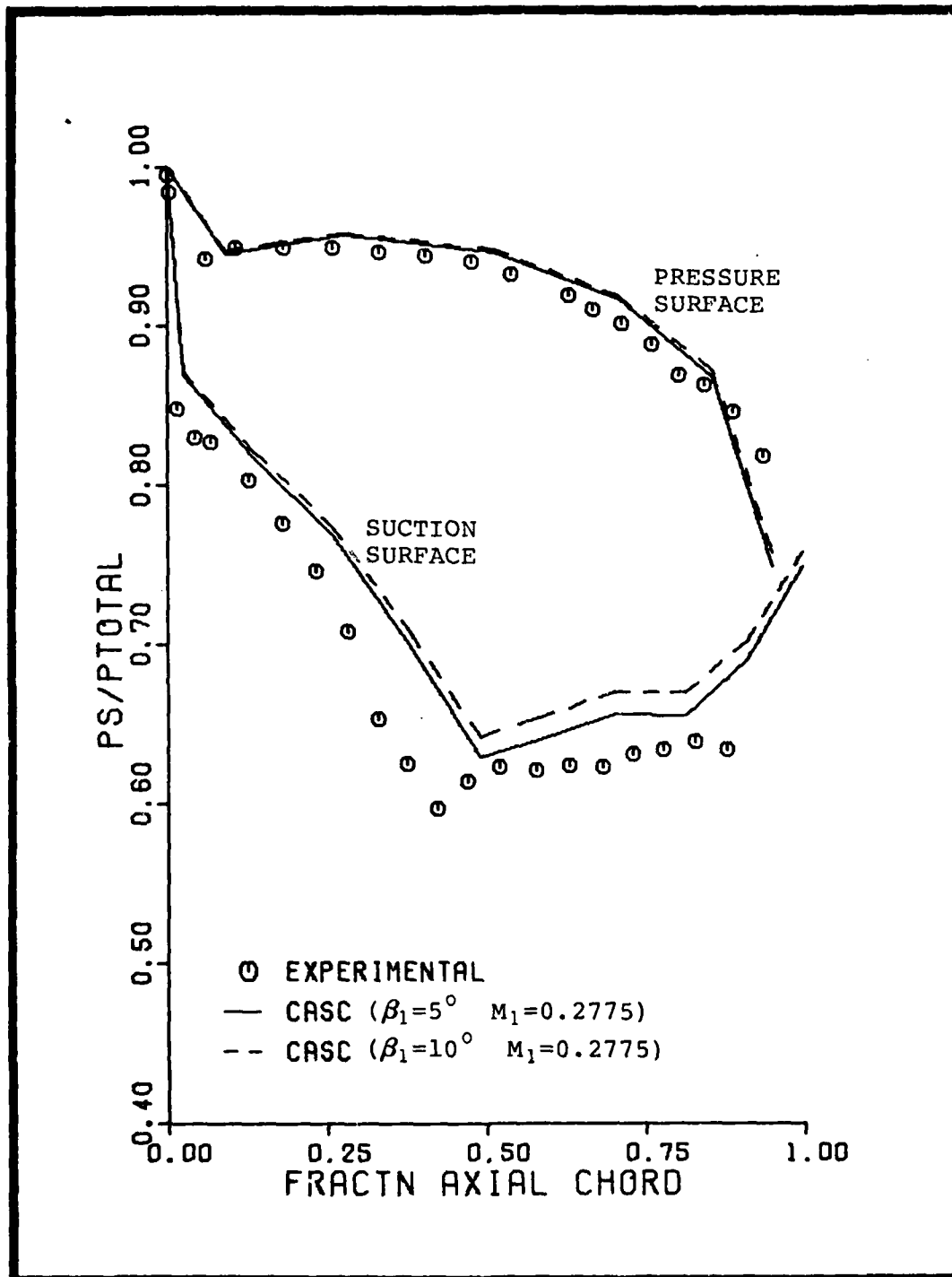
Figure 25   Case One C_p Distribution Correlation
            $(M_1 = 0.2775)$
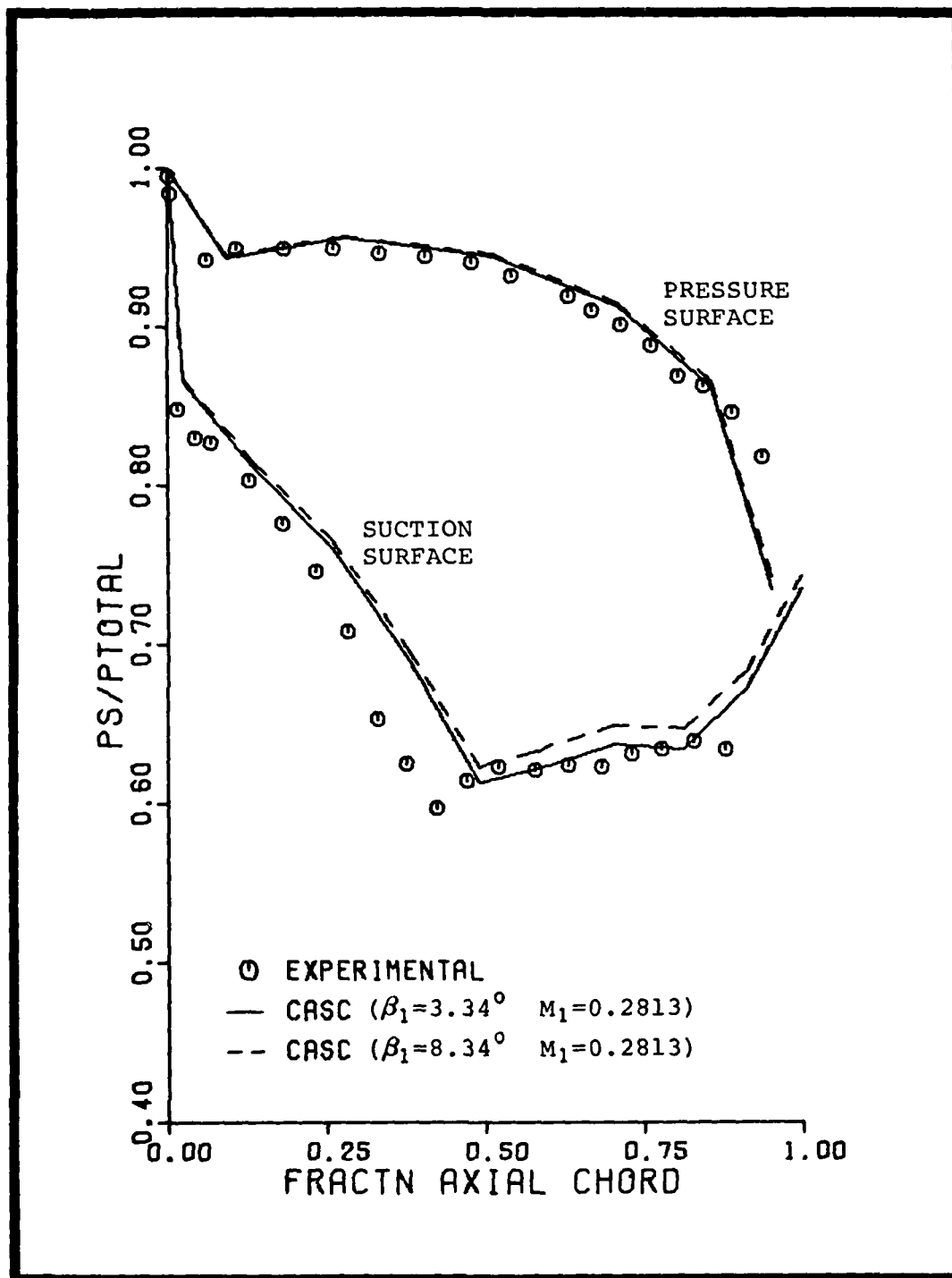
Figure 26   Case One C_p Distribution Correlation
($M_1 = 0.2813$)
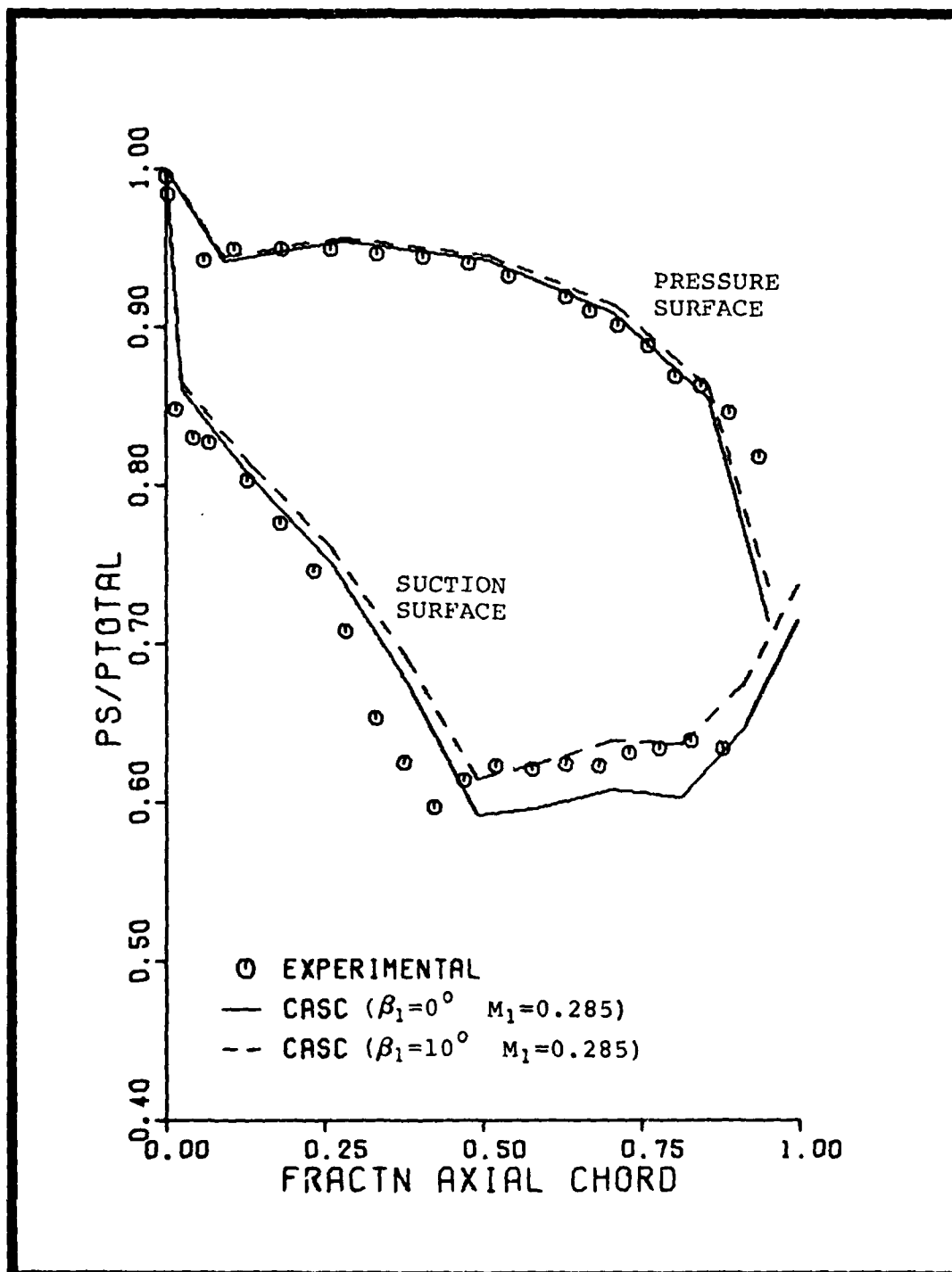
Figure 27   Case One C_p Distribution Correlation
(M_1 = 0.2850)
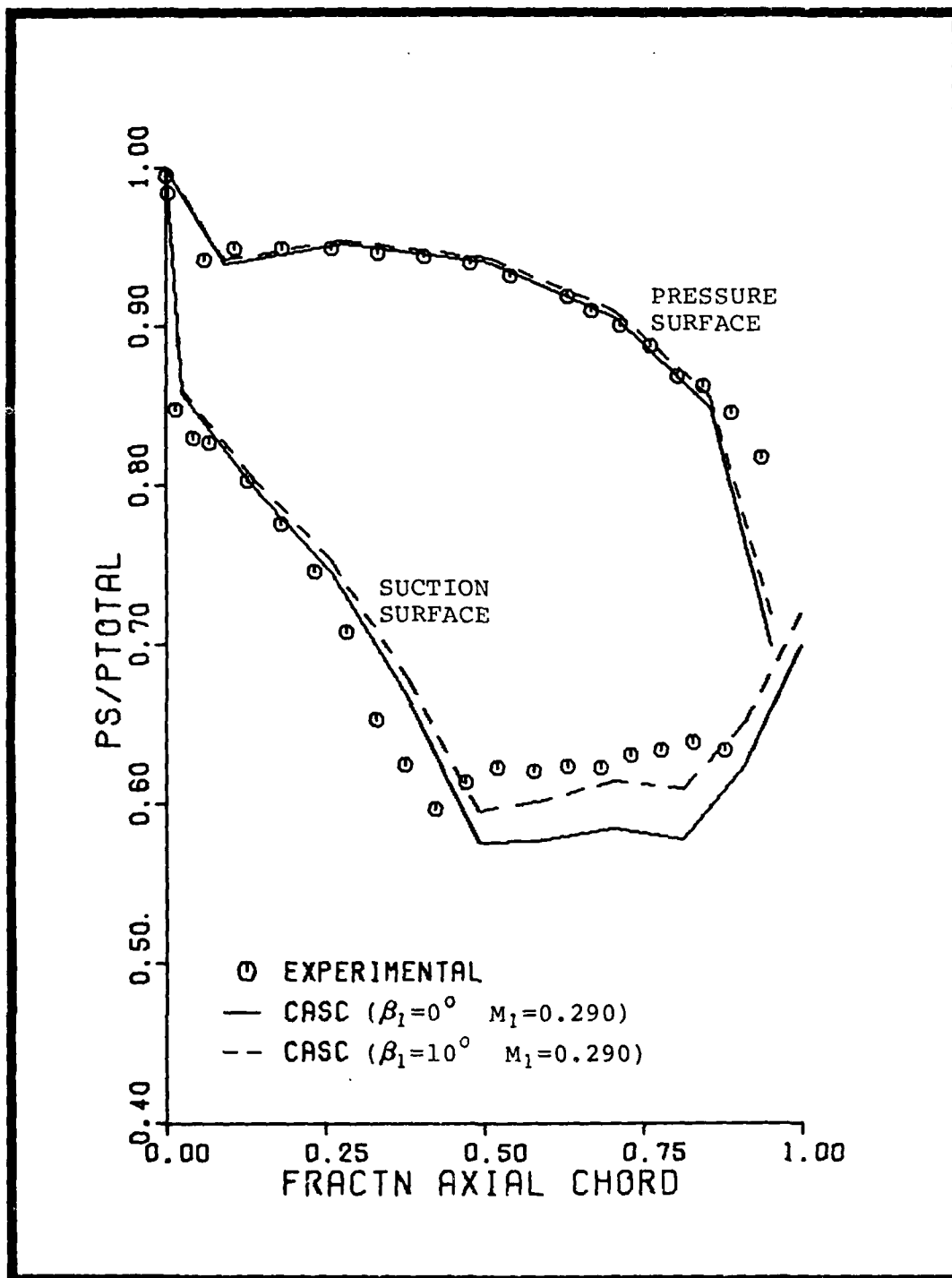
Figure 28   Case One C_p Distribution Correlation
(M$_1$ = 0.2900)

119
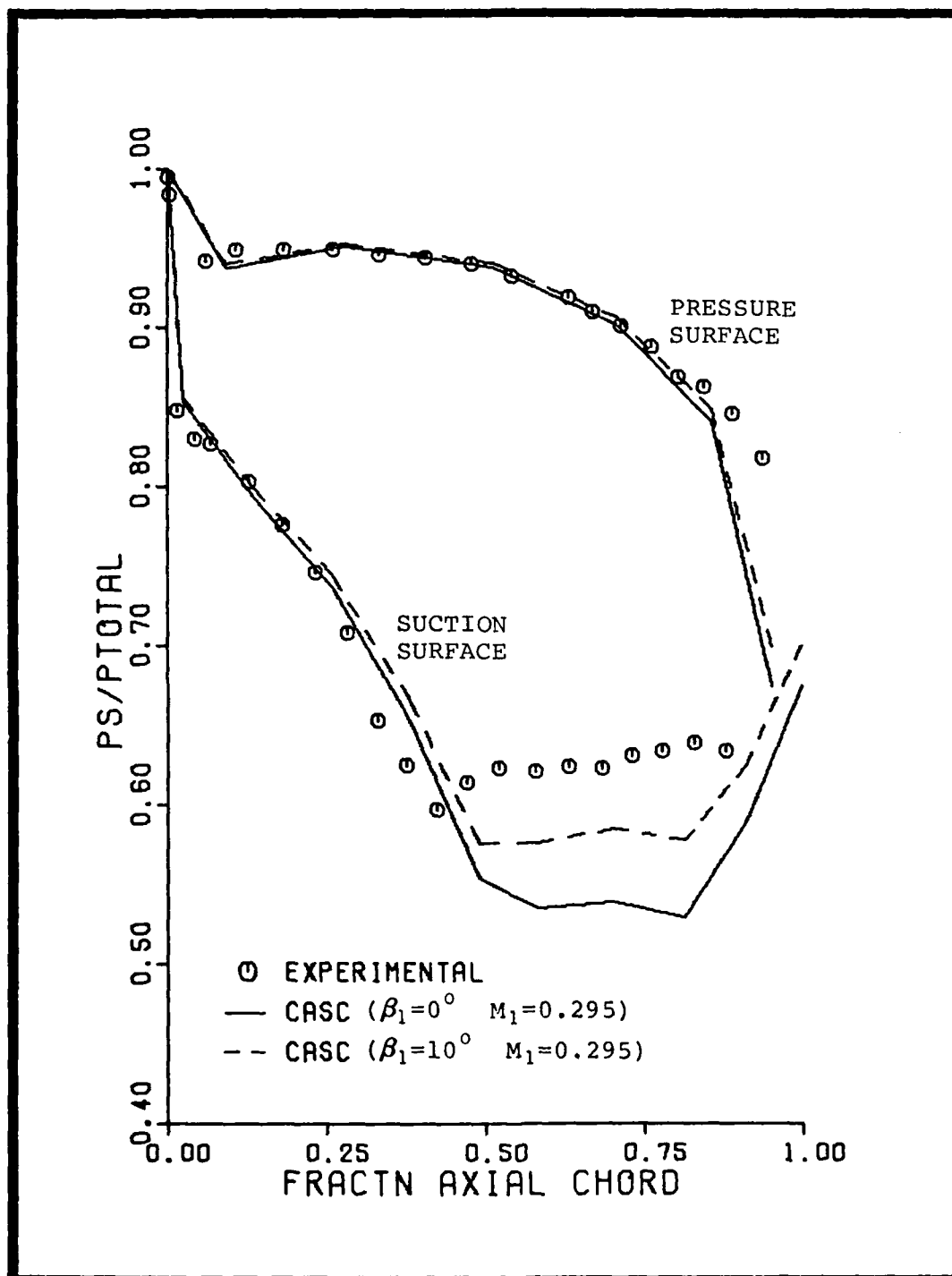
Figure 29   Case One C_p Distribution Correlation
(M$_1$ = 0.2950)

APPENDIX E

Pressure Coefficient Distributions
for Various Combinations of β_1 and M_1
(Second Test Case)
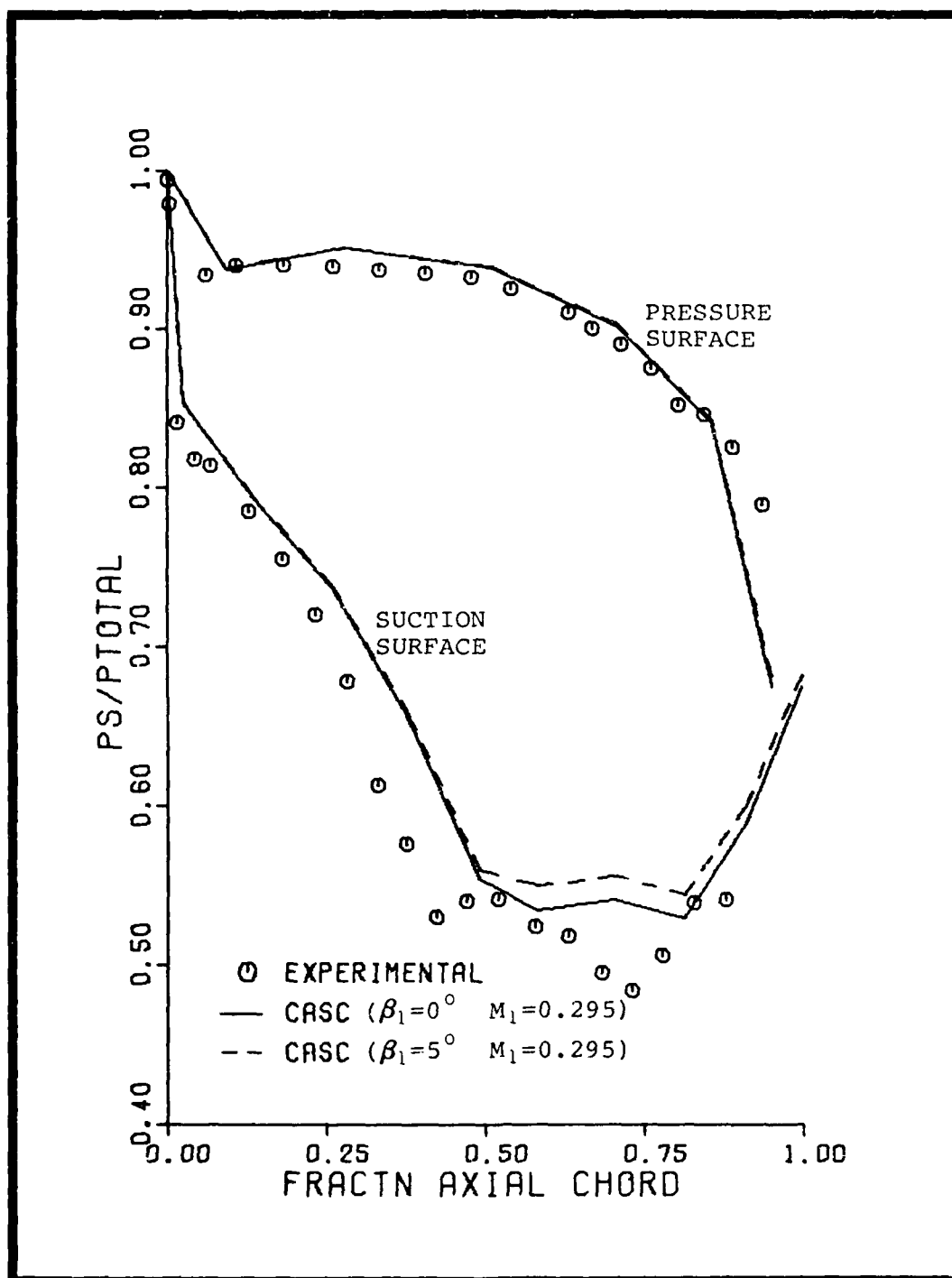
Figure 30   Case Two C_p Distribution Correlation
(M_1 = 0.2950)
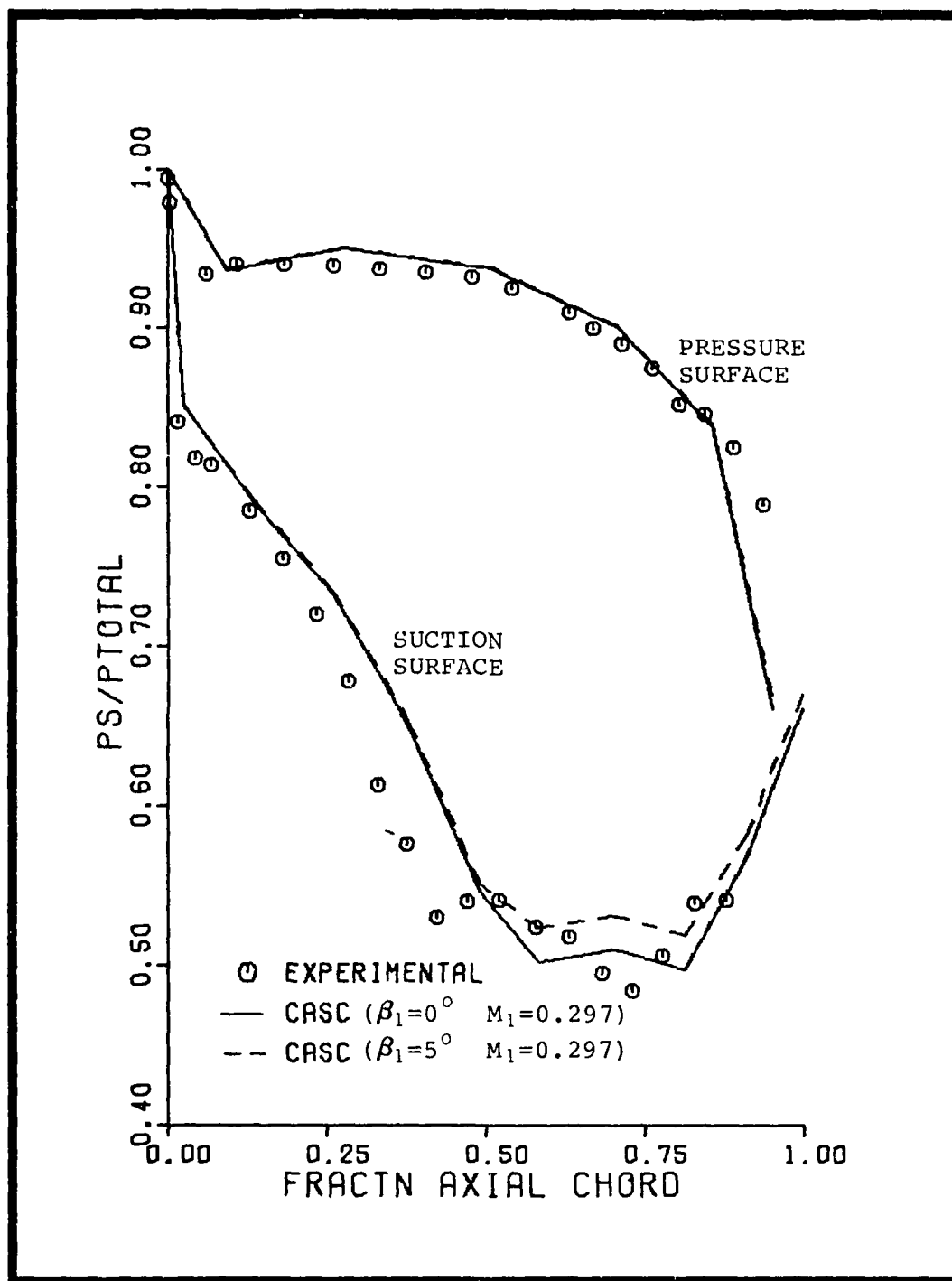
Figure 31   Case Two C_p Distribution Correlation
            (M_1 = 0.2970)

123
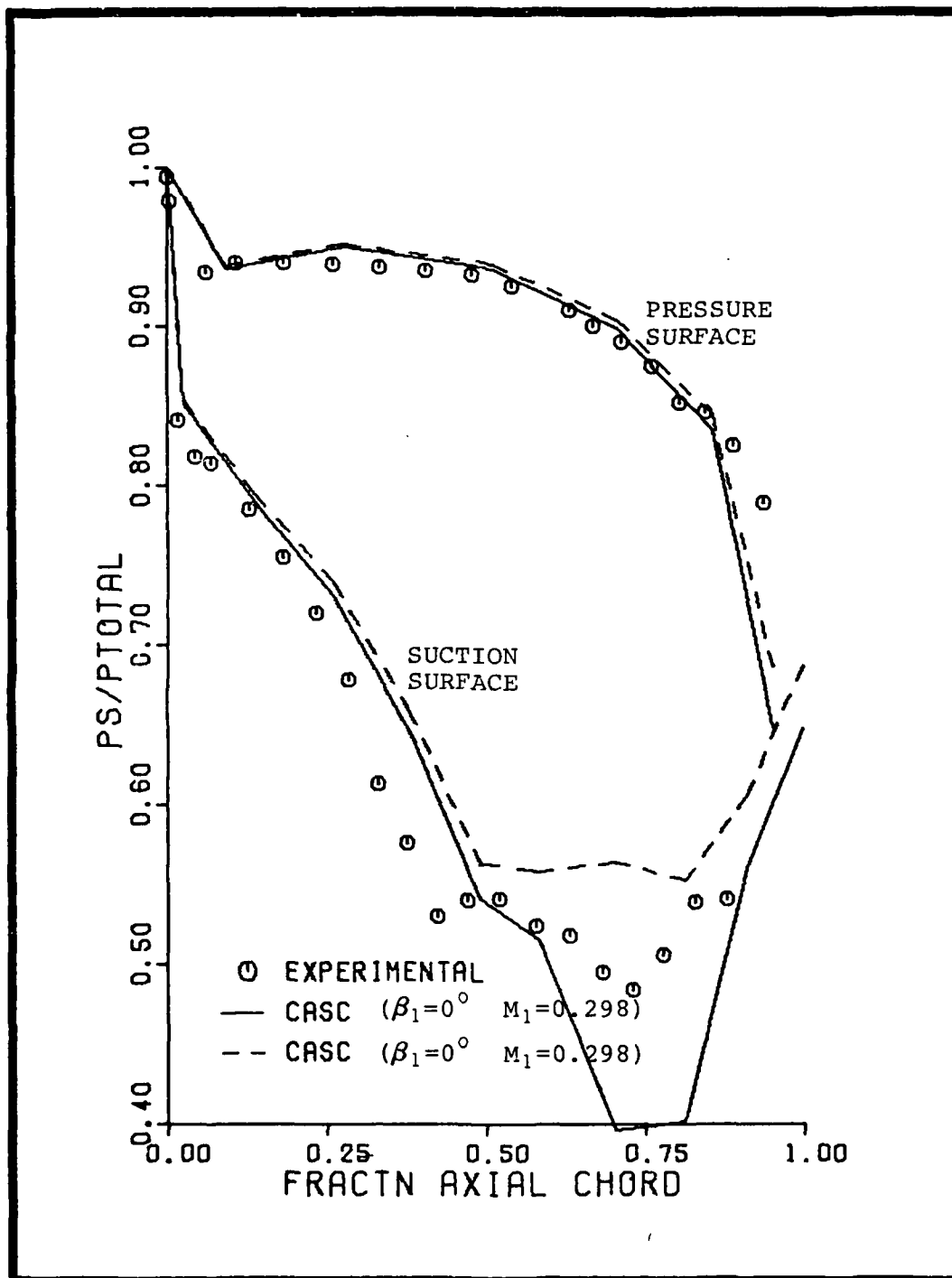
Figure 32   Case Two C_p Distribution Correlation
(M$_1$ = 0.2980)

124
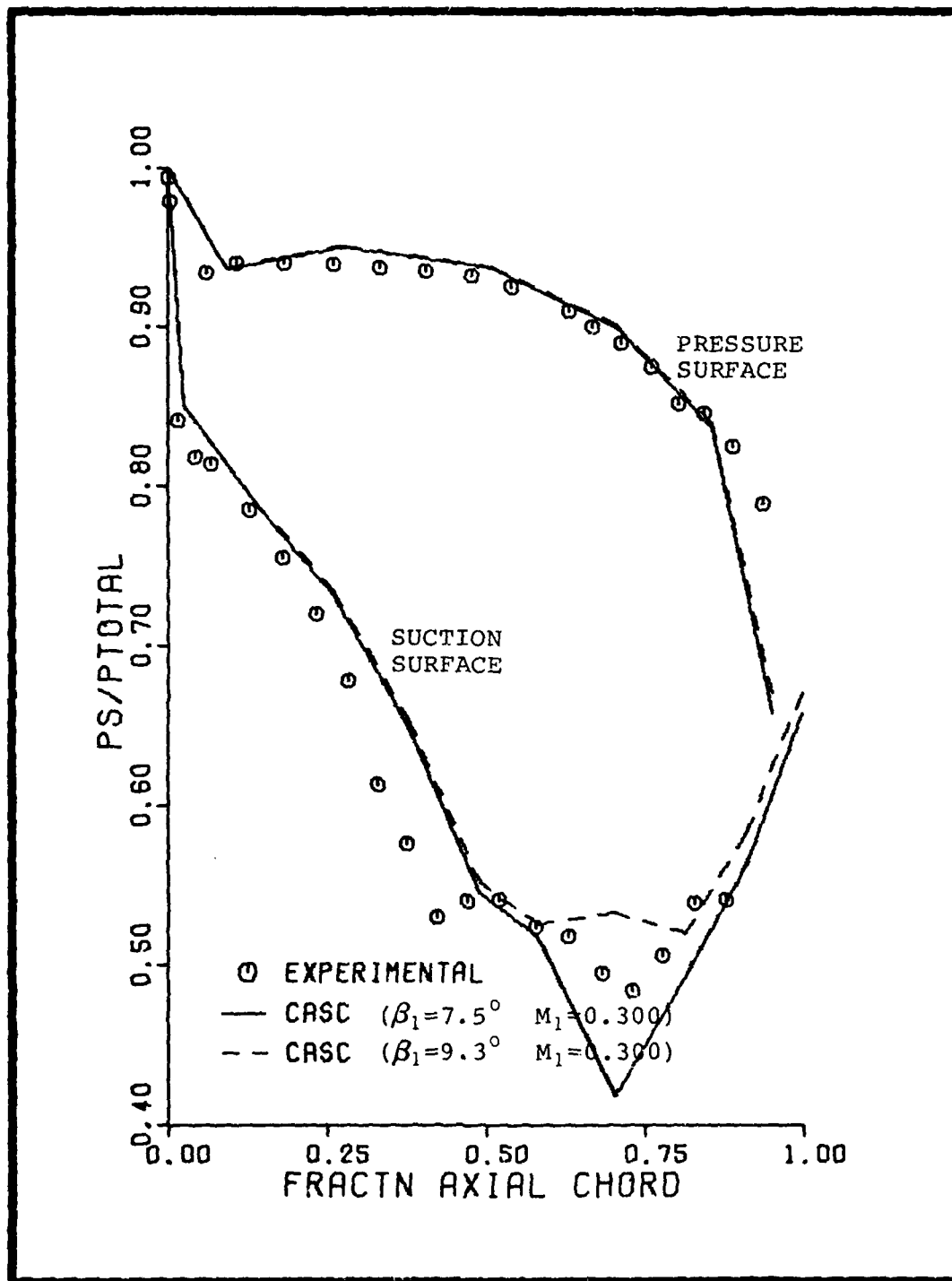
Figure 33   Case Two C_p Distribution Correlation
            ($M_1 = 0.3000$)

125
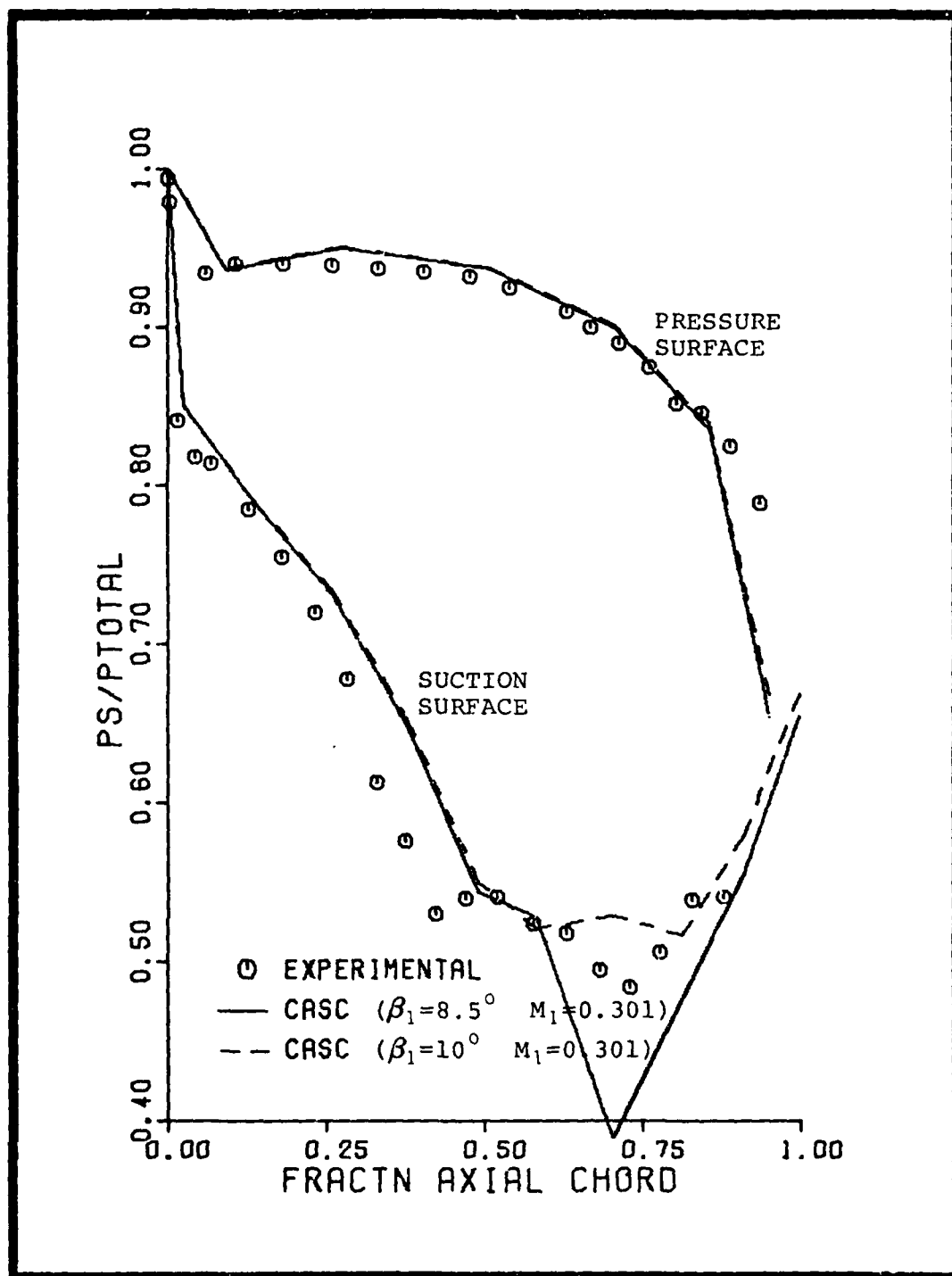
Figure 34   Case Two C_p Distribution Correlation
(M_1 = 0.3010)

126

APPENDIX F

Selected Design Versions
and
Associated C_p Distribution Predictions
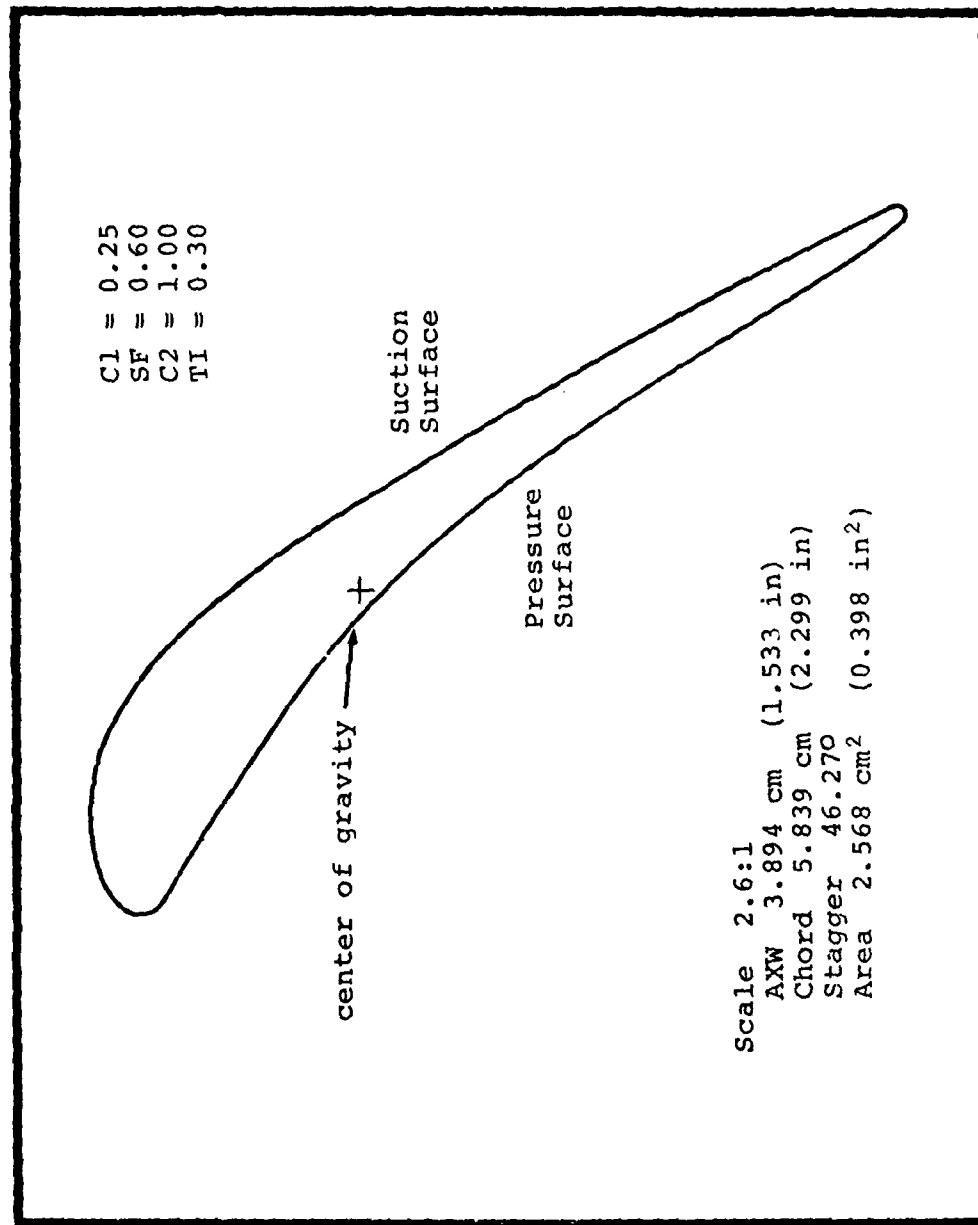
Figure 35 Design Version Two

128
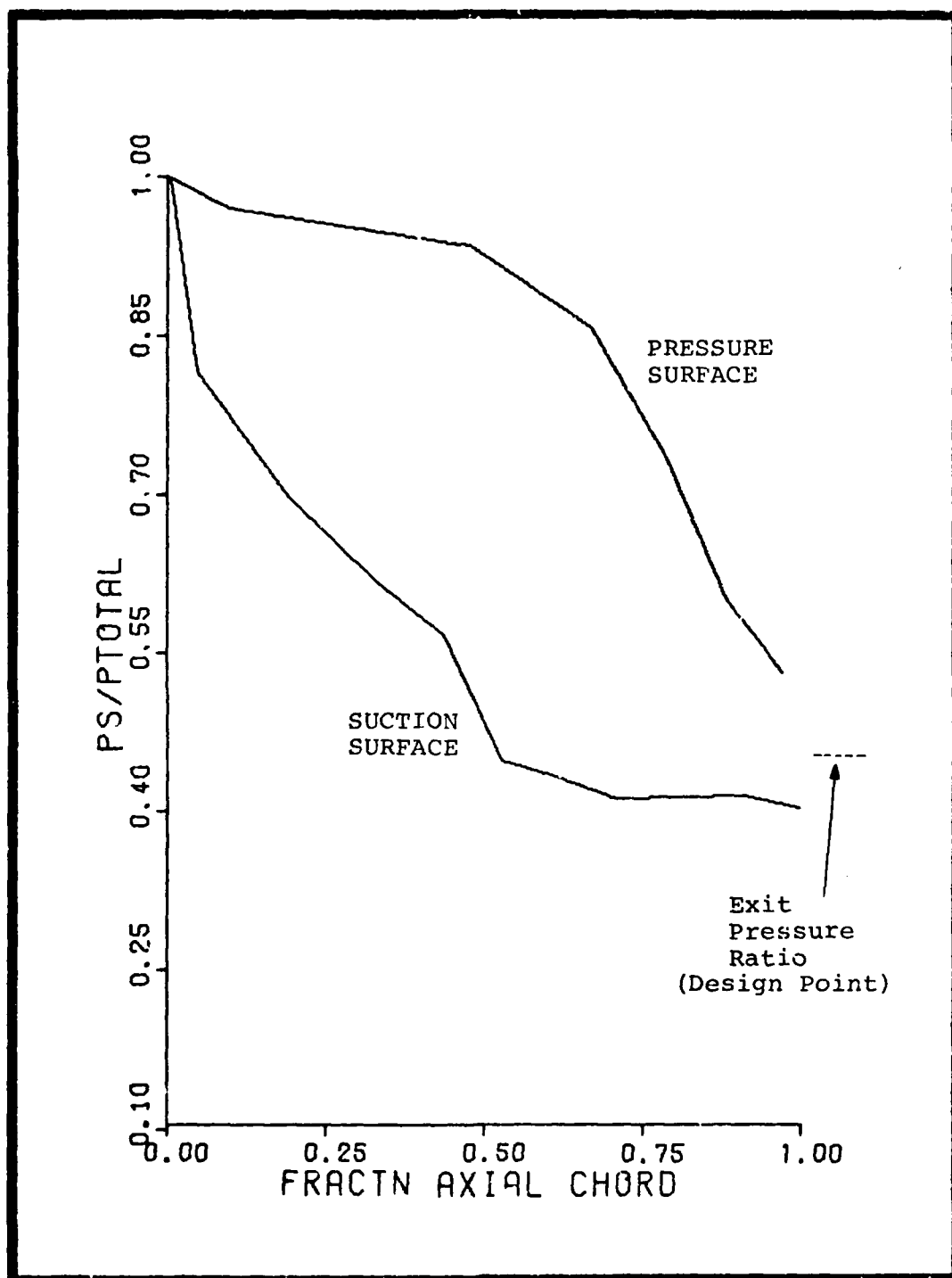
Figure 36   Design Version Two Predicted C_p Distribution
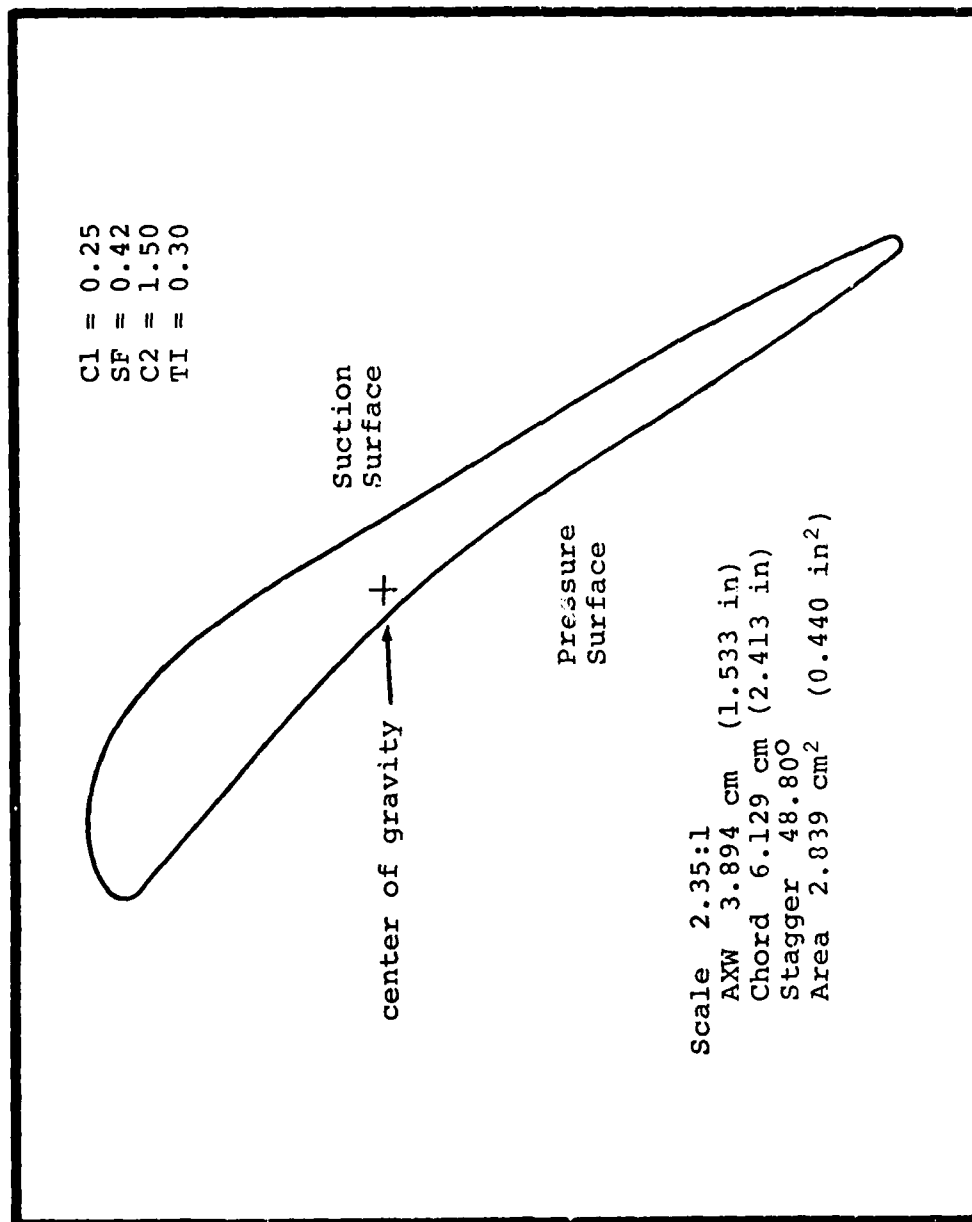
Figure 37 Design Version Twelve
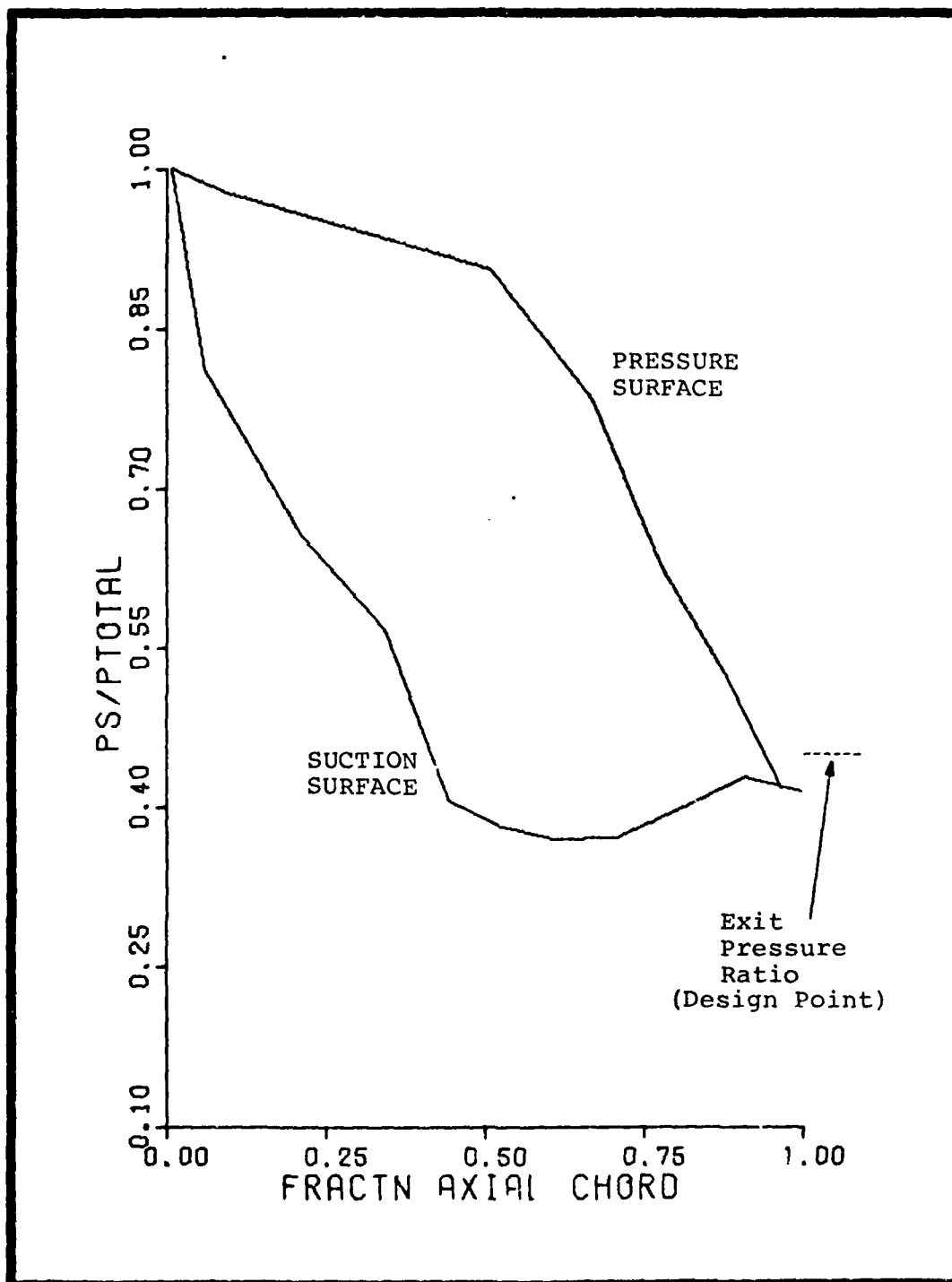
Figure 38   Design Version Twelve Predicted C_p Distribution
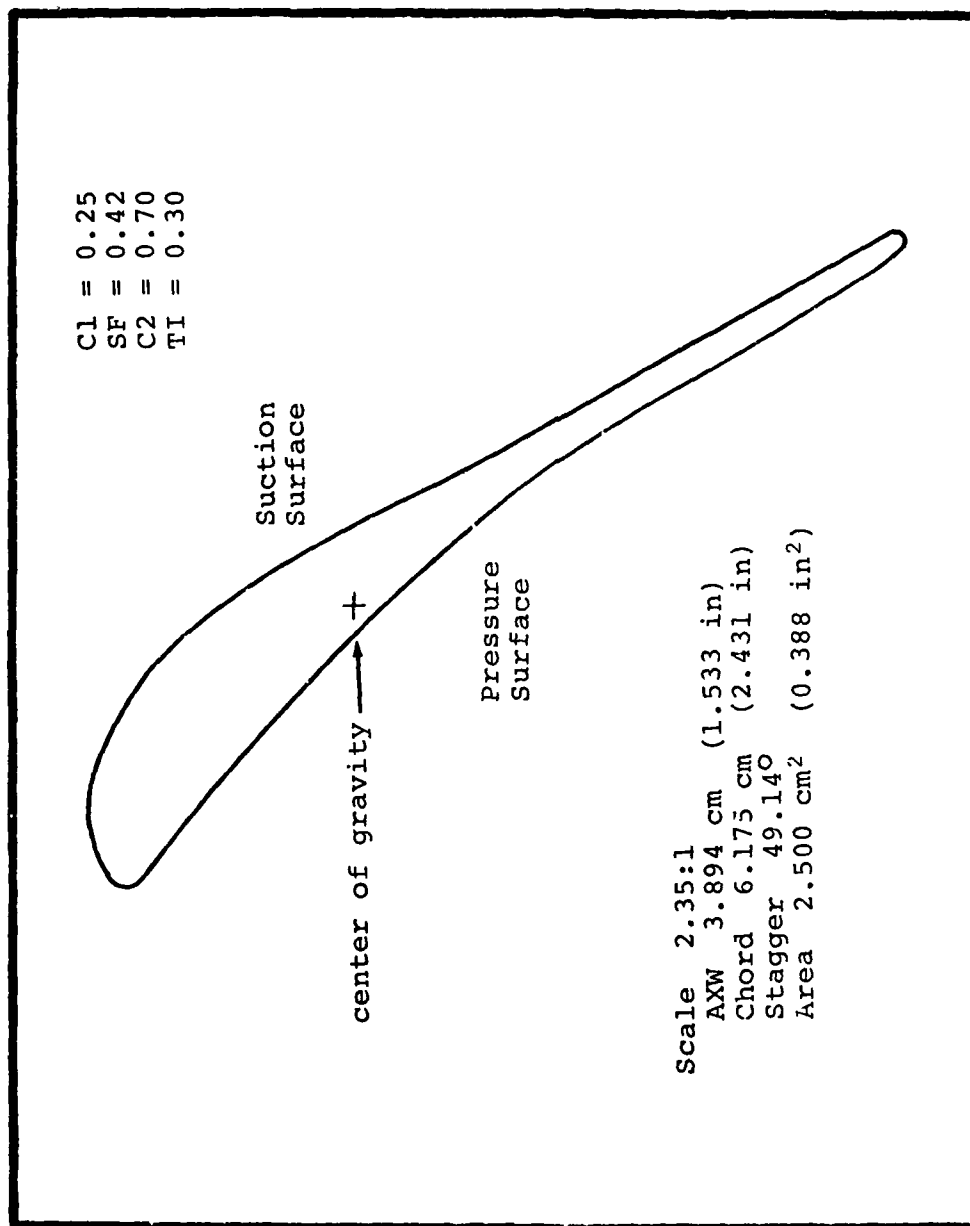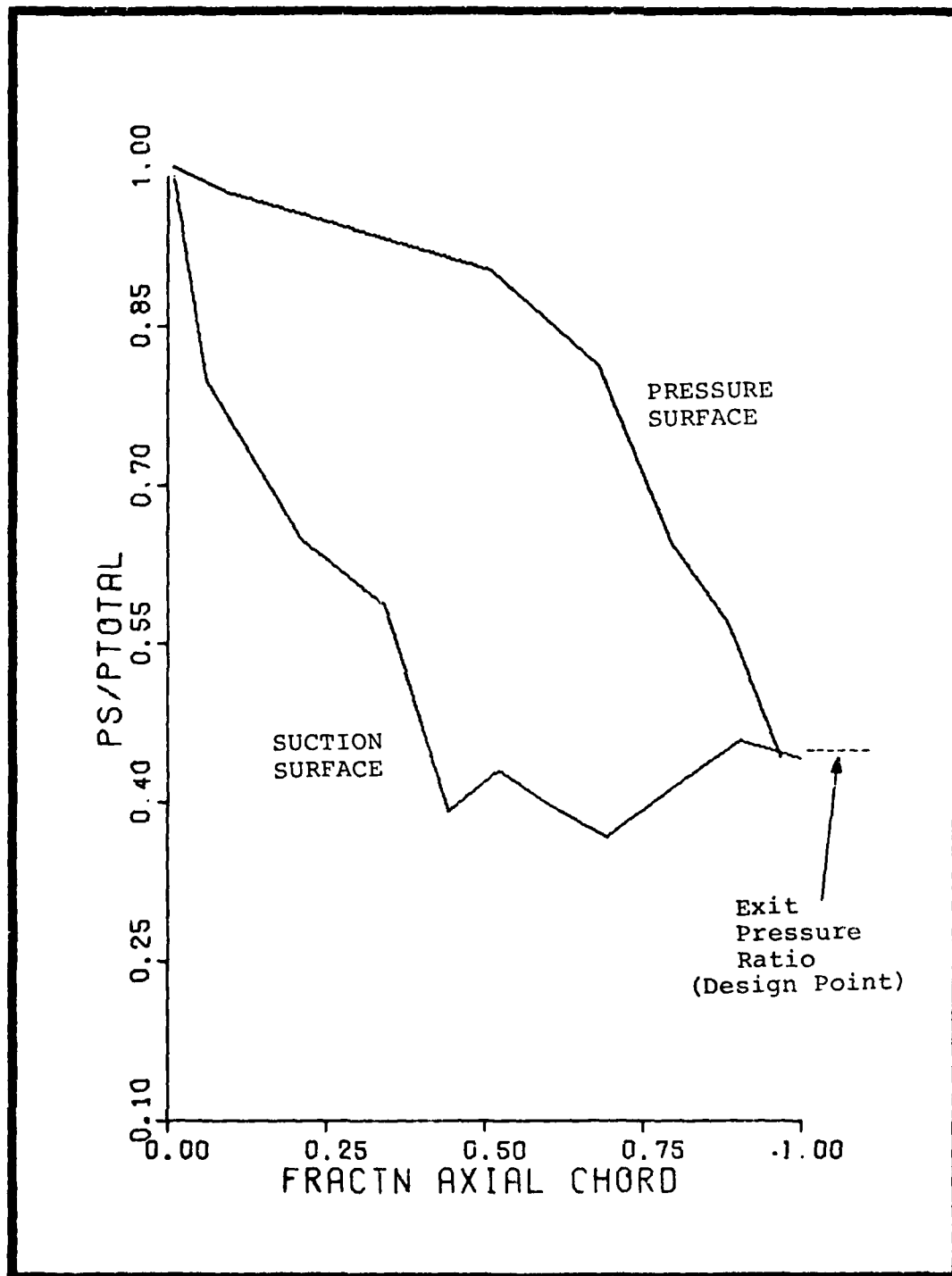
Figure 39 Design Version Fourteen

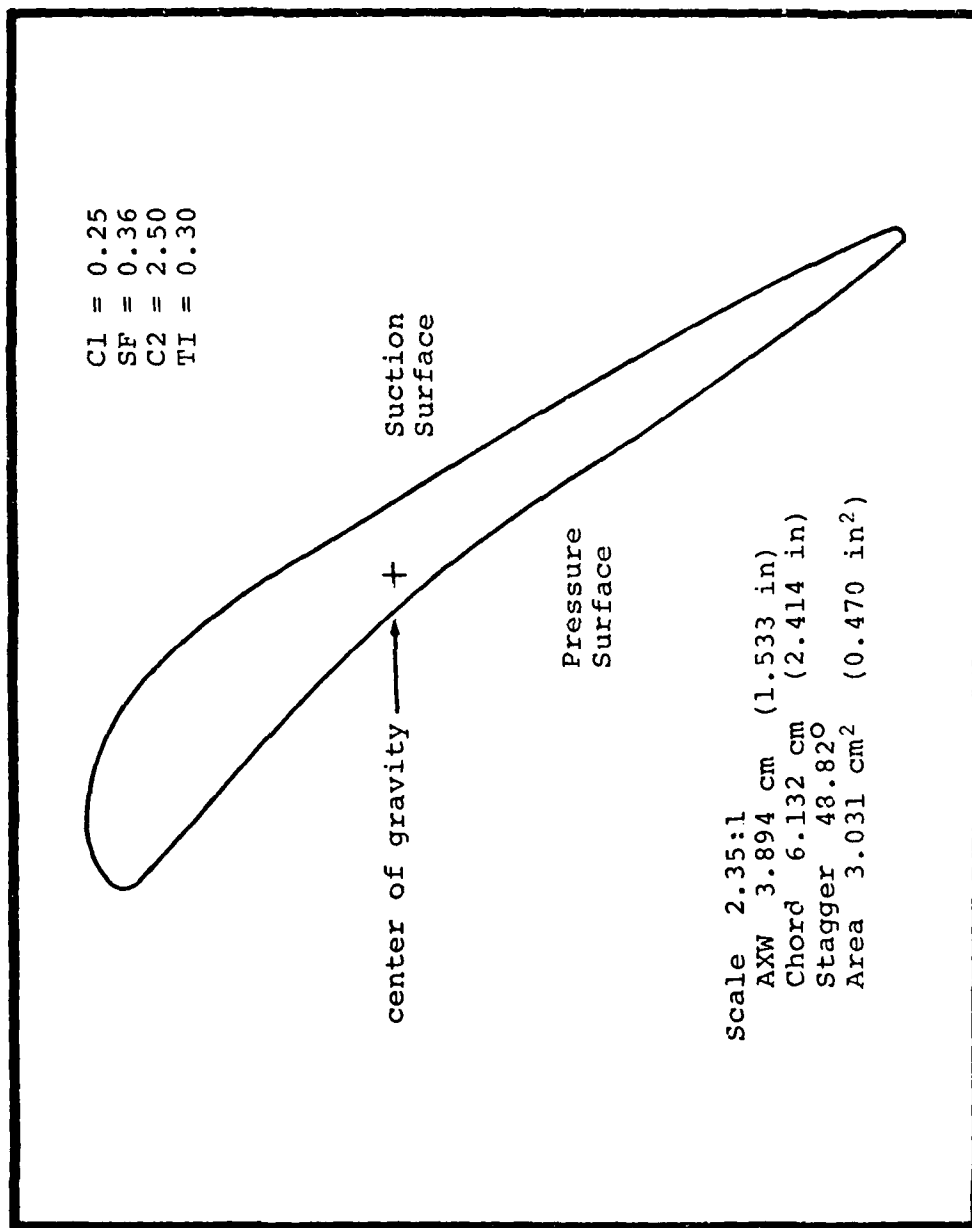Figure 40   Design Version Fourteen Predicted C_p Distribution

Cl = 0.25
SF = 0.36
C2 = 2.50
TI = 0.30

Suction
Surface

Pressure
Surface

center of gravity

Scale 2.35:1
AXW 3.894 cm (1.533 in)
Chord 6.132 cm (2.414 in)
Stagger 48.82°
Area 3.031 cm² (0.470 in²)

Figure 41 Design Version Eighteen
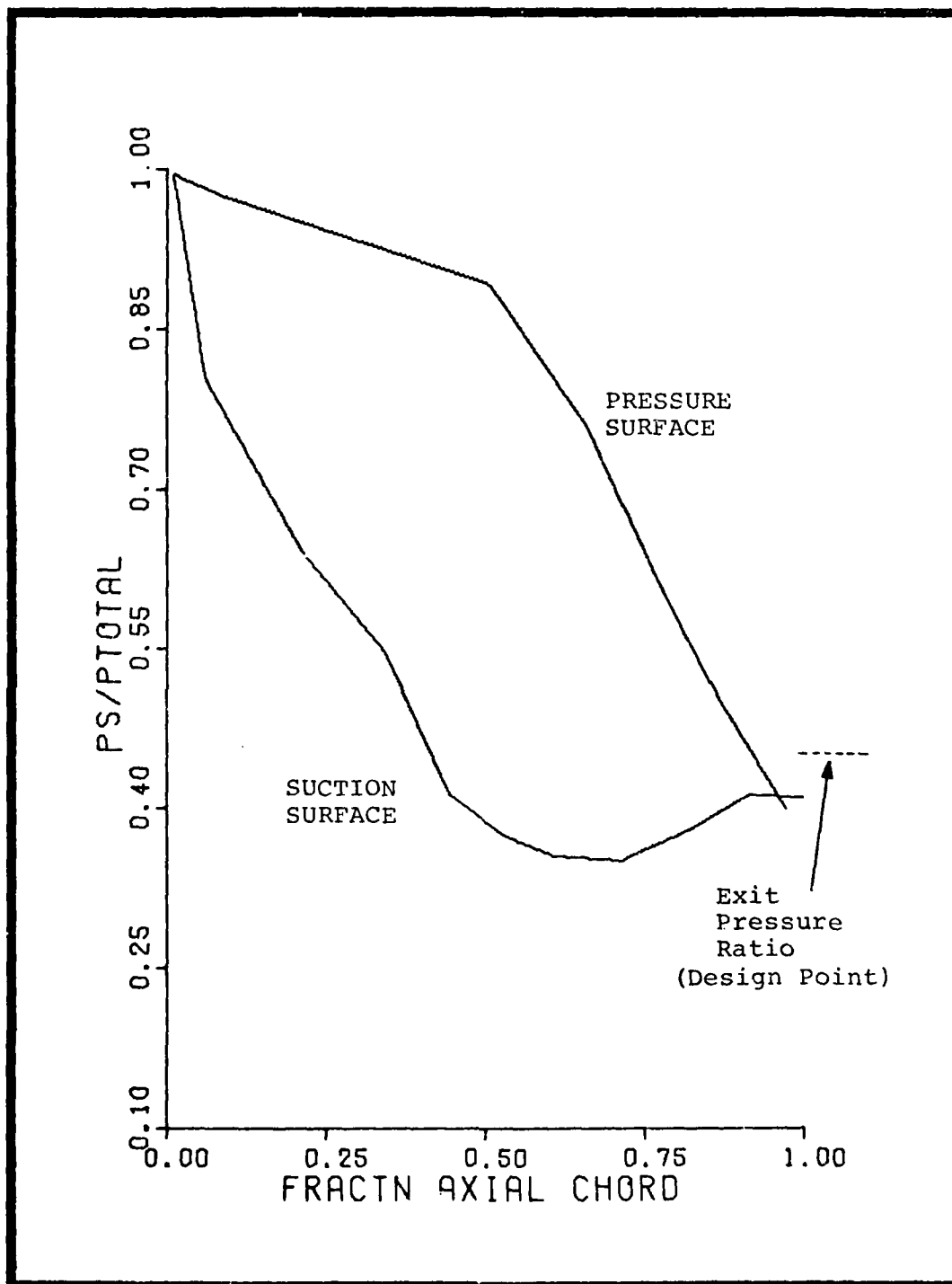
Figure 42   Design Version Eighteen Predicted C_p Distribution

C1 = 0.35
SF = 0.309
C2 = 0.95
TI = 0.60

Suction
Surface

+

center of gravity ⟶

Pressure
Surface

Scale 2.35:1
AXW 3.894 cm (1.533 in)
Chord 5.984 cm (2.356 in)
Stagger 47.71°
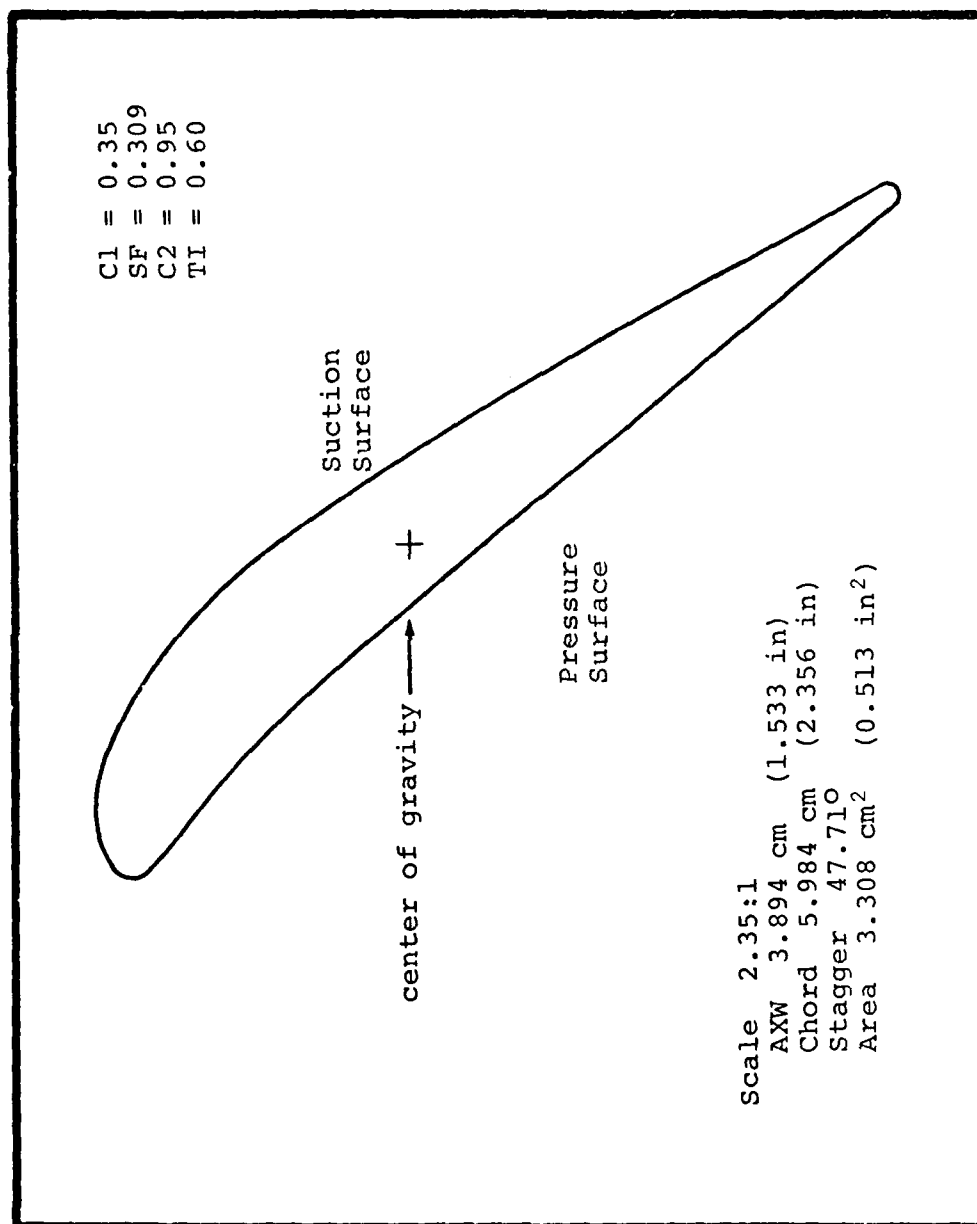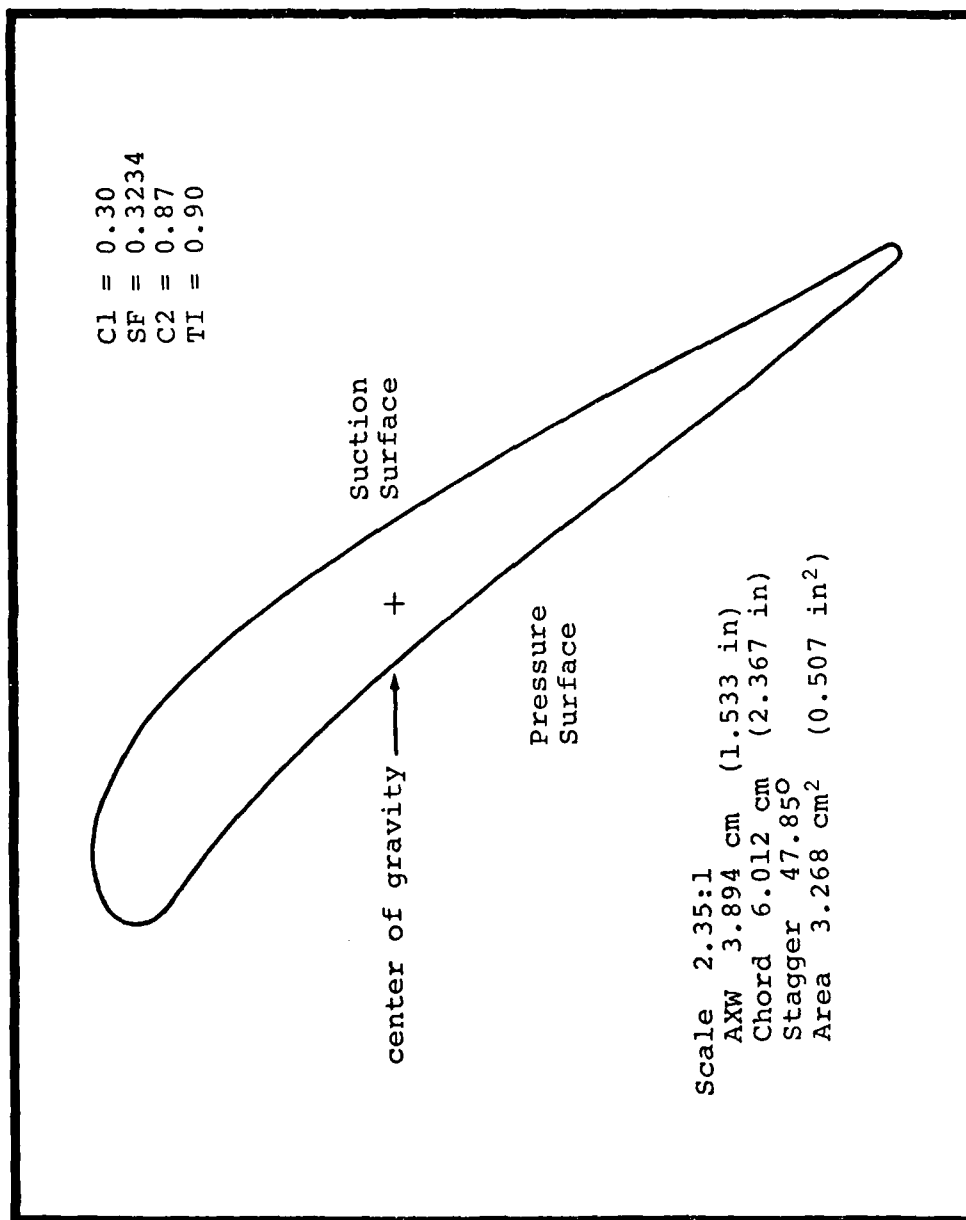Area 3.308 cm^2 (0.513 in^2)

Figure 43   Design Version Fifty-Two

136
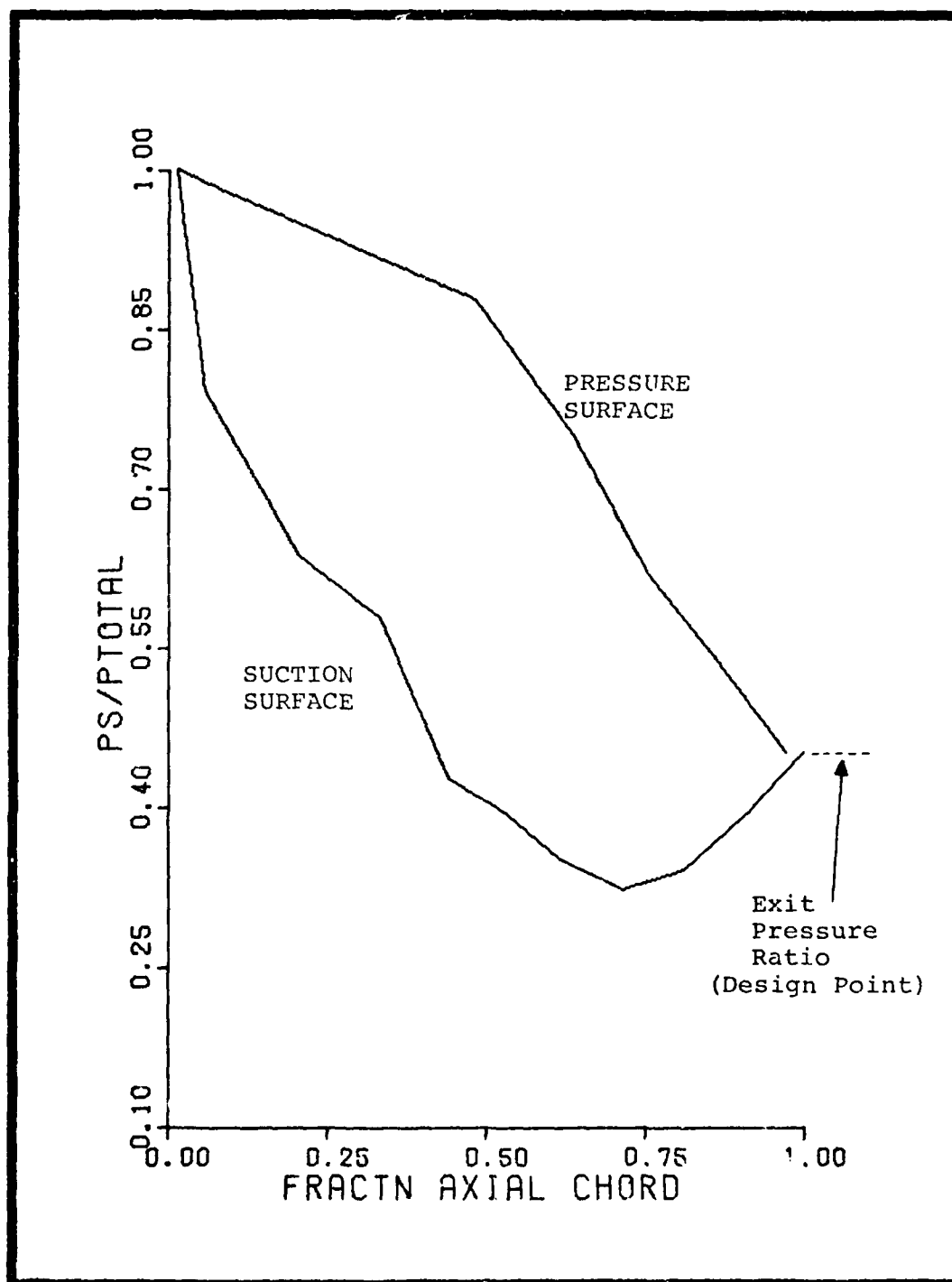
Figure 44   Design Version Fifty-Two Predicted C_p Distribution
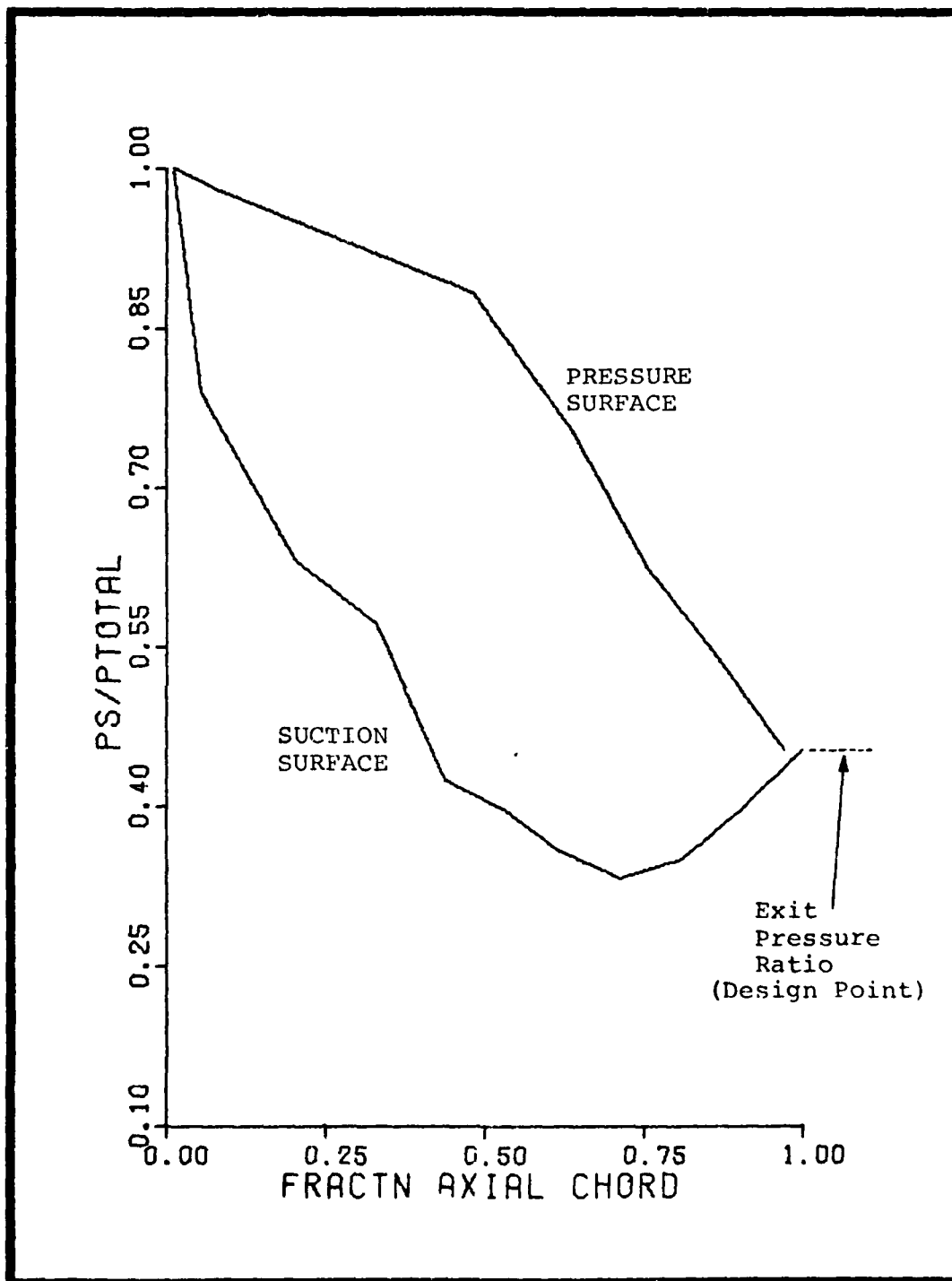
Figure 45 Design Version Fifty-Nine

138

Figure 46   Design Version Fifty-Nine Predicted C_p Distribution

C1 = 0.25
SF = 0.335
C2 = 0.757
TI = 1.20

Suction
Surface

center of gravity

Pressure
Surface

Scale 2.35:1
AXW 3.894 cm (1.533 in)
Chord 6.063 cm (2.387 in)
Stagger 48.22°
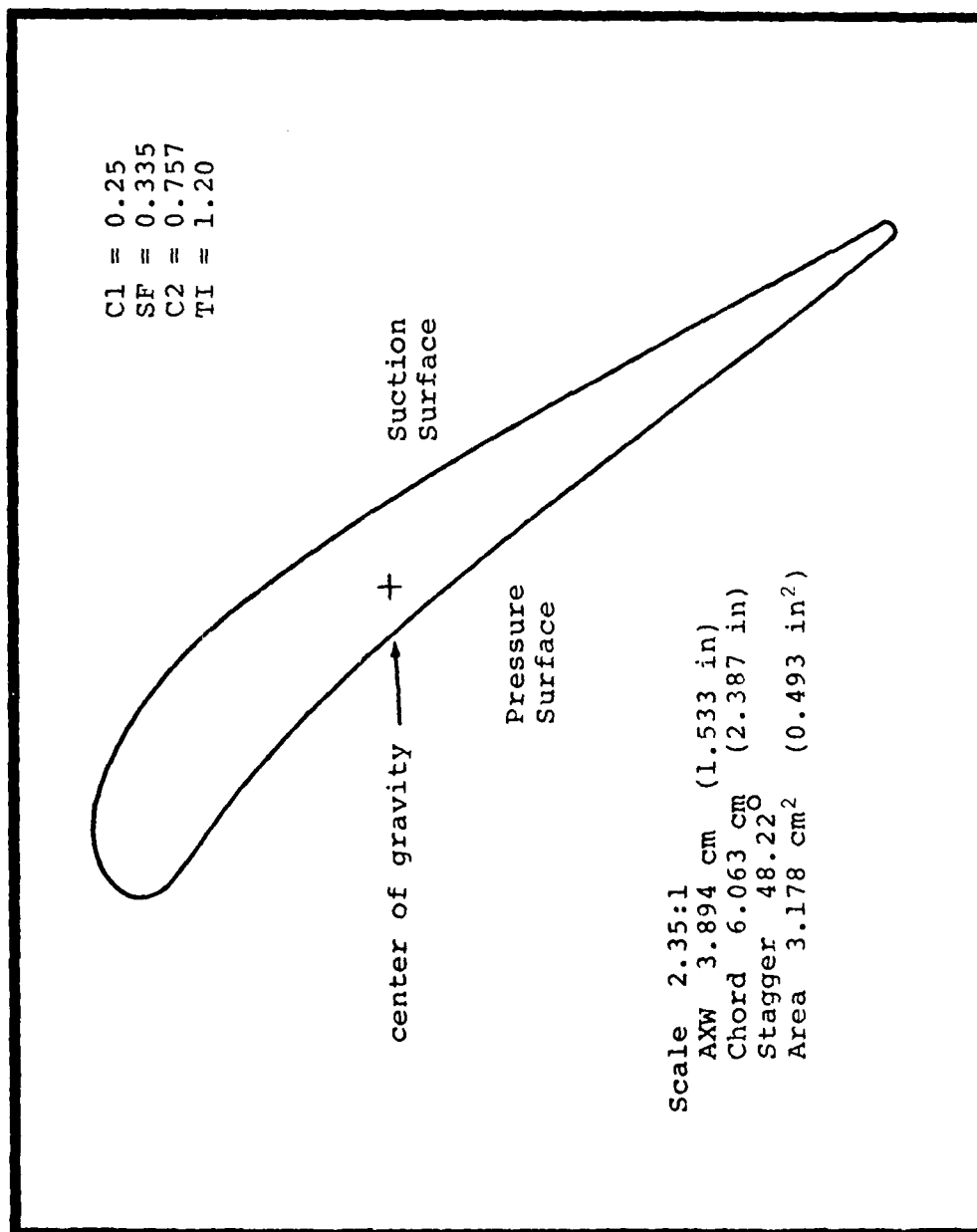Area 3.178 cm^2 (0.493 in^2)
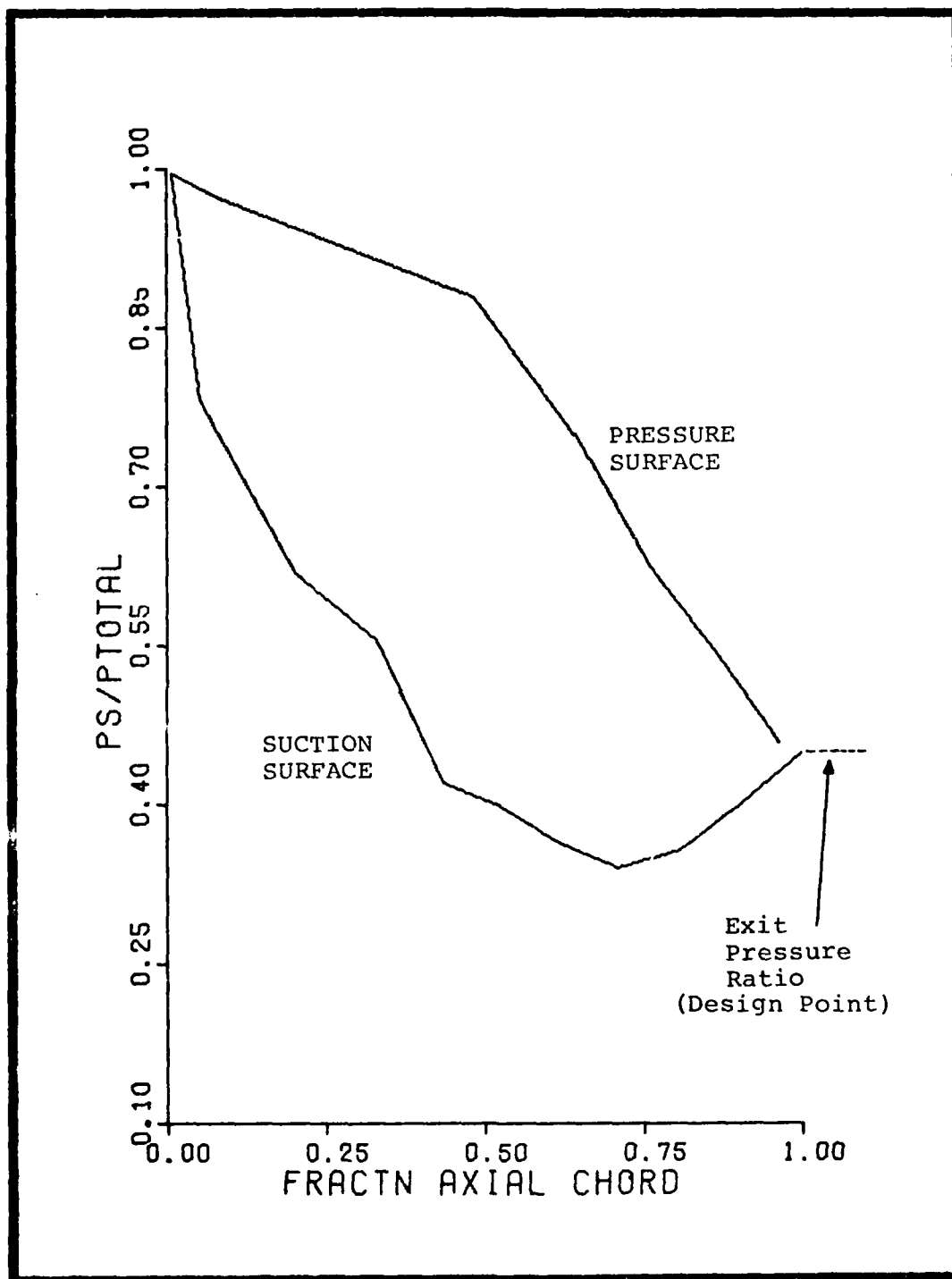
Figure 47 Design Version Sixty-Five

Figure 48 Design Version Sixty-Five Predicted C_p Distribution

Vita

Robert Normand Gamache was born on 4 July 1955 in Boston, Massachusetts, the son of Normand R. and Pauline A. Gamache. After graduation from Catholic Memorial High School in West Roxbury, Massachusetts, in 1973, he attended the University of Notre Dame graduating with a Bachelor of Science Degree in Aerospace Engineering in 1977. Upon graduation he received his commission in the United States Air Force through AFROTC. In September 1977, he reported to the Air Force Institute of Technology in the Graduate Aeronautical Engineering Program.

Permanent address: 268 Willow Street
                            West Roxbury, Massachusetts 02132

REPORT DOCUMENTATION PAGE		READ INSTRUCTIONS BEFORE COMPLETING FORM
1. REPORT NUMBER AFIT/GAE/AA/78D-7	2. GOVT ACCESSION NO.	3. RECIPIENT'S CATALOG NUMBER
4. TITLE (and Subtitle) THE DESIGN OF A TRANSONIC GAS TURBINE STATOR		5. TYPE OF REPORT & PERIOD COVERED MS Thesis
		6. PERFORMING ORG. REPORT NUMBER
7. AUTHOR(s) Robert N. Gamache, 2Lt, USAF		8. CONTRACT OR GRANT NUMBER(s)
9. PERFORMING ORGANIZATION NAME AND ADDRESS Air Force Institute of Technology Wright-Patterson AFB, Ohio 45433		10. PROGRAM ELEMENT, PROJECT, TASK AREA & WORK UNIT NUMBERS
11. CONTROLLING OFFICE NAME AND ADDRESS Air Force Aero Propulsion Laboratory AF Wright Aeronautical Laboratories Wright-Patterson AFB, Ohio 45433		12. REPORT DATE December 1978
		13. NUMBER OF PAGES 142
14. MONITORING AGENCY NAME & ADDRESS(if different from Controlling Office)		15. SECURITY CLASS. (of this report) UNCLASSIFIED
		15a. DECLASSIFICATION DOWNGRADING SCHEDULE

16. DISTRIBUTION STATEMENT (of this Report)

Approved for public release; distribution unlimited.

17. DISTRIBUTION STATEMENT (of the abstract entered in Block 20, if different from Report)

18. SUPPLEMENTARY NOTES

Approved for public release; IAW AFR 190-17

JOSEPH P. HIPPS, Major, USAF
Director of Information

19. KEY WORDS (Continue on reverse side if necessary and identify by block number)

Turbine Stator Design
Turbine Nozzle Performance
Turbine Blades
Cascades (Fluid Dynamics)
Transonic Characteristics

Transonic Flow
Transonic Nozzles

20. ABSTRACT (Continue on reverse side if necessary and identify by block number)

A turbine stator profile that is analytically predicted to exhibit good aerodynamic performance over a wide range of transonic operating conditions has been designed for the Air Force Aero Propulsion Laboratory's Heat Transfer Facility. Analytical Turbine Design System computer programs developed by General Electric Company were used to generate blade profiles/coordinates and perform 2-Dimensional cascade throughflow calculations (streamline curvature technique). Two aerodynamic performance

DD ₁ FORM 1473   EDITION OF 1 NOV 65 IS OBSOLETE

20. (Continued)

standards were applied to pressure distribution predictions of the blade contours produced from a parametric variation study; 1) equal flow expansion over both the suction and pressure surfaces, and 2) minimum suction surface diffusion. The influence of the following geometric parameters upon the design of a transonic turbine stator were investigated; axial location of maximum section thickness, stagger angle, leading edge bluntness factor, and trailing edge taper factor. Results of this study show that a good transonic turbine stator design must have a convergent-divergent flow passage and a flat suction surface aft of the throat location.